Hydrodynamics and sediment dynamics in Elkhorn Slough

A report to Monterey Bay Sanctuary Foundation

December 2005

Stephen Monismith, Nicole Jones, Megan Bela and Nicholas Nidzieko
Dept of Civil and Environmental Engineering, Stanford University

Adina Paytan, Gaurav Misra, and Joseph Street
Dept of Geologic and Environmental Sciences, Stanford University

Bank of Elkhorn Slough upstream of the Highway 1 Bridge – September 17, 2002

1. Introduction

Elkhorn Slough is a shallow coastal wetlands/lagoon complex located on Monterey Bay. While it is designated as a National Estuarine Reserve, it is subject to a number of potentially detrimental influences including nutrient and sediment loading associated with catchment agricultural practices, the loss of wetlands due to changes in erosion associated with the increased tidal action in the slough that has been observed since its opening to the ocean was expanded to build Moss Landing Harbor (P. Williams & Assoc. 1992) as well as changes in tidal prism due to subsidence (Malzone and Kvitek 1994). Recent studies carried out as part of assessing the environmental impacts of re-licensing of the power plant operated by Duke Energy that is adjacent to Elkhorn Slough have also suggested that the entrainment of larval organisms into the cooling system of power plant may be of concern.

While Elkhorn Slough generally receives little freshwater inflow it does have substantial tidal motions. Physically, the main stem of Elkhorn Slough consists of a relatively narrow channel adjoined by wide intertidal mudflats. Typical depths in the channels are 2 to 5 m. At low tides only the channels are submerged whereas at high tide they look like expanses of open water. Because the channels in these systems are narrow, velocities in them can be quite high (up to 1 m/s) and, because of nonlinearities associated with the effects of depth variations on friction, tidal motions can be complex (Friedrichs and Madsen 1992, Dyer 1997).

The primary goal of this project has been the development of a circulation model capable of modeling both sediment dynamics (erosion, deposition, and transport) and the transport of larval organisms. As we describe below, this effort has entailed both modeling activities and a program of field measurements designed to provide data needed to assess model fidelity.

The bulk of our field work was carried out during two intensive three-week long field experiments, one in Sept 2002 and one in April 2003. During these periods we deployed current meters, sea-level gauges, temperature loggers and, in one case and with limited success, a CTD[1] equipped with optical backscatter sensors to measure suspended sediment concentrations. Additionally, during the Sept 2002 experiment we also mapped velocity cross-sections at a

[1] CTD = Conductivity Temperature Depth – an instrument used to measure pressure, temperature, and salinity, the latter by measuring electrical conductivity as well as temperature.

number of stations along the slough using a boat-mounted ADCP[2] . A description of the experiments and the results of this field work are shown in section 2.

Our modeling has been based on the application of a version of the 3D circulation model TRIM3D[3] developed by Prof. Vincenzo Casulli of the University of Trento (Casulli and Cheng 1992; Casulli and Catani 1994) that incorporates modifications to scalar advection schemes (Gross et al 1999a,b) and the addition of algorithms to model cohesive sediment dynamics (Inagaki 2000, Bricker et al 2004). Elements of this work have included adapting bathymetric data acquired by the Seafloor Mapping Group at California State University Monterey Bay and by the Moss Landing Marine Laboratories for use in the model, calibrating the hydrodynamic portion of the model and exploring the behavior of the sediment model. Results from the numerical model as well as a discussion of the challenges that need to be faced in future modeling of Elkhorn Slough are presented in section 3.

Finally, in addition to physical hydrographic measurements, we also made limited measurements of the distribution of several radium isotopes. Radium isotope activities have been used in this project to derive an estimate for saline groundwater discharge and associated terrestrial non-point source nutrient loads into the Slough. Groundwater input may have direct effect on the chemical and biological characteristics of the Slough and indirectly effect sediment dynamics by influencing sea-grass, algae and phytoplankton relative abundances and the organisms higher in the food chain that depends on these autotrophs. Discharge of groundwater into the coastal estuaries is widespread; it occurs anywhere that an aquifer is connected hydraulically with the sea through permeable sediments or rocks and the aquifer head is above sea level. Submarine groundwater flows into the coast at the interface between freshwater and seawater (the mixing zone) where the unconfined aquifer outcrops at the beach (Glover, 1959; Reay et al., 1992). Towards the seaward (slough) edge of the mixing zone water is brackish due to entrainment of salt water through permeable aquifer mixing as well as wave and tidal pumping (Cooper, 1959; Li et al., 1999). The chemistry of the water in the mixing zone is altered such that it is chemically different than either the terrestrial freshwater or seawater components (Church, 1996). This area has been referred to as the subterranean estuary (Moore, 1999, 2003).

[2] ADCP= Acoustic Doppler Current Profiler - see http://www.rdinstruments.com/
[3] TRIM = Tidal Residual Intertidal Mudflat

Accordingly, we refer to submarine groundwater discharge, as the freshwater-recirculated seawater mixture that is discharging at the slough (Buddemeier, 1996).

Moore and collaborators over the last few decades have pioneered the use of the quartet of naturally occurring radium isotopes as tracers for saline groundwater input to coastal systems (Krest and Harvey, 2003). The divalent cation radium isotopes are bound to soil particles and rocks in fresh water. They readily desorb via ion exchange in the presence of solutions of higher ionic strength (Webster, et al., 1994; Yang et al., 2002). Accordingly, in coastal aquifers where seawater with high ionic strength mixes and interacts with freshwater and aquifer rocks, waters enriched in Ra are observed (Moore, 1999, 2003). Open seawater on the other hand has very low or constant radium activities because of its isolation from soil or sediment sources. Therefore, excess Ra (over the open seawater activities) suggests a groundwater source. Ra isotopes are excellent tracers for the study of saline groundwater discharge in coastal systems because of the distinct difference in activities between the end member sources (e.g. open ocean and terrestrial saline waters), and because they behave conservatively after leaving the aquifer (accounting for radioactive decay). In addition, the use of Ra isotopes has advantages over other techniques used for quantifying groundwater related fluxes, since it allows for temporal and spatial integration over the mean-life of the radionuclides (Moore, 1999), and the different timescales of decay are useful as mixing tracers. Indeed Ra isotopes have been extensively used to determine the discharge of freshwater, nutrients (Cable et al., 1996, Krest et al., 2000; Kelly and Moran, 2002), and other dissolved constituents to the coastal ocean (Shaw et al., 1998).

Activities of radium isotopes were measured several times at six sites in the Slough channel (Figure 2.25) in order to trace the spatial, tidal, and seasonal variability of groundwater and associated nutrient input to Elkhorn Slough. In all seasons, and under all tidal conditions, high activities of the short-lived isotopes were measured near the head of the Slough at Kirby Park, declining toward oceanic activities at sites closer to the mouth of the Slough (Figure 2.26). This work is discussed in section 4. We summarize our findings in section 5.

2. Field measurements

The primary aim of our field work has been to obtain high quality velocity and water level data to calibrate and verify the numerical model. In addition, as we will discuss below, the field data reveal important features of the complex flows found in Elkhorn Slough.

2.1 Description of field work

Two main experiments were carried out. The first of which took place 4-24 September 2002 and involved deployment of the instruments shown in Table 1. The station locations are shown (approximately) on figure 2.1. Following recovery, we were able to download data from all instruments excepting the Vector at Station 2, which had flooded. Due to a firmware glitch, the ADP at station 4 did not record data while the ADP at station 3 fell over during deployment, something we were not aware of until after recovery. In addition to fixed instrumentation several sets of cross-channel velocity transects were acquired on the 10th and 17th of September with a 1200 KHz RDI ADCP mounted on a small boat. The primary data obtained during this experiment were approximately three-week long records of:

(1) water levels at stations 1,2,3,&5

(2) velocities at stations 1,2,&5

(3) temperatures at stations 1 to 5

(4) salinities and OBS[4] voltages at 3 heights at station 2

(5) turbulent bottom stress at station 5

Although water samples were collected to calibrate the OBS sensors, conversion of these records into suspended sediment concentrations was not pursued since all 3 sensors had "pinned", i.e. at reached their maximum output voltage at sediment concentrations less than the maximums to which the sensors had been exposed. Nonetheless, the OBS data does give some qualitative sense of how suspended sediment concentrations vary both tidally and subtidally.

The second experiment took place from 7-29 April 2003. The locations and combinations of instruments are listed in Table 1. During deployment and retrieval water samples were taken and CTD drops performed at each of the locations. Data was successfully collected from all of the instruments with the exception of the SBE26s and the OS200 which malfunctioned. Furthermore, data indicates that the frame at station 2 turned onto its side at day 11. We

[4] OBS = Optical backscatter instrument – an instrument that uses reflectance of infra-red light to measure concentrations of suspended sediment

speculate that a boat attached to our surface buoy and dragged the frame over. No ADCP transecting was done as part of this experiment. Thus, the primary data obtained during this experiment were approximately three-week long records of:

(1) water levels at stations 2, 3, 4 & 5

(2) velocities at stations 1,2,3,4&5

(3) temperatures at stations 1 to 5

(4) bottom stress at station 5

In all cases, raw data (in whatever form was native to the instrument) was converted to text files and then was loaded into the data analysis program Matlab™ to proceed with analysis.

2.2 Results: Tidal observations

As expected the dominant motions we observed in Elkhorn Slough were tidal. Typical depth-averaged velocities at Stations 1 (Near the Highway 1 bridge - figure 2.2) and 2 (landward of Seal Bend - figure 2.3) were as high as 1 m/s with a tidal range of approximately 2 m. An important feature of currents in Elkhorn Slough is easily seen in these records: Higher high water is always followed by lower low water such that maximum ebb currents are markedly stronger than are maximum flood currents. This characteristic is termed “ebb-dominance” (Friedrichs and Aubrey 1988), i.e. although they are of shorter duration, ebb currents are more intense than are flood currents.

The implications of this behavior can be seen in the acoustic backscatter recorded by the ADCPs. The strength of the acoustic backscatter recorded by the ADCP is known to be a proxy for sediment concentration (Holdaway et al 1999), i.e. high scattering return implies high sediment concentration. In this case, both tidal and spring-neap variations in scattering return and hence sediment concentration are apparent. On the tidal time scale, the strongest returns coincide with the peak ebbs, whereas returns from the flood tides are always weaker. In general, ADCP backscatter at a given range can be related to sediment concentration through a relationship of the form

$$10\log\left(C_s\right) = aEI + b \qquad (1)$$

where C_s is the sediment concentration, a and b are constants determined by sediment size (and size distribution), and EI is the echo intensity (in decibels = db). If we knew maximum and minimum sediment concentrations (C_{max} and C_{min}), we could determine a and b from (1) as

$$a = \frac{10}{EI_{\max} - EI_{\min}} \log\left(\frac{C_{\max}}{C_{\min}}\right)$$
$$b = 10\log\left(C_{\max}\right) - aEI_{\max} \tag{2}$$

Based on the small number of water samples originally taken for calibration of the OBS, as well as on values reported by Malzone (1999), for illustrative purposes we might guess that C_{max} = 100 mg/l and C_{min} =1 mg/l. C_{min} is not very important so long as it is small and non-zero. The relatively large value of C_{max} is not entirely speculative given that we measured concentrations of 30 to 40 mg/l at times when the currents were weaker than their maximum values. The results of this approximate calibration are shown in figure 2.4, where we have also estimated the cross-sectionally averaged sediment flux as

$$F_s = A_c C_s U \tag{3}$$

where A_c is average cross-sectional area and U is the time-varying along-channel velocity, (see also Malzone and Kvitek 1994). The implication of this asymmetry in currents and inferred sediment concentrations is that since currents and sediment concentrations are stronger/larger on ebbs than on floods, sediments eroded from the sides and bottom of the Slough are, in effect, pumped downstream and ultimately out of the estuary. This appears as an average flux (to be taken as a very approximate number) of 23,000 tons/year, or about 10,000 m^3, of sediment.

Another way to look at tidal flows in the Slough is to look at tidal excursions, i.e. the displacements of (fictional) water parcels due to tidal currents. Mathematically the displacement, ξ, is defined as:

$$\xi\left(x_0, t\right) = \int_0^t U\left(x_0, \tau\right) d\tau \tag{4}$$

where x_0 is the point where u is measured and t is the time of interest. ξ approximates how far up and down the channel water parcels are likely to go during a single tidal cycle. An example of a computation of ξ by (4) is given for Sta. 2 in figure 2.5. Note that using only velocities at Sta. 2, water parcels would be expected to exit the Slough on ebbs and to make it to the head of the estuary on floods. This reflects the fact that the tidal prism is comparable to the volume of the estuary below MLLW: In 1993 the volume of water in Elkhorn Slough at MHHW[5] was

[5] MHHW= Mean Higher High Water – the average height of the water surface at the greater of the two daily highs.

approximately 1.2 x 10^7 m^3 whereas at MMLW it was 6 x 10^6 m^3 (Malzone 1999), thus giving a tidal prism of 1.2 x 10^7 - 6 x 10^6 = 6 x 10^6 m^3, i.e. approximately the volume below MLLW.

While the currents at Stations 1 and 2 were quite similar, measured currents at Stations 4 and 5 show the expected weakening of the mean flow with distance from the ocean (Figure 2.6), with currents generally weaker at the head of the estuary than at the mouth. This behavior demonstrated in figure 2.7, where we have plotted the rms along-channel velocity

$$U_{rms} = \sqrt{\frac{1}{T}\int_0^T U^2\, dt} \tag{5}$$

as a function of distance from the mouth. The difference between the two distributions is due to the different tidal conditions observed during the two experiments; the ratio of U_{rms} at any station to that at the mouth is the same for the two experiments. This variation in tidal velocities with distance implies tidal excursions that are corresponding smaller near the head than at the mouth, e.g. ± 2 km near Kirby Park versus ± 6 km downstream of Parson's Slough. Thus, it seems possible that the much if not all of the water in Elkhorn Slough downstream of Parson's Slough at high tide may have exited the Elkhorn Slough/Moss Landing Harbor complex by the end of the following ebb tide.

The velocities at Station 2 show significant subtidal means that are modulated over the spring-neap cycle. As discussed (e.g.) in Li and O'Donnell (1997), such mean velocities can be driven by rectification of tidal velocities, i.e. the averaged effect of the advection of momentum can give a driving force that varies like the square of the rms tidal velocity, i.e. which can vary significantly over the fortnightly spring-neap cycle. Similar mean velocities (and variation over the spring-neap cycle) were also observed at Station 2 during April 2003, so the behavior seen in figure 2.4 is not an artifact. In contrast, the mean velocities observed at all 3 other main channel stations were somewhat smaller. It may be worthwhile in future work to explore this subtidal flow, as it may enhance longitudinal dispersion and exchange in the Slough (Fischer et al 1979).

Comparing water level records for all 4 stations in Sept 2002 (figure 2.8) shows that phase differences (time lags) along Elkhorn Slough are relatively small, i.e. less than 1 hour (see Malzone and Kvitek 1994), a direct consequence of the short length of the Slough relative to the

wavelengths of the diurnal and semi-diurnal tides. For non-rectangular cross-sections, the phase speed, C, can be estimated to be (Henderson 1966):

$$C \simeq \sqrt{g \frac{A_c}{W}} \tag{6}$$

where A_c is the cross-sectional area and W is the width at the free surface. The approximation comes about because in shoal-channel systems, the velocity is not uniform across the cross-section as is assumed in deriving (3). Nonetheless, (3) provides a good first guess, e.g. at Station 2, A_c ! 300 m^2 and W ! 120 m (Malzone and Kvitek 1994), so C ! 5 m/s, whereas at Station 5, A_c ! 65 m^2 and W ! 100 m, giving C ! 2.5 m/s. For an average value of 4 m/s, we would expect a phase difference of 8000/4 = 2000 s, or slightly more than 30 minutes. The details of the observed phase behavior are more complex: for the day shown in figure 2.6, the time difference between stations 1 and 5 are 39 min. (HHW), 28 min. (LHW), 26 min. (HLW), and – 6 min. (LLW). More precise estimates of phase could be had through harmonic analysis (Schureman 1940), but this difference in phase behavior with depth may reflect the fact that in a shoal-channel system, the phase velocity can decrease with increased depth when this increased depth results in filling of substantial intertidal mudflats (Friedrichs pers. comm. 2005).

A cursory inspection (which could be confirmed by harmonic analysis) of water level and velocity records together suggests a phase shift of 90 deg between currents and elevation, i.e. maximum ebb currents take place when the depth, h, is half way between high water and low water, or when dh/dt is a maximum. This too is a consequence of the "shortness" of Elkhorn Slough. In the limit of no phase difference between the head and the mouth, aka co-oscillation of Elkhorn Slough with Monterey Bay, the local cross-sectionally averaged velocity $\overline{U}(x,t)$, is easily shown to be related to the rate of change with time of the depth, viz:

$$\overline{U}(x,t) = \frac{\overline{\frac{dh}{dt}}(t)}{A_c(h,x)} \int_x^L W(x,h)\,dx = \frac{dh}{dt}\frac{A_s}{A_c} \tag{7}$$

where A_s is the surface area upstream of where $\overline{U}(x,t)$ is measured. If the ratio A_s / A_c were constant, then $\overline{U}(x,t) \propto dh/dt$. Examples of this relation are shown in figures 2.9 to 2.11 and results for all 4 main channel stations are given in table 2.3. While the match is not perfect, it

does seem that as a first approximation, tidal currents can be directly calculated using only bathymetric data and knowledge of the tidal water elevation. Thus, if we look at the behavior of dh/dt (figure 2.12), we can see that the ebb-dominance that characterizes Elkhorn Slough tidal currents, which arises because LLW follows HHW, is possibly attributable to the inherent phasing of the tidal constituents in Monterey Bay.

Given that our experiments were both conducted about half way between the equinoxes and solstices, the behavior observed in figure 2.10 may not characterize tides throughout the year. Thus, it is worthwhile to assess the variation of dh/dt, in particular the evident asymmetry between floods and ebbs seen in figure 2.12, throughout the year. Absent long-term water level data, this can be done using harmonic predictions[6] for Moss Landing water levels. A comparison of histograms for the along-channel velocities for all of 2002 and 2003 with histograms for Sept 2002 and April 2003 (figure 2.13) shows that the tides observed during our experiments were not unusual.

The ebb dominance of Elkhorn Slough can be examined in light of the modeling and observational work carried out by Aubrey and colleagues (Speer and Aubrey 1985, Friedrichs and Aubrey 1988, Friedrichs et al 1990) examining the behavior of a number of small east coast estuaries. They showed that estuaries characterized by a relatively large tidal prism on shallow intertidal shoals relative to the volume of water stored in the deep channel (V_s/V_c) *and* relatively small ratios of the tidal amplitude to mean depth (a/h) tended to be ebb dominant. Assuming that all the water above MSL: is on the shoals and taking conditions downstream of Seal Bend, a quick calculation for Elkhorn Slough shows that:

$$\frac{V_s}{V_c} \approx \frac{3\times10^6}{9\times10^6} \approx \frac{1}{3}$$

$$\frac{a}{h} \approx \frac{1}{6}$$

According to Friedrichs et al (1990, figure 10), this places Elkhorn Slough firmly in the ebb dominant regime. On the other hand, the fact that the water surface level changes little along the Slough, suggests that tide propagation in the Slough does not change the water surface profile much and hence that much of the ebb dominance may originate from the nature of tides in the

[6] We used the version of X-Tide, a tide predictor based on using harmonic constants, available at http://tbone.biol.sc.edu/tide/tideshow.cgi

near shore regions of Monterey Bay. Testing these alternative hypotheses will be left for future work.

2.3 Results: Vertical and lateral variability of tidal flows

Beyond the tidal variations in depth and average velocity, flows recorded by the ADCPs were vertically and laterally sheared. For example at station 1 (figures 2.14 and 2.15), along-channel tidal velocities are vertically sheared as would be expected for a turbulent channel flow. More remarkably, the cross-channel flows show a persistent secondary flow, most notably on ebbs, that is defined by flows to the south side of the channel at the bottom ($V < 0$), and towards the north side near the surface ($V > 0$). This secondary flow comes about because of curvature of the channel (Kalkwijk and Booij 1986), which produces a centrifugal force directed outwards that is generally balanced by a free surface pressure gradient directed towards the center of curvature. The appropriate momentum balance is:

$$\frac{\partial}{\partial z}\left(\nu_t \frac{\partial V}{\partial z}\right) \cong -\frac{U^2}{R_c} + g\frac{\partial \zeta}{\partial r} \tag{8}$$

Here R_c is the radius of curvature, ζ is the free surface displacement, ν_t is the eddy viscosity, V is the transverse flow, and r is the local radial distance directed outwards from the center of curvature. As shown by Kalkwijk and Booij, solutions to (8) can be approximated by a linear variation with height in V which gives a top-bottom shear

$$\Delta V \cong \frac{2\left|\overline{U}\right| h}{\kappa^2 R} \tag{9}$$

where h is the local depth and $k = 0.41$ is von Kárman constant. The linear relation predicted by (9) is seen clearly in figure 2.16; note that the slope of the relation between ΔV and U implies a radius of curvature of approximately 310 m.

Overall, this secondary flow should represent a downwards flow on the north bank, upwards flow on the south bank, and cross-flows (as seen in figures 2.14 and 2.15). The effects of this secondary flow can be seen in transect data taken near station 1 (figure 2.17 – plots of velocity magnitude and acoustic backscatter). The secondary flow notwithstanding, the velocity magnitude primarily reflects the along-channel velocity. Overall, across the channel there was an almost 0.5 m/s variation in the tidal flow, with flows on the north side having been notably

stronger than on the south side. Comparing this transect data with the station 1 time series makes clear that the fixed ADCP did not record the most energetic part of the flow in this cross-section.

Evidence for the importance of the secondary flow can be seen on the south side of the channel where the slowing of the flow due to bottom friction extends much higher into the water column than on the north side. Evidently this reflects the effects of vertical advection of slow, near-bottom fluid by the upwelling flow. On the north side, the concomitant effects of downwelling result in the highest velocities being found at depth rather than at the surface. The effects of this secondary flow are pronounced in the backscatter field, i.e., in the sediment concentrations, where it appears that more turbid water from the shallows on the south side is being carried into the channel at the surface, whereas less turbid water from the north side is being carried under and across. The result is that local sediment concentrations might be higher near the surface than in mid water column as otherwise might be expected.

In contrast to station 1, the flow at station 2 seems simpler (figures 2.18 - 2.20): secondary flows are much weaker and at any point in the cross-section, the maximum velocities at any point in the cross-section are at the surface, and the depth averaged velocities vary inversely with depth as would be expected for a flow in which frictional effects are important. At station 2, the highest sediment concentrations can be inferred to be near the sides and bottom, although there are still high scattering returns, and thus probably high sediment concentrations, near the surface.

A final example of cross-sectional complexity can be seen in figure 2.19 – 2.21, time series of velocity profiles at station 3 in April 2003. This station was located inside Parsons Slough, nominally in the center of the channel. In this case, we appear to see flooding only; evidently ebbing took place somewhere else in the cross-section!

In any event, the cross-sectional variability seen in the ADCP transects makes clear that it will be difficult to infer fluxes of mass, sediments, nutrients, or larvae etc. from single point or even single profile measurements.

2.4: Flow results: turbulence

In shallow systems like Elkhorn Slough, the turbulent bottom shear stress plays an important role in the overall flow dynamics. As a first approximation, the streamwise momentum balance for the depth-averaged flow is (Friedrichs and Aubrey 1988):

$$\frac{\partial \overline{U}}{\partial t} + C_D \frac{\overline{U}\left(\overline{U}\right)}{h} \simeq -g\frac{\partial \zeta}{\partial x} \tag{10}$$

where the bottom drag coefficient $C_D \approx \left(2-6\right)\times 10^{-3}$ (see below). If we assume a tidal current $\overline{U} = U_0 \cos\left(2\pi t/T\right)$, with T= 12.42 h = the period of the M2 tide and U_0 = 0.5 m/s, we can estimate the relative importance of inertia and friction in the momentum balance in the Slough by computing the ration of inertia to friction:

$$\frac{\dfrac{\partial \overline{U}}{\partial t}}{C_D \dfrac{\overline{U}\left(\overline{U}\right)}{h}} = \frac{\dfrac{2\pi U_0}{T}}{C_D \dfrac{U_0^{\,2}}{h}} = \frac{2\pi h}{C_D U_0 T} \sim \frac{2\pi\left(5\right)}{\left(4\times 10^{-3}\right)0.5\left(4.2\times 10^{4}\right)} = 0.4 \tag{11}$$

Thus, it would appear that both friction and inertia are important.

More importantly, from the standpoint of erosion of Elkhorn Slough and its adjacent marshes, bottom stress also directly determines rates of sediment erosion and deposition. If the water column can be assumed to be well-mixed, then standard model for the rate of erosion of cohesive sediments takes the form (Mehta 1989):

$$\frac{\partial C_s}{\partial t} = \frac{P}{h}\left(\frac{\tau_b}{\tau_c} - 1\right) \quad \text{for} \quad \tau_b \geq \tau_e \tag{12}$$

where C_s is the local sediment concentration in the water column (in kg/m^3), P is the erodability (kg/m^{2}s), τ_b is the bottom stress (Pa), and τ_c is the critical stress (Pa) for erosion. Deposition is modeled as

$$\frac{\partial C_s}{\partial t} = \begin{cases} \dfrac{-2V_s}{h} C_s \left(1 - \dfrac{\tau_b}{\tau_d}\right) & \text{for} \quad C_{sed} < C_c \\ \dfrac{-2V_s}{h}\left(\dfrac{C_s}{C_c}\right)^{2/3} C_s \left(1 - \dfrac{\tau_b}{\tau_d}\right) & \text{for} \quad C_{sed} \geq C_c \\ 0 & \text{for} \quad \tau_b > \tau_d \end{cases} \tag{13}$$

where V_s is the settling velocity, τ_d is the critical stress for deposition, and C_c is the critical concentration for concentration dependent sedimentation

The model parameters *P* etc. depend on the particular composition of the sediments, their degree of consolidation, and the presence or absence of benthic infauna. They are completely empirical and must either directly measured (see McNeil et al 1996) or extrapolated from other systems using "engineering judgement", i.e. they must be guessed. For example, the sediment modeling reported in McDonald and Cheng (1997) and Bricker et al (2004) relied on values of *P* and τ_c measured in one set of experiments by the late Ray Krone in the early 1960's (Krone 1962). There are also subtleties: Brennan et al (2003) reported values of P/τ_c computed from direct measurements of the erosional sediment flux. Their observations suggested that the erosion of surficial sediments that had been deposited during the previous phase of the tide was much faster than of deeper sediments.

Bottom stress was measured directly at Station 5 in both experiments using Nortek Vector ADVs. Bottom stress is computed from measured time series of the fluctuating velocities by computing the velocity covariance (see e.g. Pope 2000) near the bed (z ! 0):

$$\tau_b = -\rho \left\langle u'w' \right\rangle \Big|^{z \approx 0} \tag{14}$$

Here < > represents a 10 minute time average that is designed to filter out turbulence while leaving tidal variations in velocity. The fluctuating horizontal (u') and vertical velocities are defined using the traditional Reynolds decomposition:

$$u' = u - \left\langle u \right\rangle = u - U \tag{15}$$

Velocities and stresses for April 2003 are shown in figure 2.22. As with the other stations, ebb dominance in the currents is readily apparent. This leads to an ebb-dominance in the stresses, with peak ebb stresses being typically 2 to 3 times larger than peak flood stresses. In light of the basic model above (12), this suggests greater erosion of sediments of ebbs than on floods and hence a downstream flux of sediments.

A standard way of representing the bottom stress (one used by many circulation models), is to connect τ_b to the velocity measured 1 m above the bottom:

$$\tau_b = \rho C_D U_1 \left| U_1 \right| \tag{16}$$

Thus

$$C_D = \frac{-\left\langle u'w' \right\rangle \Big|^{z \approx 0}}{U_1 \left| U_1 \right|} \tag{17}$$

i.e., C_D can be found by performing linear regression on the bottom Reynolds stress as a function of $U_1|U_1|$. Doing so for the 2002 data gives $C_D = 0.0015$ and for the 2003 data $C_D = 0.002$. These are less than the canonical value of $C_D = 0.0025$, and likely reflect the fact that the bottom at station 5 is effectively "smooth" from a hydrodynamic standpoint.

This is not the case for station 1. As part of ongoing studies for LOBO[7], a group from the EFML at Stanford[8] deployed several 1200 KHz ADCPs near LOBO mooring 1 (which is approximately 1 km upstream of Station 1 in the 2002/2003 experiments). These instruments were configured to record single ping data from which turbulent stresses can be computed (see Stacey et al. 1999). The main results of this work will be reported elsewhere, but in figure 2.23 we plot measured stresses and stresses computed using C_D=0.0043, a drag coefficient that is more typical of a rough bottom in an estuary. However, as at station 5, the ebb-flood asymmetry of the bottom stresses is striking.

In the absence of direct measurements of the bottom stress, fitting observed velocity profiles to the law of the wall can also be used to infer C_D. For a rough wall, the law of the wall is usually written as (Pope 2000)

$$U(z) = \frac{u_*}{\kappa} \ln\left(\frac{z}{z_0}\right) \tag{18}$$

where z_0 is the roughness height. This can be expressed in terms of C_D as follows

$$C_D = \left(\frac{u_*}{U(1)}\right)^2 = \kappa^2 \left(\ln\left(\frac{1}{z_0}\right)\right)^{-2} \tag{19}$$

Thus by regressing U as a function of $\ln(z)$, u_* and z_0 can be determined. Table 2.4 shows values for Stations 1,2, and 4. Two values are given for station 4, one near the bed ($z < 0.85$) and for higher up in the water column. This difference may reflect flow distortion near the ADP by the ADP and its support frame, although the fit of the log variation of velocity with height near the bed seems quite good (r^2=0.99), and so the difference may be real. It is reassuring that the value of C_D for station 1 calculated from log fitting is not too far from the value measured directly.

[7] Land Ocean Biogeochemical Observatory – see http://www.mbari.org/lobo/
[8] Derek Fong, Jim Hench and Nicholas Nidzieko

2.5 Temperature and salinity variations in the Slough

During the both experiments, a substantial temperature difference was observed between the head and mouth of the estuary. For example, during the September experiment (figure 2.24), the coldest temperatures at station 1, those seen at the end of the floods, were approximately 12 deg, presumably reflecting the temperature of surface waters of Monterey Bay. In contrast, the warmest temperatures at Station 5, observed at the end of the ebbs, were over 23 deg. In general, the longitudinal temperature difference between stations 1 and 5 was between 3 and 8 deg, being weakest at the end of the ebb and strongest at the end of the flood. During spring tides at the beginning of the experiment, water temperatures at station 5 at the end of the flood were roughly the same as those at station 1 at the end of the ebb, indicating that in one half tidal cycle, water parcels had traveled over 7 km, nearly the entire length of the Slough. During neap tides in the middle of the experiment water parcels travel only from as far as Station 2 between high water and low water, i.e. about 5 km.

In addition to temperature variations, as seen in tidal variations in salinity (figure 2.25) indicate that the salinity also varied along the length of the Slough in September 2002. The fact that the highest salinities at Station 2were observed at the end of the ebb, indicates that, as might be expected in an estuary with little inflow and a non-zero evaporation rate (Largier et al 1997), the head of the slough was hyper-saline, i.e. had salinities that were greater than oceanic values. Interestingly, the combined effects of temperature and salinity gradients lead to longitudinal density gradients that are relatively small and, in fact, reverse during the experiment (figure 2.26). A measure of the likely importance of these gradients to baroclinic circulation is the horizontal Richardson number (Monismith et al 2002):

$$Ri_x = \frac{\frac{\partial \rho}{\partial x} g h^2}{\rho C_D U^2} \approx \frac{10^{-4}\left(10\right)\left(4\right)^2}{10^3\left(5\times 10^{-3}\right)\left(1\right)^2} = 3\times 10^{-3} \qquad (20)$$

Given that $Ri_x << 1$, significant gravitational circulation and stratification are unlikely to have been important in Elkhorn Slough.

2.6 Summary

The major results of the hydrographic field work are:

(1) Water levels in the Slough are nearly in-phase; i.e., the water surface in the Slough moves up and down in response to tides in Monterey Bay as though it were a flat surface. As a result, tidal currents are proportional to the rate of change in sea-surface elevation, enabling first-order predictions of currents to be made using predicted water level variations.

(2) Currents below Parsons Slough are relatively constant in strength, partially reflecting the fact that much of the tidal prism of the system is upstream of the confluence of Parson's Slough and the main stem of Elkhorn Slough. The decrease in cross-sectional area with distance from the Highway 1 Bridge also contributes to maintaining the strength of tidal currents below Parson's Slough.

(3) Currents in Elkhorn Slough are ebb dominant – i.e., the shorter duration ebbs have stronger currents than are observed during floods. The likely effect of this on sediment transport is pronounced since bottom stresses, which drive erosion of sediments, are substantially larger on ebbs than on floods. The net effect is a mean ocean-ward flux of sediments. This flux would appear to be strongly modulated by the fortnightly spring-neap cycle.

(4) Tidal excursions are a considerable fraction of the length of the Slough. As observed in measured temperatures and inferred from integration of current measurements, at spring tides, a water parcel that is located at Kirby Park at the end of the flood can travel nearly the entire length of the Slough on the following ebb. During neap tides, water motions are somewhat reduced.

(5) Flows in many sections of Elkhorn Slough are spatially complex. In most cross-sections, flows are stronger in the deepest section, although in Seal Bend, the region of maximum ebb current wanders from side to side through the bend. Immediately upstream of the Highway 1 Bridge, there are pronounced secondary flows on ebbs. These lead to predictable variations in acoustic backscatter intensity that suggest cross-sectional variations in the distribution of sediments.

(6) Bottom drag coefficients, "constants" that relate bottom stress to local velocity vary from the canonical value of 0.002 near Kirby Park to values as large as 0.0075 in the reach below Parson's Slough.

Table 2.1: Location of field sites and associated instruments – Sept 2002 experiment

Station No	1	2	3	4	5
Station Description	East of Hwy. 1 bridge	East of Seal Bend	Parson's Slough	South of Kirby Park	Head of Slough
Station location	N 36^{O} 48.658' W 121^{O} 46.997'	N 36^{O} 48.859' W 121^{O} 45.350'	N 36^{O} 48.835' W 121^{O} 44.717'	N 36^{O} 49.543' W 121^{O} 44.697'	N 36^{O} 50.621' W 121^{O} 45.232'
Instruments	600 kHz RDI ADCP	1200 kHz RDI ADCP	2 MHz ADP	1.5 MHz HR-ADP	Vector ADV
	SBE39	Vector ADV	SBE26	SBE39	SBE39
	SBE26	OS200 CTD	SBE39		
		OBS			
		OBS			
		OBS			

Table 2.2 Location of field sites and associated instruments – April 2003 experiment

Station No	1	2	3	4	5
Station Description	East of Hwy. 1 bridge	East of Seal Bend	Parson's Slough	South of Kirby Park	Head of Slough
Station location	N 36^{O} 48.658' W 121^{O} 46.997'	N 36^{O} 48.859' W 121^{O} 45.350'	N 36^{O} 48.835' W 121^{O} 44.717'	N 36^{O} 49.543' W 121^{O} 44.697'	N 36^{O} 50.621' W 121^{O} 45.232'
Instruments	600 kHz RDI ADCP	1200 kHz RDI ADCP	1200 kHz ADCP	1.5 MHz HR-ADP	Vector
	SBE39	SBE39	SBE26	SBE39	SBE39
	SBE26	OS200 CTD	SBE39		
		OBS			
		OBS			
		OBS			

Notes:
ADP/ADCP: Acoustic Doppler (Current) Profiler – measure vertical distributions of currents
SBE 39: Temperature logger
SBE 26: S Water level logger
Vector ADV: Acoustic Doppler Velocimeter – measures mean and turbulent currents at a point
OS200 CTD: Conductivity/Temperature/Depth logger – measures salinity, water level and temperature
OBS: Optical backscatter sensor – measures (after calibration) suspended solids concentration

Table 2.3: Velocity – elevation data

Station	Slope: U vs dh/dt	A_c (m^2)	A_p(m^2)
1	6000	400	2.4×10^6
2	6000	335	2×10^6
4	3100	240	7×10^5
5	2040	65	1.3×10^5

Table 2.4: Drag coefficients and roughness lengths derived from the law of the wall

Station	C_D	z_0 (mm)
1	0.005	3
2	0.0075	9
4 (upper)	0.0075	9
4 (lower)	0.0125	26

Figure 2.1 Sampling stations for field work.

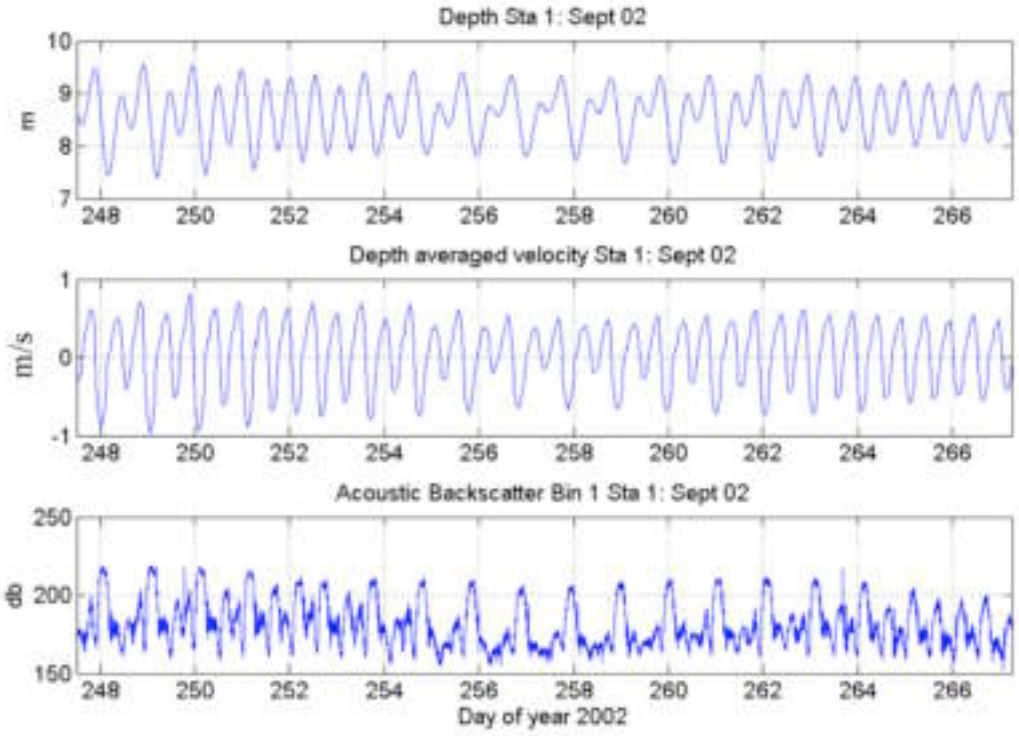

Figure 2.2 Water levels, currents and ADCP backscatter at Station 1, Sept 2002.

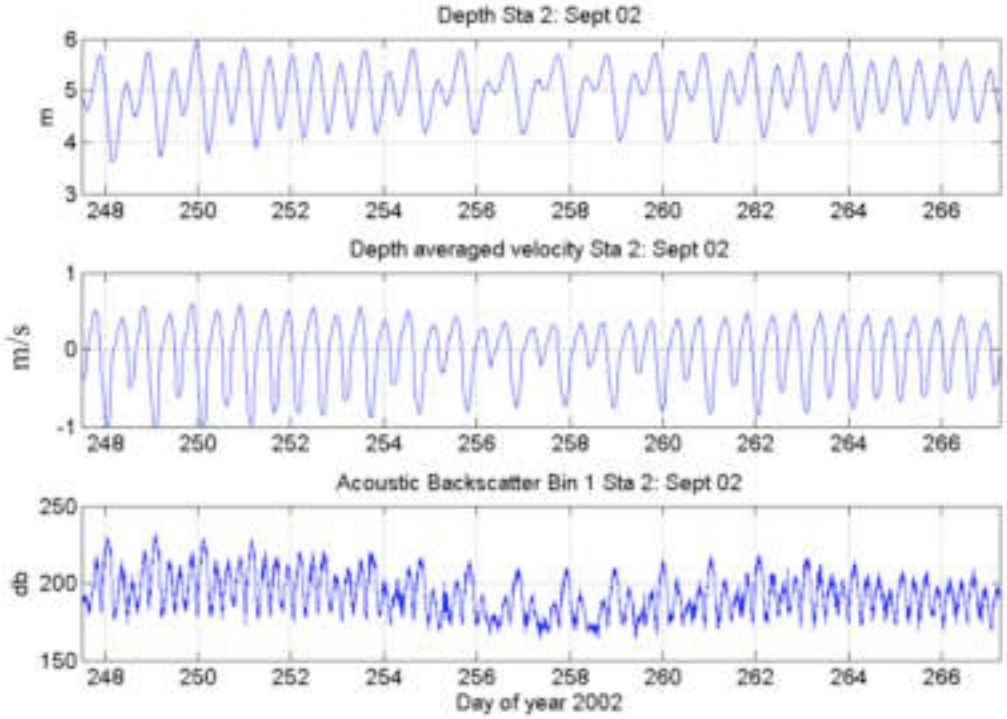

Figure 2.3 Water levels, currents and ADCP backscatter at Station 2, Sept 2002.

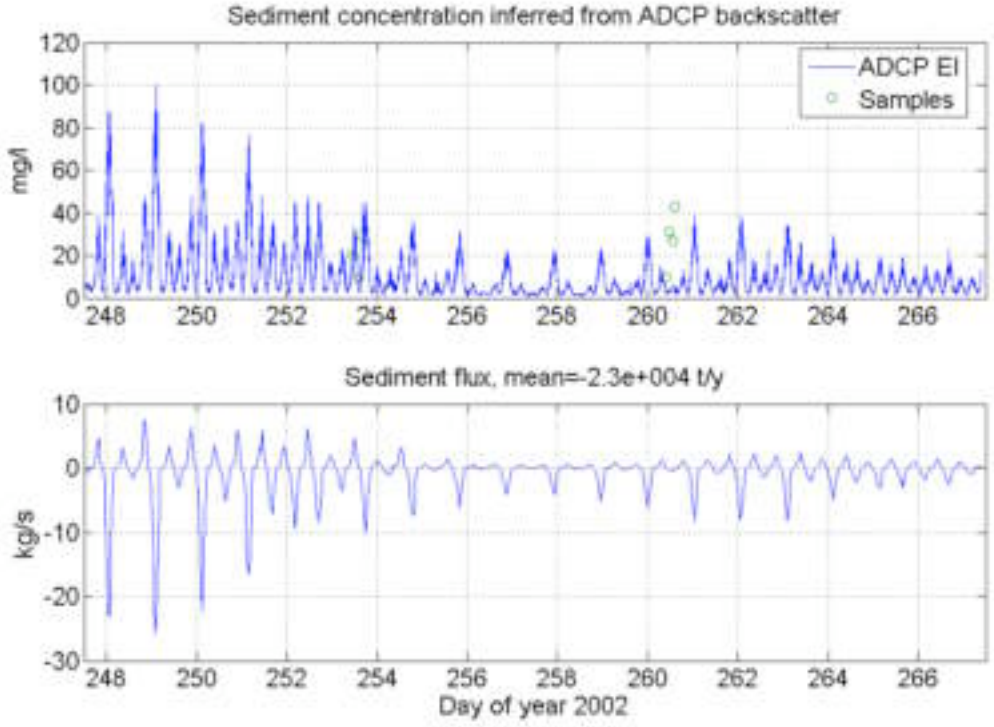

Figure 2.4: Inferred sediment concentration (based on ADCP backscatter) and sediment flux. The open circles show the results of a small set of water samples taken at Station 2.

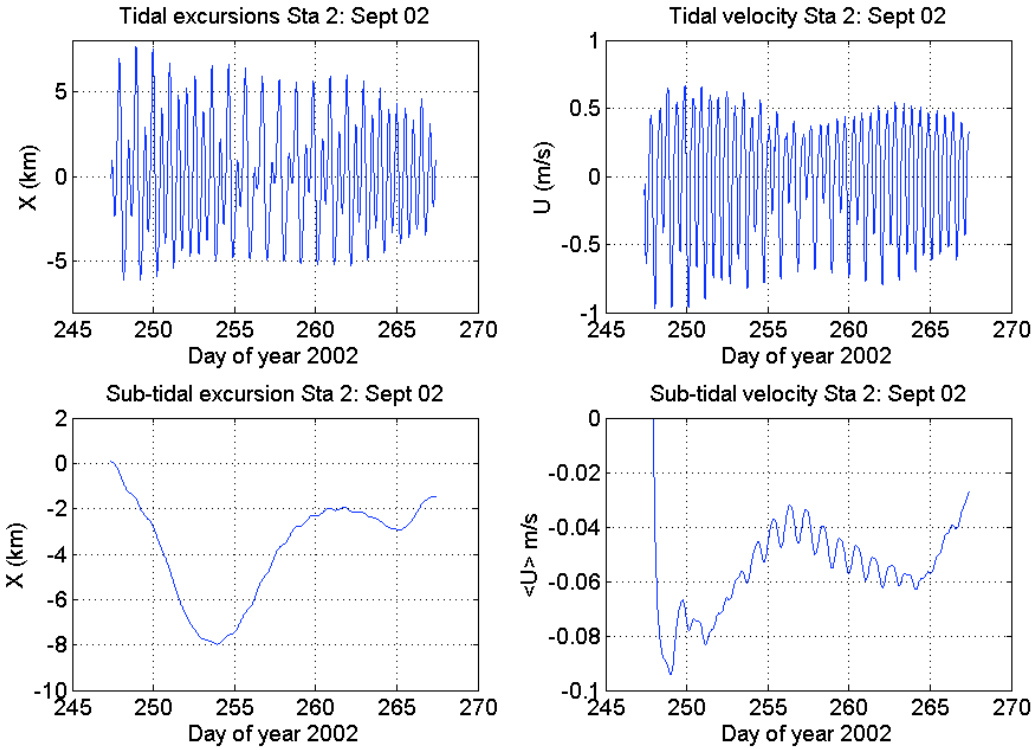

Figure 2.5: Tidal and subtidal excursions and velocities at Station 2 Sept 2002.

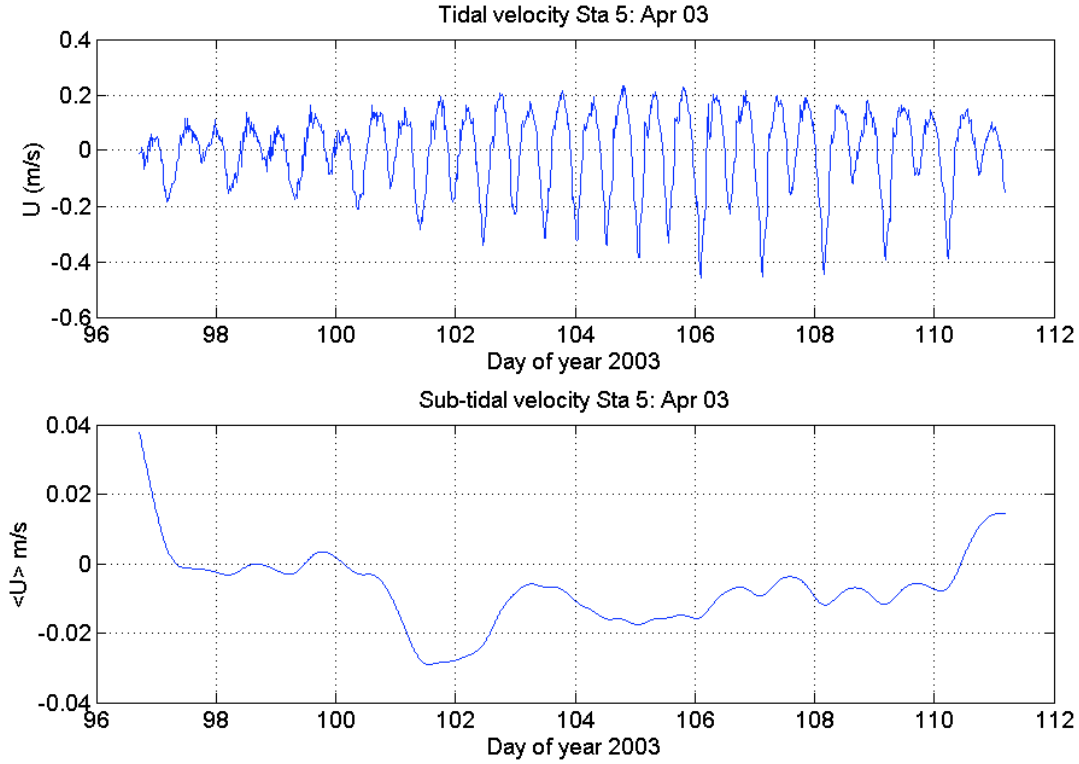

Figure 2.6 Tidal and subtidal velocities at Station 5 April 2003.

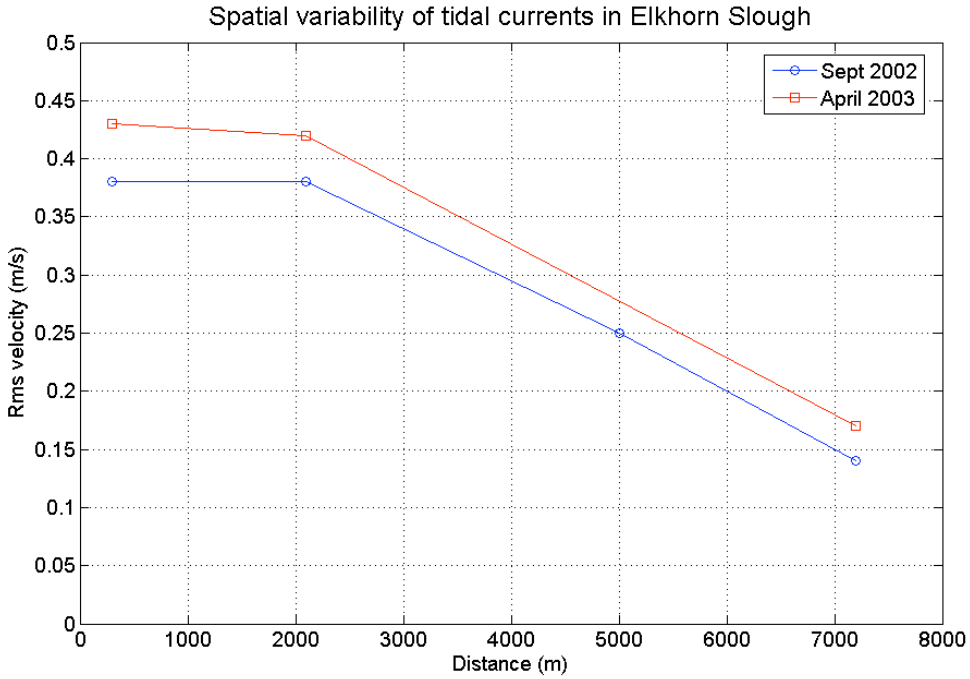

Figure 2.7 RMS depth averaged velocities in Elkhorn Slough Sept 2002 and April 2003.

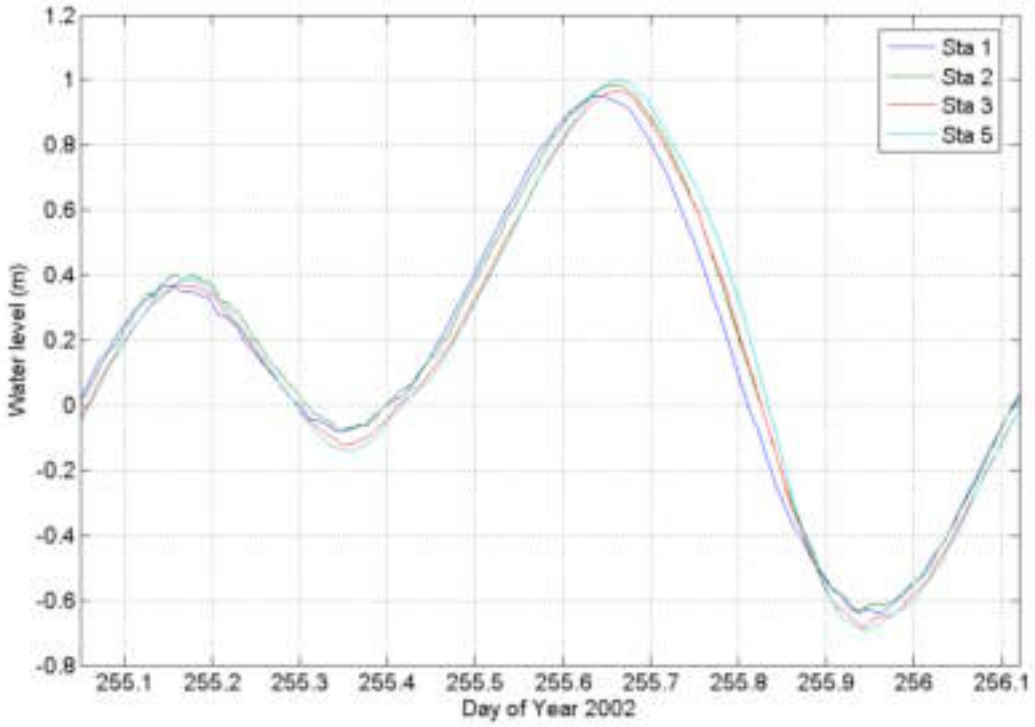

Figure 2.8 Water levels throughout one tidal cycle, Sept 2002.

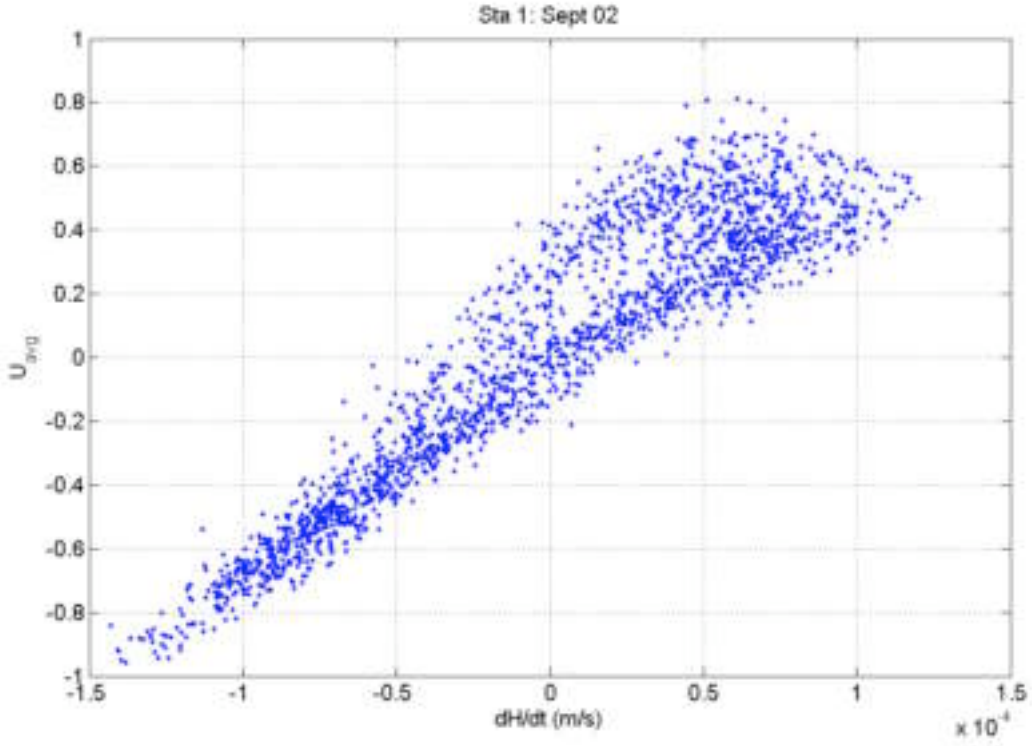

Figure 2.9 Depth averaged velocity as a function of dh/dt at Station 1, Sept 2002.

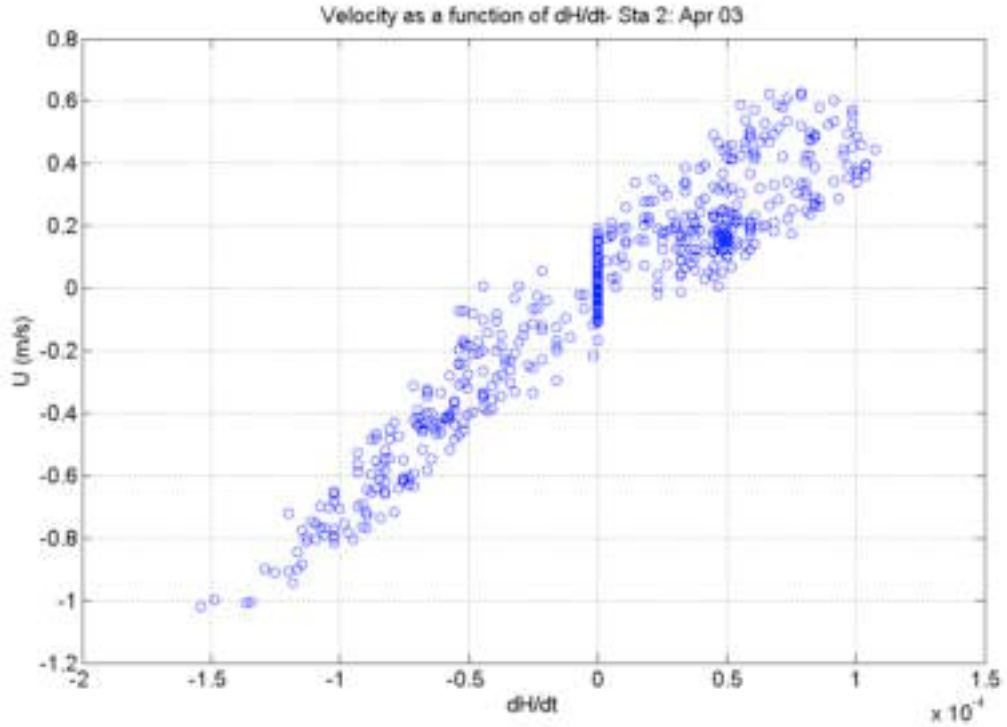

Figure 2.10 Depth averaged velocity as a function of dh/dt at Station 2, April 2003.

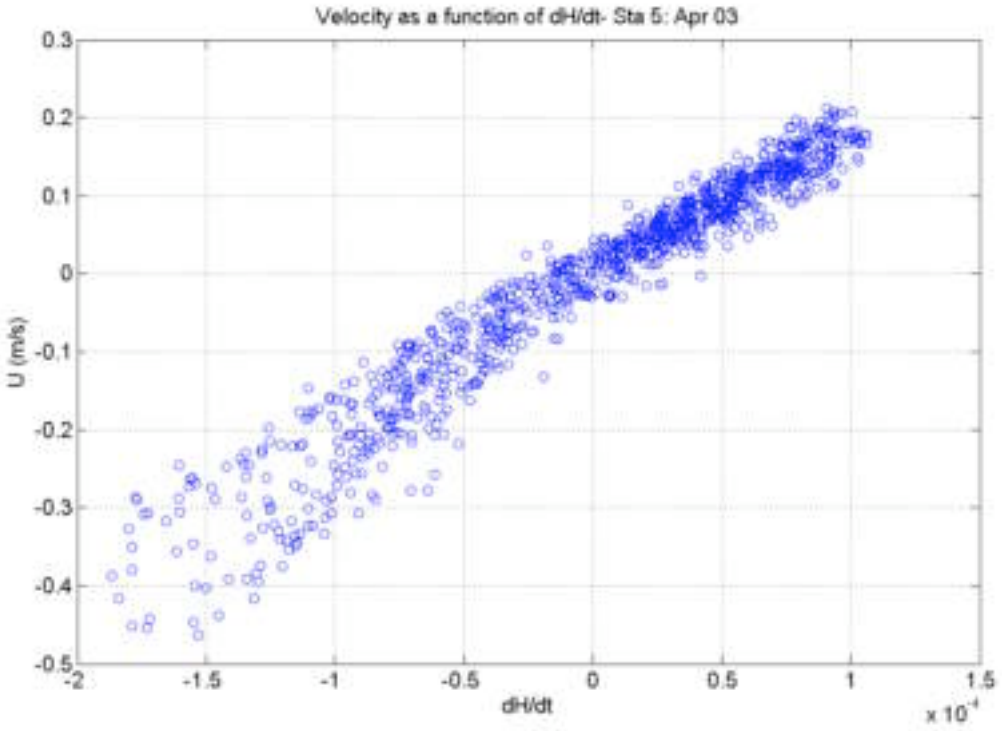

Figure 2.11 Depth averaged velocity as a function of dh/dt at Station 5, April 2003.

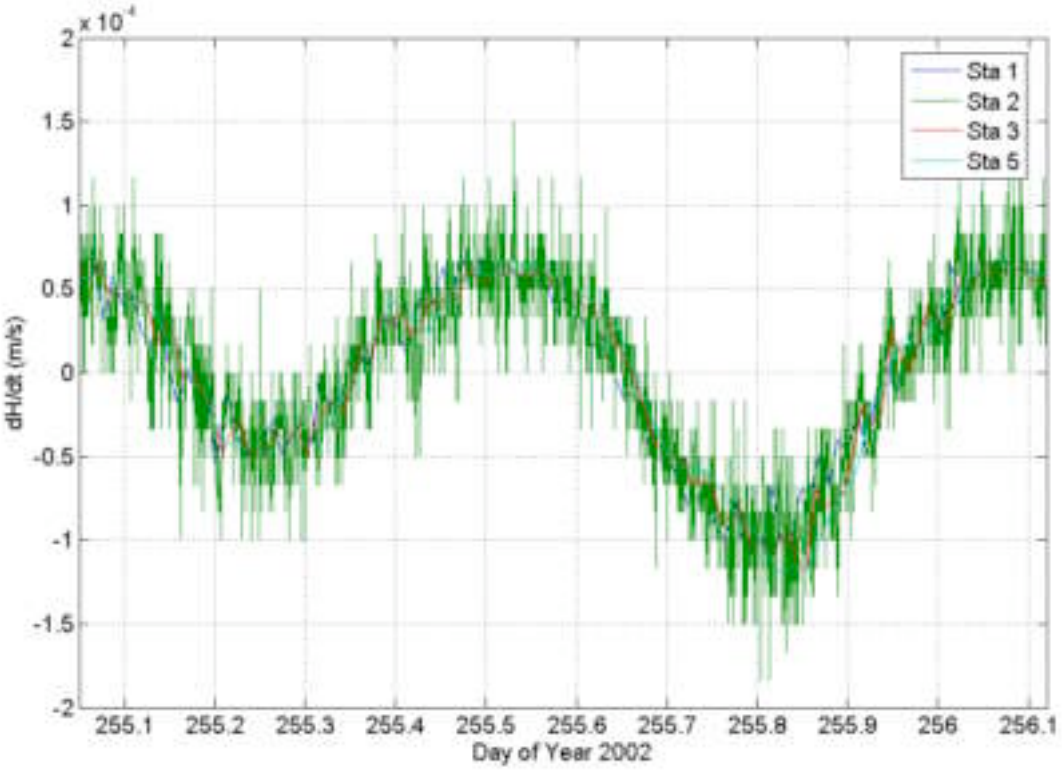

Figure 2.12 Tidal variation in dh/dt Sept 2002.

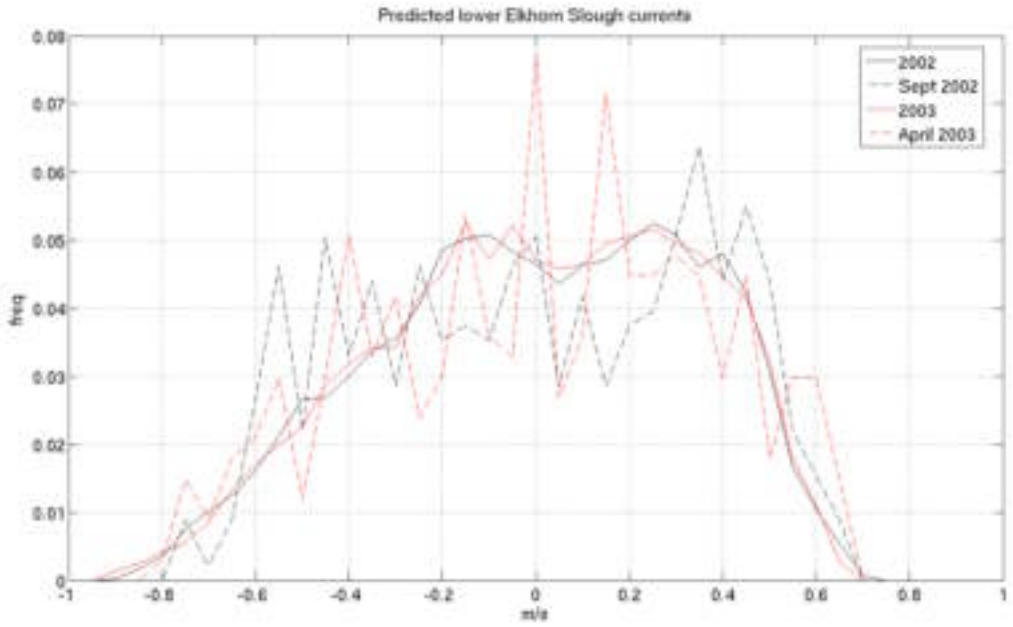

Figure 2.13 A comparison of the frequency of currents of different strengths observed in the two field experiments and inferred for 2002 and 2003 from predicted sea-level variations.

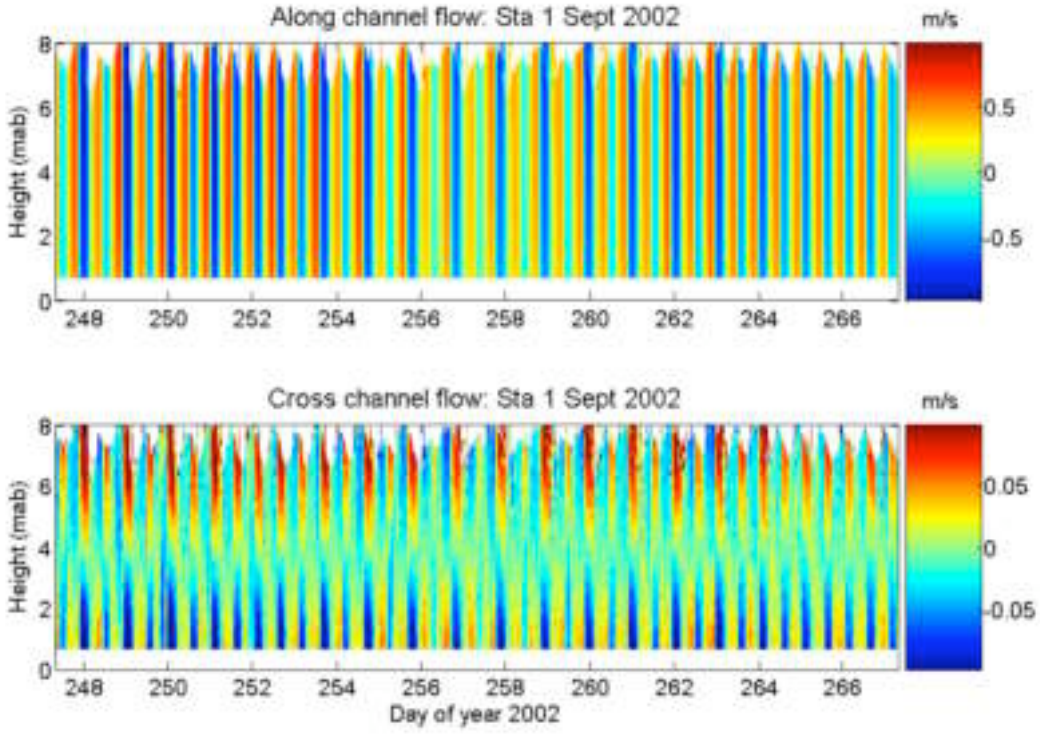

Figure 2.14 Vertical and temporal structure of along-channel and cross-channel flows at Station 1, Sept 2002.

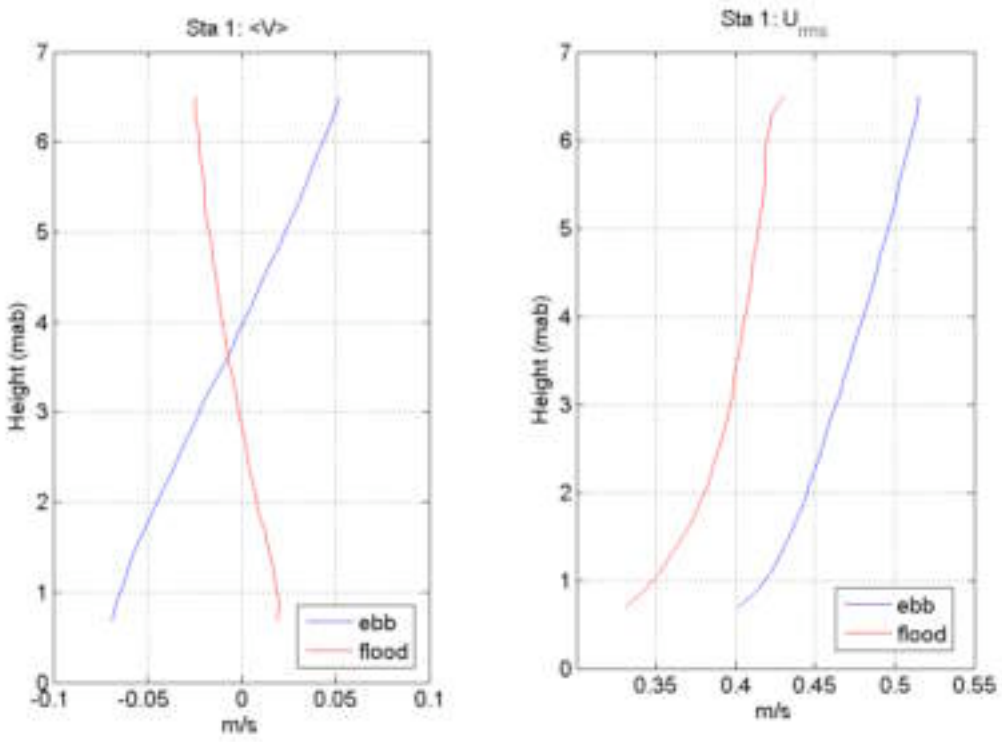

Figure 2.15 Vertical structure of averaged cross-channel and along-channel flows at Station 1, Sept 2002.

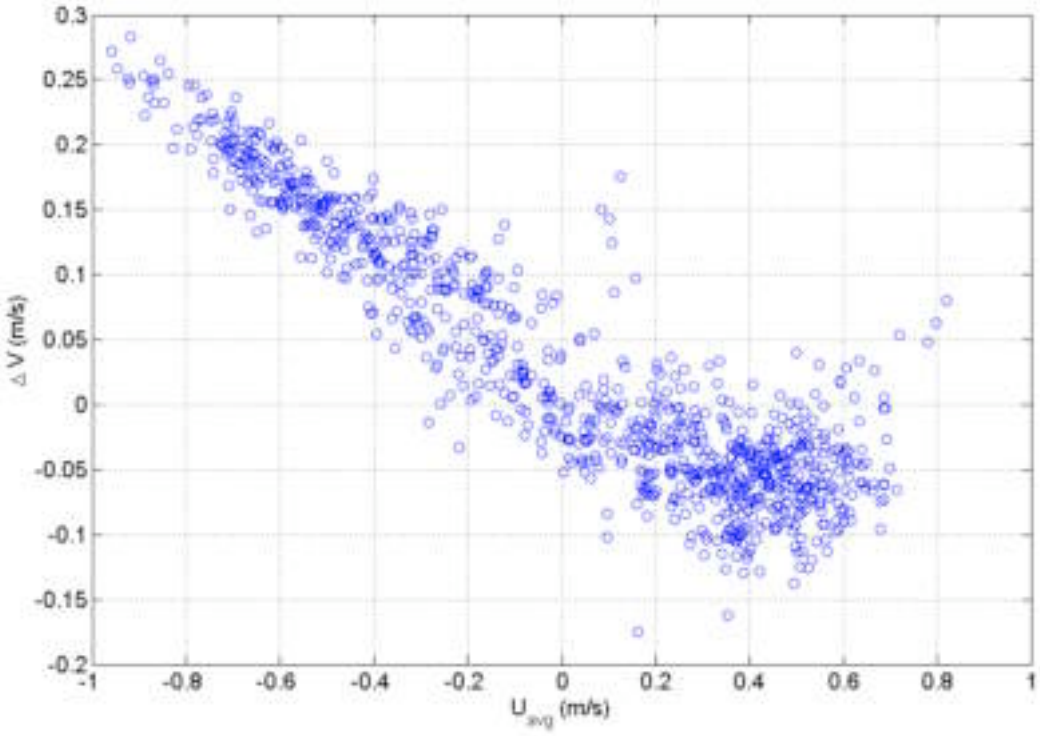

Figure 2.16 Cross-channel shear as a function of depth-averaged along-channel flow at Station 1, Sept 2002.

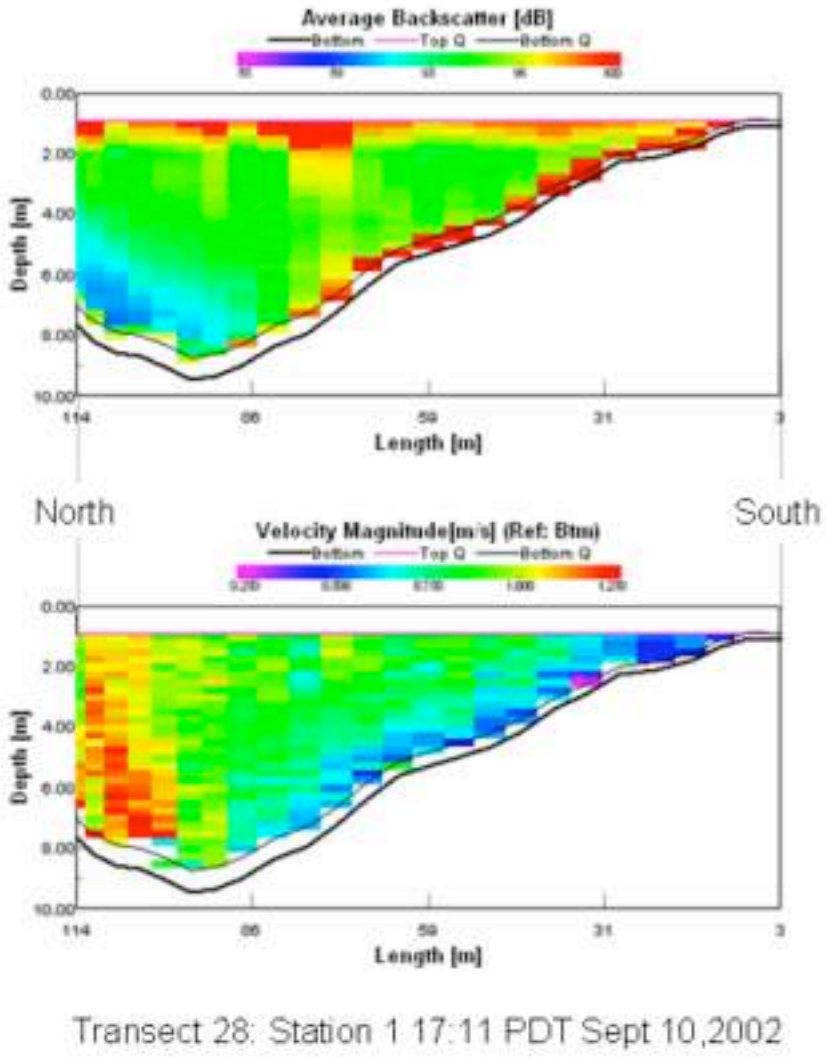

Figure 2.17 Transverse structure in the measured flow and acoustic backscatter intensity at Station 1, Sept 10, 2002

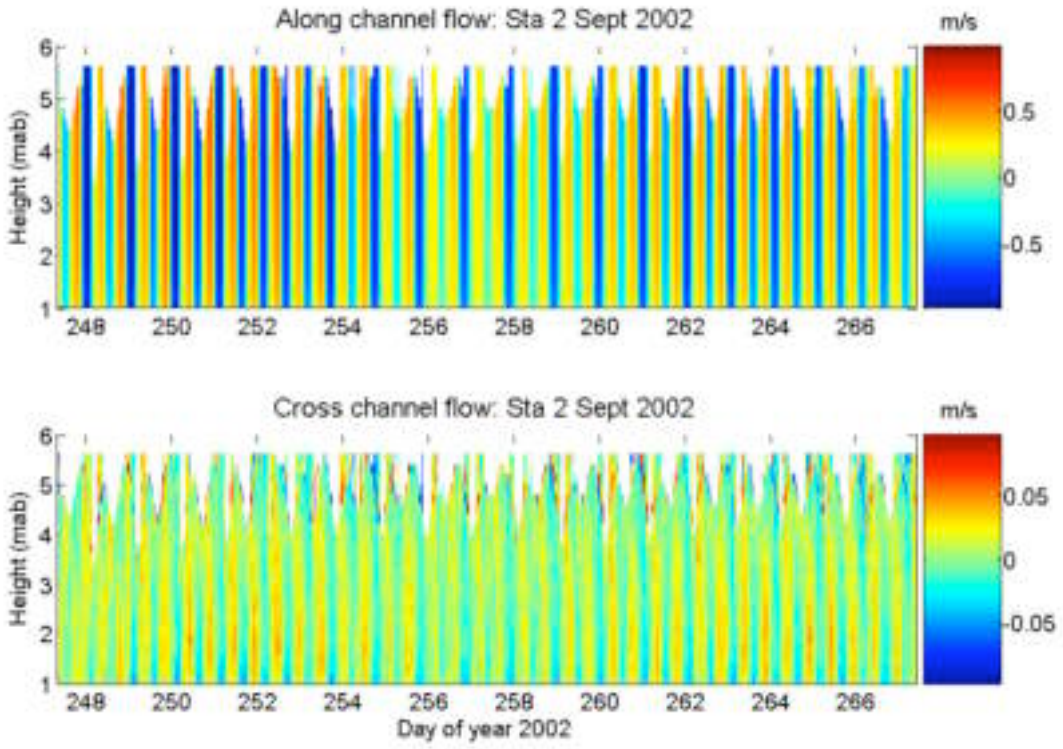

Figure 2.18 Vertical and temporal structure of along-channel and cross-channel flows at Station 2, Sept 2002.

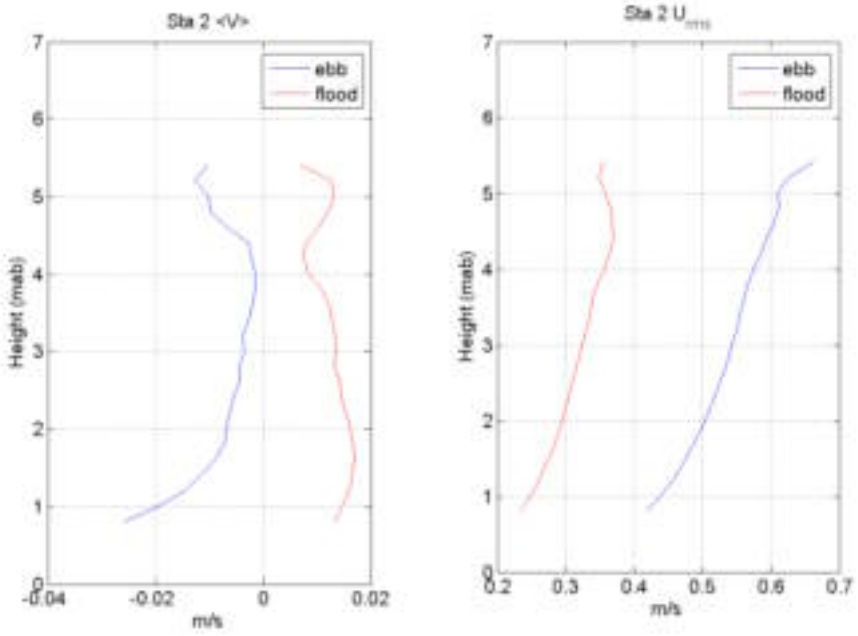

Figure 2.19 Vertical structure of averaged cross-channel and along-channel flows at Station 2, Sept 2002.

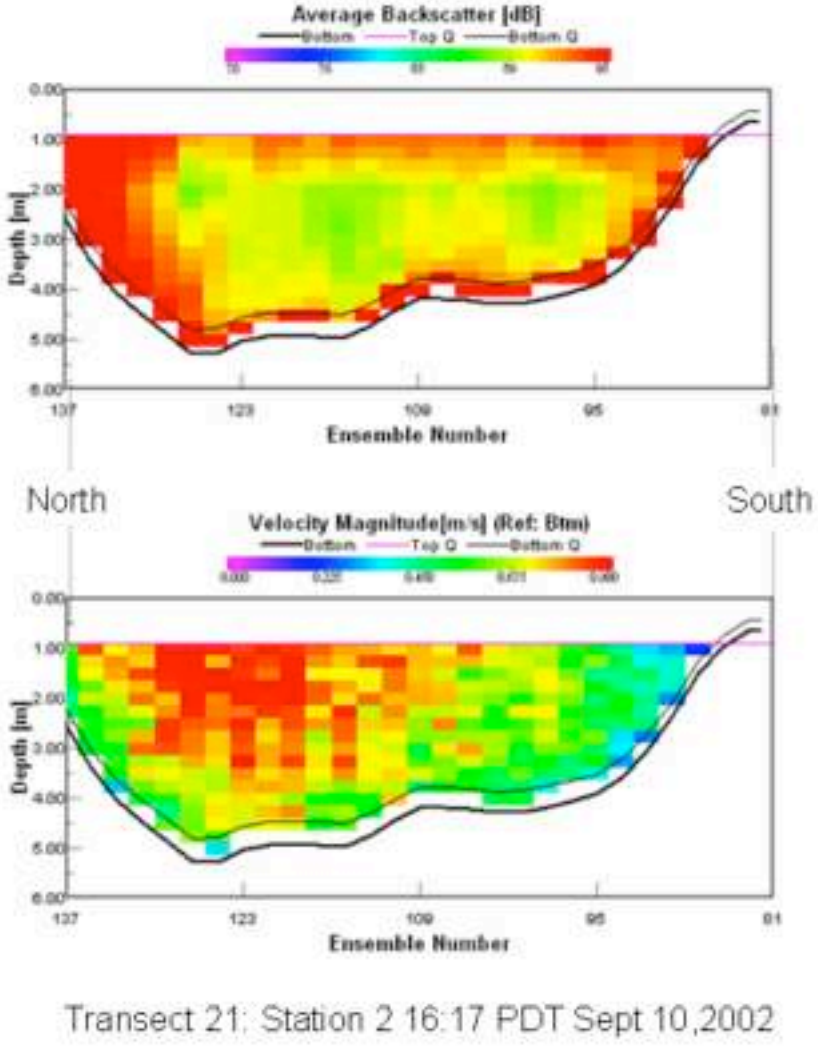

Figure 2.20 Transverse structure in the measured flow and acoustic backscatter intensity at Station 2, Sept 10, 2002

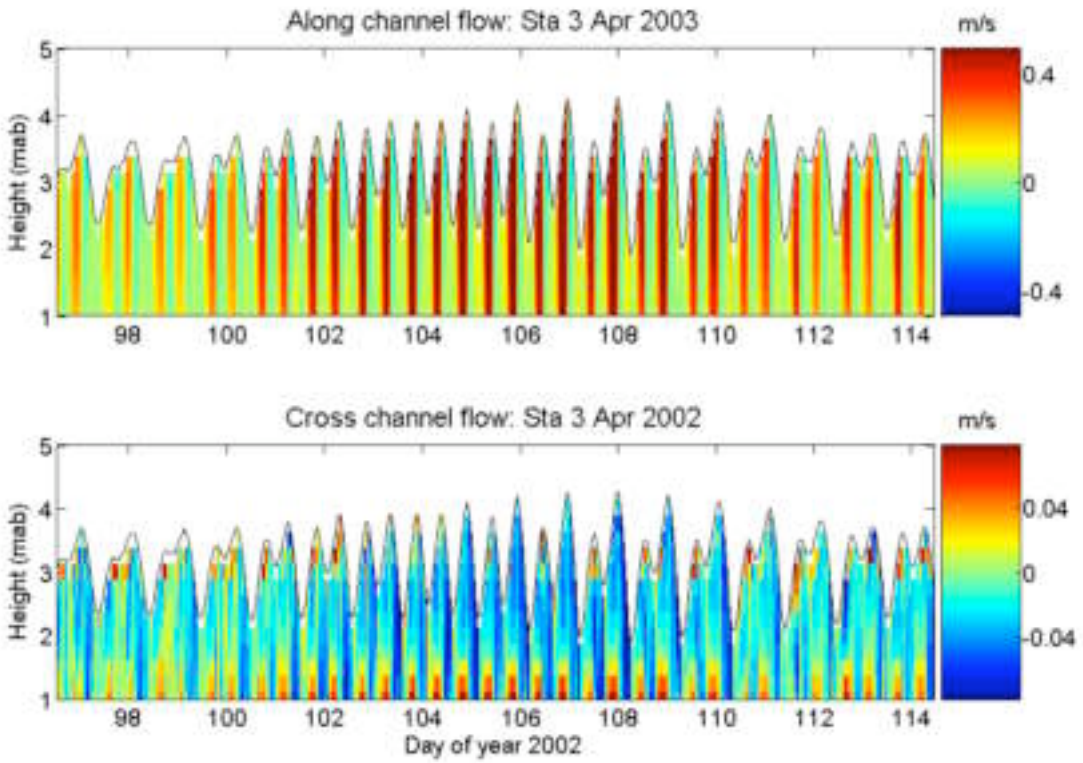

Figure 2.21 Vertical and temporal structure of along-channel and cross-channel flows at Station 3, April 2003.

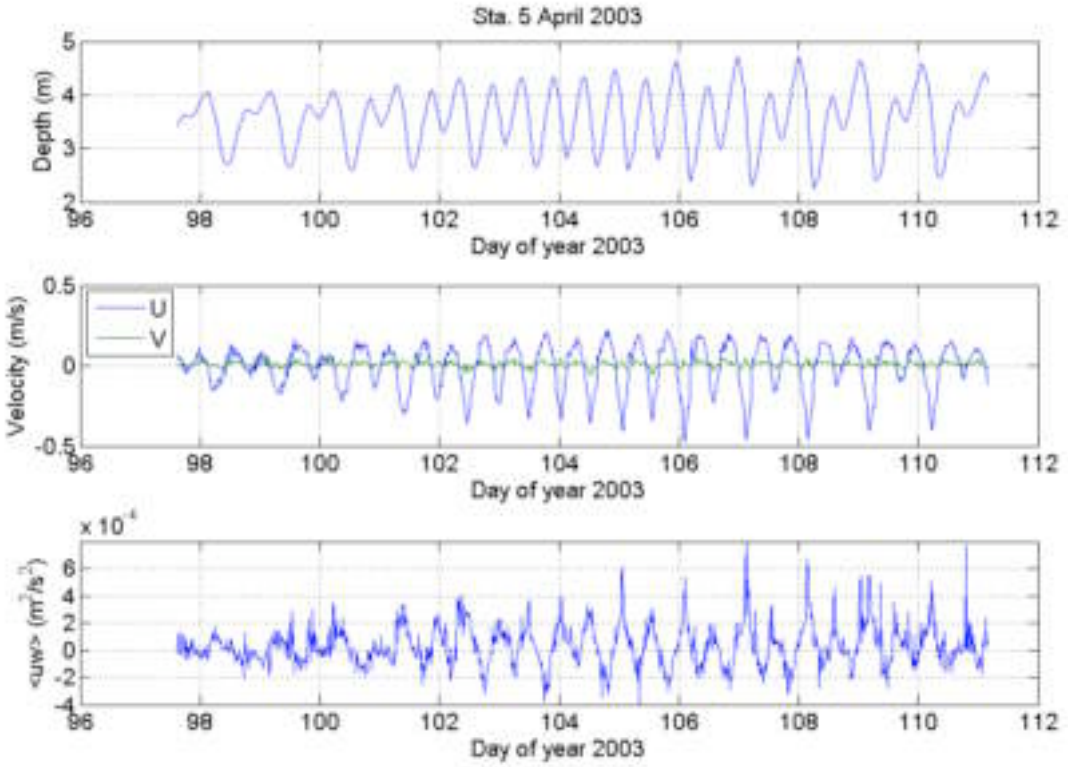

Figure 2.22 Time series of depth, along-channel and cross-channel velocities, and bottom stress at Station 5, April 2003.

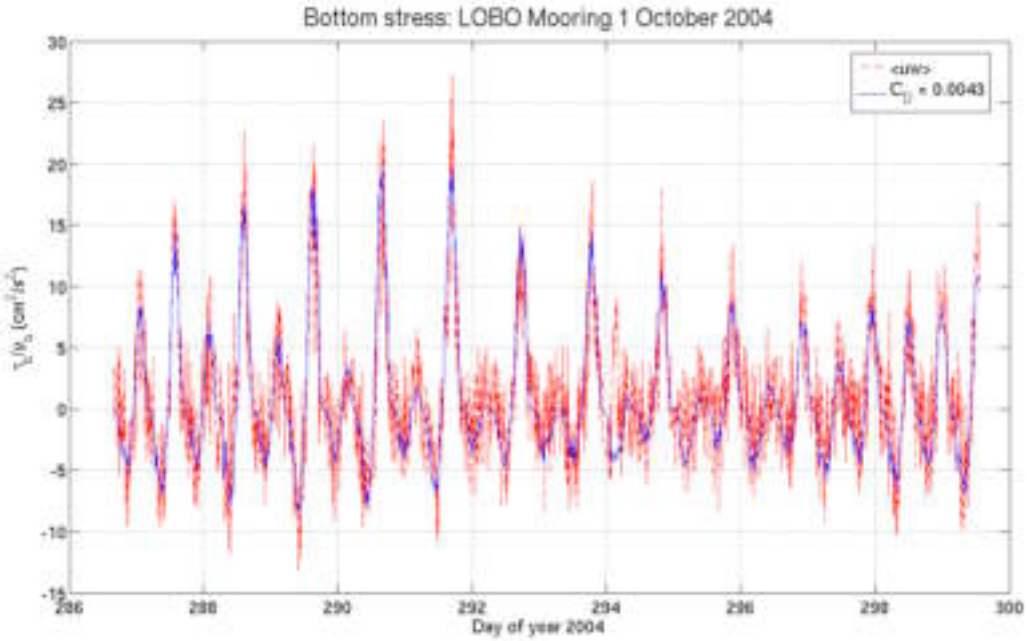

Figure 2.23 Time series of measured and computed bottom stress near LOBO mooring 1, October 2004.

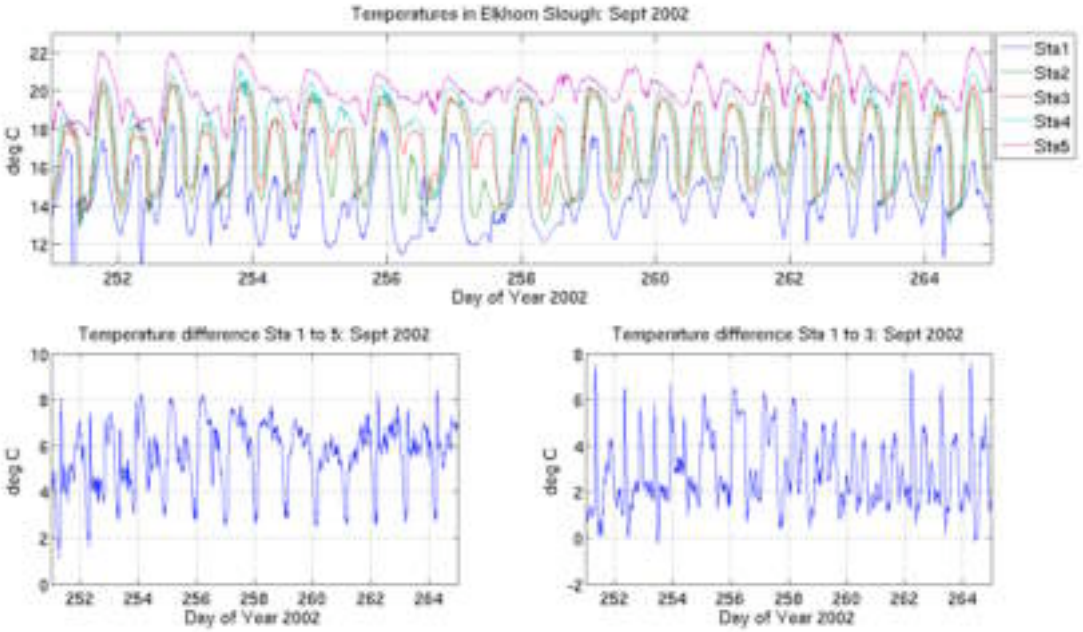

Figure 2.24 Temperatures and temperature differences in Elkhorn Slough, Sept 2002.

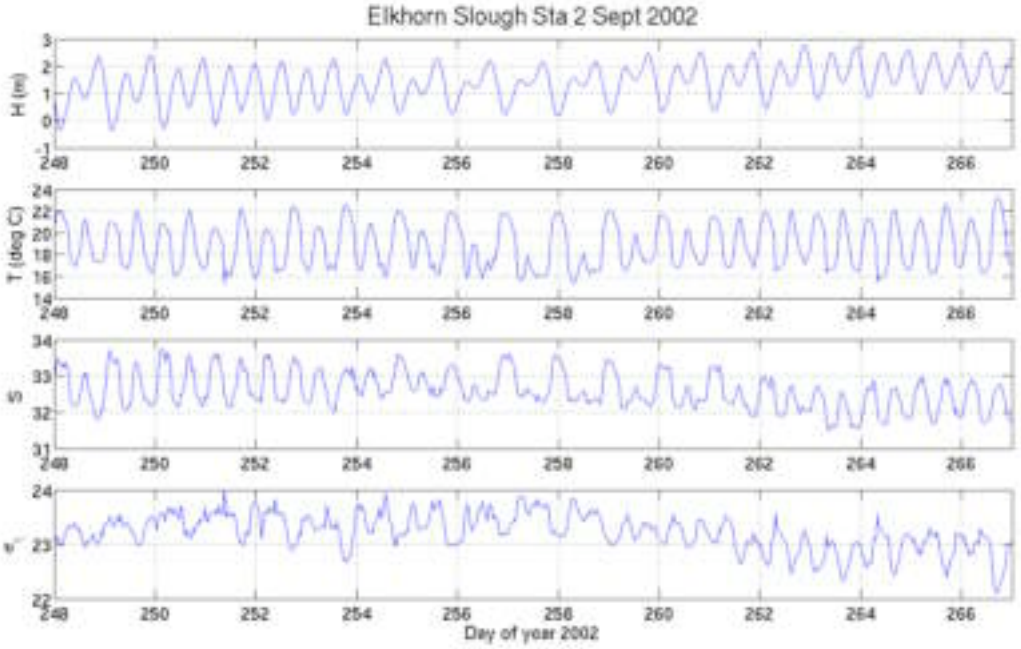

Figure 2.25 Time series of depth, temperature, salinity, and density (σ_t) measured at Station 2, Sept 2002.

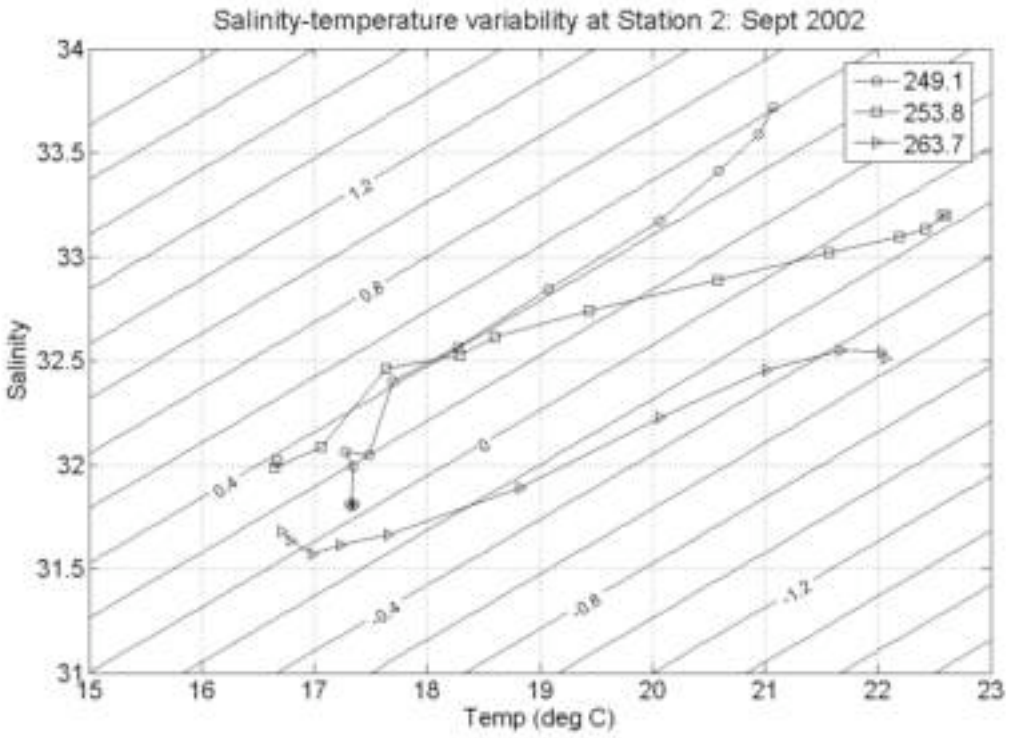

Figure 2.26 Salinity (S) –temperature (T) variations during single tidal cycles plotted as S as a function of T. The solid line reflect lines of constant density in units of σ_t , (1000*(ρ-1)), relative to the density at (S,T)=(31,15)

3. Numerical Modeling

3.1 TRIM3D

All of the numerical modeling carried out in this project made use of the 3D finite difference circulation code TRIM3D (Caulli and Cheng 1992, Casulli and Catani 1994, Gross et al 1999a,b). TRIM3D solves the three dimensional hydrostatic Navier-Stokes equation including the effects of variations in density, turbulent mixing and a free surface. Although the code itself is proprietary[9], the algorithms used in TRIM3D have been described extensively in the open literature. The heart of TRIM3D is a semi-implicit free-surface solver that permits relatively large time steps. Typically, free surface codes like TRIM must choose time steps, Δt, that are small enough to make the Courant number

$$Co = \frac{\sqrt{gh}\Delta t}{\Delta x} \leq 1 \tag{21}$$

remain stable (less than unity). Here Δx is the spacing of the points on the finite difference grid. For the 10 m grid we used to model Elkhorn Slough, this would imply

$$\Delta t \leq \frac{\Delta x}{\sqrt{gh}} = \frac{10}{\sqrt{80}} \approx 1\text{sec}$$

In contrast, in our computations we used Δt = 30 sec. However, there are limits to the size of the time step that are imposed by the process of wetting and drying cells in the intertidal region. TRIM3D is thought to be good for flows with extensive wetting and drying (Casulli and Catani 1994, Gross et al 1999b), as is the case with Elkhorn Slough, although we will return to this point below.

Another advantage of TRIM3D is that because the majority of the computational effort is associated with solving for the free surface, an aspect of the code that is relatively insensitive to the vertical resolution used, the vertical resolution can be improved for relatively little additional computational cost. The version of TRIM3D we use incorporates high-performance (low numerical diffusion) conservative advection schemes (Gross et al 1999a,b) as well as standard cohesive sediment algorithms (Mehta, 1989; discussed in Inagaki 2000)[10]. Turbulence is modeled using the Mellor-Yamada level 2.5 closure (Galperin et al 1988) used in many coastal and estuarine circulation models.

---

[9] As a consequence, our TRIM3D Elkhorn Slough model cannot be transmitted to any other parties without Prof. Casulli's permission.

[10] See discussion in §2.4

One "weakness" of TRIM3D is that the scheme it uses for advection of momentum, the Euler-Lagrange method (ELM - Casulli and Cheng 1992), is not conservative (Monsen 2000). Lack of conservation in the model is not generally problematic since real physical momentum is not conserved: momentum is lost from the flow due to bottom friction. We compensate for momentum loss due to the ELM by a suitable reduction of bottom drag, C_D. Following Cheng et al (1992) and Gross et al (1999b), bottom drag is parameterized in terms of z_0, with particular values of z_0 specified for different depth ranges, as opposed to for particular areas in the model.

3.2 Application of TRIM3D

To apply TRIM3D to Elkhorn Slough we used 3 sets of data: bathymetry, boundary condition data, and interior hydrodynamic data for calibration verification. The general procedure is to start by "gridding" the available bathymetry data, next acquiring the needed boundary condition data (tidal heights), and then running the model with varying depth-variable values of z_0 so as to produce model velocities and water surface elevations that best agree (in a least squares sense – see Blumberg et al 1999) with observations. Table 3.1 details the specific computer setup used in the modeling effort.

In the present case, we started with a 10 m resolution grid based on bathymetry obtained in the late 1990s from Moss Landing Marine Laboratories. In early 2004 we developed a new 10 meter grid based on bathymetric surveys of the main channel conducted by the Sea Floor Mapping Lab at CSUMB ca. 2002. The current model domain is plotted in figure 3.1. The area outside of the main channel region has been modeled as extended mudflats with an elevation of 0.3 meters. Our progress towards implementing an improved grid based on LIDAR measurements of the mudflats is described in the final section.

As described in section 2, we obtained field data to generate the boundary conditions for the model, i.e. water level at (near) the Highway 1 Bridge. For the sediment and other scalar calculations, the concentration need only be specified during floods. Given a lack of suitable data, we assume that all concentrations are zero (excepting salinity which we set equal to an ocean salinity of 33.5 PSU) at the Highway 1 Bridge during floods. This may be a reasonable approximation to reality if (as we suspect) the water that exits the Slough bypasses the Moss Landing harbor and enters directly into Monterey Bay. Nonetheless, our model approach essentially assumes that the entire tidal prism is replaced each tidal cycle; thus we may

underestimate residence times in the Slough as well as overestimate likely fluxes of materials, e.g. sediment, out of the Slough. Clearly, a preferred approach would be to extend the model grid into Monterey Bay and thus to explicitly model exchange between the Slough and the ocean.

3.3 Model results

In general, the modeled water surface elevations match observed ones quite well (Figure 3.2). However, this is not surprising given that the length of the slough is short compared to the wavelength of the diurnal and semi-diurnal tidal constituents, such that the water surface of the estuary moves up and down almost as a rigid lid in response to the forcing of the tides. Initially, we had some difficulty in getting model velocities to match field data both in phase and magnitude. However, with the improved bathymetry, we have improved the phasing of the velocities (Figure 3.3). The accuracy of the modeled velocities is important because sediment transport depends roughly on the cube of the velocity. If we are off by a factor of two in the velocities, the error in suspended sediment is likely to be incorrect by a factor of eight. It must be recognized that the problem of predicting sediment erosion is not limited to that of correctly computing the velocity: the parameters pertaining to the erodability of the sediment in Elkhorn Slough are uncertain, so inasmuch as we can resolve the velocities accurately uncertainty will remain in sediment deposition and erosion rates.

In the following sections, we will assess model results and performance in light of attempts at improving model fidelity by: (a) increasing model resolution; (b) incorporating the sediment model; and (c) synthesizing field and model data.

3.3.1 Model implementation

We have found that the current ten-meter horizontal resolution does an adequate job of resolving the main flow and sediment dynamics within the slough and that the computational costs associated with increasing the horizontal grid resolution are not warranted. Instead, we have focused on changes in the vertical resolution. One of the primary trade-offs in numerical modeling is between the cost of computation and the resolution of the model grid. The goal in modeling is to accurately represent the processes with a minimal amount of computation. Increasing resolution comes at the expense of more computation. As an example, if we improve the model's resolution from ten to five meters we would end up with four times as many grid

cells and would subsequently need to reduce the time step used in the model from 30 to 15 seconds in order to maintain the stability of the numerical method where wetting and drying occur. Thus, an eight-fold increase in computation occurs every time the resolution is halved. Currently the model runs two weeks worth of real-time computations in just over two days (Table 3.1) Eight times as many computations could result in a model that runs at near real-time, i.e., hardly a useful long-range forecasting tool.

We increased the vertical resolution of the model from two to seven layers. Initially we used a two-layer model that had an upper layer with an average thickness of one meter to cover the mudflats and a thicker second layer that encompassed only sub-tidal portions of the main channel. Velocities were only slightly affected by increasing the number of layers (Figure 3.4) but this change resulted in a roughly 50% increase in total suspended sediment load (Figure 3.5). The benefit of the higher vertical resolution is that is allows better tuning of the bottom roughness, which varies with depth in the model formulation we are using. This roughness element, z_o, factors into the drag coefficient (see (19)) and thus affects both velocities and sediment transport via shear stress at the bed. The two-layer model does not have the fine-tuning ability of a model with more vertical cells because the depth variations of the roughness element are averaged out. With the current bathymetry, variations in z_0 have only a minor effect on velocities while small changes to z_0 result in huge differences in sediment transport. (Figure 3.3) A run with $z_0 = 0.0025$ m set at a constant depth resulted in increased sediment erosion, though with a pattern that was nowhere close to those of field measurements. By contrast, variations in depth of z_0 (0.001 m in the shallows and 0.00002 m in the channels) resulted in a pattern of erosion and deposition that resembles actual observations (see below).

The cost associated with increasing the vertical resolution is not prohibitive, either, because additional vertical cells often are either out of the model domain (in the mud) or are dry part of the time (high mudflats) and thus do not significantly increase the computational costs. In addition, the majority of computational cost is associated with solving for the free-surface elevation. Given that the sediment yields differ so vastly between the two- and seven-layer runs while only increasing runtime by 40% we believe that it is well worth the additional computational time to more accurately resolve the vertical.

We have tried model runs with more than seven layers but have run into the problem of numerical instabilities overwhelming the solution. (Figure 3.6) The model has a difficult time

dealing with large velocities in cells that border dry cells. There is a limit, imposed by the Courant number described above, to the maximum velocity entering into a dry cell. As seen in Figure 3.4, once this condition is exceeded the model produces errors (i.e. dividing by zero) and this error quickly overwhelms the whole domain. The instabilities in the velocity fields of the two- and seven-layer runs (the wide peaks in the 2-layer U velocity) seen in figure 3.4 are generated in the same region but the thickness of the cells is just enough to keep the solution stable. The 7-layer solution appears to do a better job of damping out the instabilities, further supporting its use.

3.3.2 Field/model synthesis

The end goal of improving bathymetry and tuning vertical roughness elements is to represent the real velocities and sediment transport patterns that we see in the slough today. Qualitatively, the model appears to do reasonably well with regard to direction of flow. (Figure 3.7a,b) The magnitudes of the model results are clearly not as large as in the field measurements. The effect of the instabilities can be seen in the flood direction of the modeled station 1 (red in Figure 3.7b).

We can quantify the model's performance numerically by comparing harmonic analyses of the velocity data produced by the model to those of the field data. For simplicity we have chosen only to compare the dominant frequency, the M2 tide, and its first overtide, the M4. Table 3.2 contains the results of this analysis for model and field along-channel velocities. In the field data, the amplitude of the M2 frequency remains relatively un-muted through Seal Bend and towards station 2, but is much weaker farther up-slough at Seal Bend. By contrast, the model reduces the amplitude of the M2 tide quickly, producing a slight phase shift towards the upper end of the slough. In addition, all of the velocities in the model have a different phase than the field measurements. The combination of muted amplitude and lagged phase suggests that the model is too diffusive and that the bottom friction needs to be reduced further.

As an application of the model results, we can look at the flow structure around Seal Bend, a task that is difficult to do with great detail in real time. The model does a good job of representing the areas of higher velocity around Seal Bend and this will continue to improve with better bathymetry. In Figure 3.8, shortly after high slack water, higher velocities (represented by black vector arrows) are seen on the outside of the eastern portion of the bend. This faster water

then shoots inside the 180 degree turn and increases velocities towards the western edge of that turn. The water is then diverted to the southern side of the westernmost bend. This flow pattern is exactly what we have observed in the course of transects through the region. (Figure 3.9) The accuracy to which this is modeled will improve dramatically with better bathymetry, particularly given the fact that there shouldn't be any flow *over* Seal Bend. The elevation of the southern side of the model is much too low in the present bathymetry. A new bathymetry set fixes this and we are already seeing better results in the trial runs of the model, as discussed in the final section.

3.3.3 Sediment erosion

The patterns of erosion and deposition predicted by the model are generally in good agreement with the long-term observations of erosion in the slough, despite the crude bathymetry. A comparison of model results (Figure 3.10a) to changes reported between 1993 and 2001 by Wasson et al (2002) (Figure 3.10b) shows several areas where erosion in the model closely matches the field measurements. There are some areas where the model incorrectly predicts a net gain where erosion actually occurred. The most notable discrepancy is on the eastern portion of Seal Bend and is due to a combination of factors. In the first place, the lack of accurate bathymetry across Seal Bend allows water to flow across the bend, rather than through it, reducing peak velocities. Also, the model's erodability and critical shear stress parameters are constant throughout the slough while the actual slough bed is extremely variable with some areas covered in shell hash and others in fine muds. Finally, erosion processes involving the marsh edge are not represented by the present model; it is likely that some of the these dynamics, such as the mass wasting of steep banks, might not be captured in a sediment model as simple as this.

An example of the instantaneous spatial variability of the sediment field can be seen in Figure 3.8, with the color scale represent suspended sediment concentrations ranging from zero (blue) to 0.05 kg/m^3 (red). At the start of the ebb tide, a high concentration of suspended sediment is located east of Seal Bend (Figure 3.8a). During the course of the ebb tide, that mass is advected around the turn, as seen in Figure 3.8b, and the concentration on the western side of Seal Bend increases. Some loss of sediment occurs through Seal Bend, as noted on the inside of the eastern portion of the bend. Some of this loss is due to the effects of the false bathymetry, but it also natural for sediment to build up on the inner portion of the turn, where velocities are

weaker. We lack a good long-term record of instantaneous suspended sediment concentrations at locations throughout the slough, however, for validating some of these dynamics.

Even though we have no direct field comparisons for the suspended sediment concentrations, model results from station 2 east of Seal Bend (Figure 3.11) are qualitatively similar to what we inferred from ADCP backscatter and to what Malzone and Kvitek (1999) report. The pattern of ebb-dominance is quite clear in these results as the large peaks in suspended sediment concentration occur on the ebb tide while the smaller peaks coincide with the flood tide. The model currently does not have any way to retain sediment that is flushed out of the slough mouth during ebb tide and, as a result, all water entering on the flood tide has zero suspended sediment concentration. While this might not be entirely accurate, it is nevertheless reasonable to assume that dynamics away form the immediate vicinity of the Highway 1 bridge are well represented. Because the head of the Monterey Canyon is immediately outside the slough mouth, it is likely that the majority of sediment flushed during ebb tide is lost to the canyon and that the flood tide is reasonably clear water. Our personal observations from fieldwork in the slough support this hypothesis as we regularly see clear, cold ocean water flush into the slough in a sharp front at the start of the flood tide. These observations suggest that having no sediment input from Monterey Bay is thus not a problem for the model.

To confirm this behavior, we constructed a zero-dimensional version of the sediment model using the same erosion and deposition models as used in the 3D calculation. Such a model takes the form

$$\frac{\partial C_s}{\partial t} = -U\overline{\frac{\partial C_s}{\partial x}} + \frac{1}{h}\left(\dot{M}_E - \dot{M}_D\right) \tag{22}$$

where the mass fluxes due to erosion and deposition $\dot{M}_E$ and $\dot{M}_D$ have been given in §2.4, and the effects of sediment transport are represented by the advection in the presence of a sediment concentration gradient $\overline{\frac{\partial C_s}{\partial x}}$. Since the simple model does not solve for $\overline{\frac{\partial C_s}{\partial x}}$, this parameter must be specified *a priori*. Based on the discussion above, when the flow is ebbing, we assume that $\overline{\frac{\partial C_s}{\partial x}} \approx 0$, whereas when the flow is flooding we assume that the water entering the Slough from Moss Landing Harbor (and Monterey Bay) has zero sediment, giving an approximate sediment concentration gradient

$$\overline{\frac{\partial C_s}{\partial x}} = \frac{C_s}{\Delta x} = \frac{C_s}{3000\,m}$$

The resulting "asymmetrical advection" model does a good job at reproducing temporal variations in sediment concentration seen in the field and in the 3D model. The resulting sediment flux (3 x 10^4 t/y) is similar to what we have inferred from the ADCP backscatter data.

3.4 Modeling residence time

A central aspect of understanding many biogechemical processes in estuarine systems like Elkhorn Slough is the amount of time that materials spend in the system before being transported out into the ocean. This transport is generally accomplished by the tidal flows that transport materials back and forth inside Elkhorn Slough, thus acting to reduce longitudinal gradients, i.e. to disperse materials.

Often the dispersive effects of the tidally varying flow are averaged in time and across the cross-section to produce a diffusion (dispersion) equation that takes the form (Fischer et al 1979)

$$A_c(x)\frac{\partial C}{\partial t} + \frac{\partial}{\partial x}(QC) = \frac{\partial}{\partial x}\left(K_x A_c \frac{\partial C}{\partial x}\right) + \text{sources} - \text{sinks} \qquad (23)$$

where Q is the cross-sectionally averaged flow (negative if there is flow out to the ocean) and K_x is the dispersion coefficient. As discussed in Fischer et al, K_x, is the result of a variety of physical processes (shear, gravitational circulation, etc. - see Dronkers and Zimmerman 1982, Zimmerman 1986); for Elkhorn Slough it is likely that the most important of these is lateral shear in the tidal currents.

An example of how this works can be seen in Figure 3.12, where we have plotted the concentration field computed using the 2-layer model. In this model run, the Slough was initially filled with fresh water and then gradually got saltier due to the inflow of salty water on flood tides. In this case salt serves only as tracer; the density was held constant in this model run. The salinity field is shown at 48h (mid flood) and at 68 hours (end of ebb) after first making the estuary "fresh". The clear tendril of saltier fluid can be seen in the center of the channel in both cases is the result of faster upstream and downstream transport where the velocities are higher. However, at the same time, turbulent mixing and secondary flows work to mix out the resulting cross-sectional concentration gradients, leading to net upstream transport of salt.

For tidal systems like Elkhorn Slough, Fischer et al (1979) show that

$$K_x \simeq 0.02\overline{U^2}T\left[\frac{T_c}{T} f\left(\frac{T}{T_c}\right)\right] \tag{24}$$

where T is the tidal period, $T_c = 0.4W^2/hu_*$ is the cross-sectionally mixing time, and the expression in square brackets (plotted in chapter 7 of Fischer et al) is a function of T/T_c that reflects the fact that when cross-sectionally mixing is slow compared to tidal variations, there is little net dispersion. For Elkhorn Slough we can estimate (downstream of Parson's Slough):

$$W = 120\,m\; u_* = 0.03\,m/s\; d = 3m \Rightarrow T_c = 4\times10^4 s$$
$$T = 12.42\,h = 4\times10^4 s \Rightarrow T/T_c \approx 1 \Rightarrow F \approx 0.5$$
$$\overline{U^2} \approx 0.5\,m^2s^{-2} \Rightarrow K_x \approx 0.02\times0.5\times\left(4\times10^4\right)\times0.5 = \underline{200\,m^2s^{-1}}$$

We will use this value of K_x in the context of computing groundwater fluxes in chapter 4. However, we can compute a first-order estimate of the time required to mix out concentration gradients in the Slough using this value of K_x from the relation

$$T_{mix} \sim \frac{L^2}{K_x} \sim \frac{8000^2}{100} = 6\times10^5\, s \approx 7\, days \tag{25}$$

Here we have assumed that an appropriate value of K_x is one half the value computed above for the lower Slough, and that L is the length of the Slough.

An alternative approach to the use of the diffusion equation is that of box models, for which mixing is represented by a quantity known as the "Residence Time". While many definitions of residence time are possible (see, e.g. Monsen et al 2002), the simplest definition is based on the first-order exchange process:

$$V\frac{dC}{dt} = -Q_{ex}C$$
$$\frac{dC}{dt} = -\frac{Q_{ex}}{V}C = -\frac{C}{T_R} \tag{26}$$

where V is the volume of the system, Q_{ex} is the effects of exchange (as represented by a pseudo flowrate), and T_R is the residence time. Note that in this model, if we start with concentration C_0 at $t = 0$, when $t = T_R$ the concentration is reduced to $e^{-1}\, C_0$.

Using the numerical model, we can carry out a series of experiments in which we place different tracers in different parts of the Slough (Figure 3.13) and then as the flow evolves keep track of their mass both in the region they were initially placed and in the Slough as whole (Figure 3.14a-e). As with the sediment modeling, the artificial element of this approach is that

we must assume that none of the material that exists the Slough at the Highway 1 Bridge returns on the following flood.

The results of these calculations (Figure 3.14a-e) show clearly the fact that residence time is very short in the lower portion of the Slough, i.e. $T_R < 1$ day, and thus that it also depends on what phase of the tide the tracer release is carried out. In contrast, upstream of Parson's Slough the residence time increases dramatically such that for the region near Kirby Park (tracer 9), little of the initial mass has left Elkhorn Slough after 2 weeks, i.e $T_R > 2$ weeks. Thus, while we may assume 1 well-mixed box in the calculation of groundwater fluxes given in Chapter 4, it is important to keep in mind the substantial variation along the Slough in residence time seen in the model results; i.e. the Slough is not really a single well-mixed box as we shall, for simplicity sake, assume.

3.5 Modeling: Ongoing and future efforts

With support from NSF through LOBO, at the time this report was prepared, we continue to work towards improving the model results. Our main focus is to fix the overdamping of velocity field in the upper reaches of the slough. Our second goal, one which will require more field data for calibration and testing, is to better model sediment transport patterns. This work will be centered on improvements to bathymetry and bottom roughness. It is easy to change the bottom roughness on an estuary-wide scale, but implementing specific bottom roughness and erodability parameters on a point-by-point basis will be much more time consuming.

We will soon be able to take a big step towards capturing some of the mudflat and larger tidal-channel circulations in the existing model. At the end of 2004, we obtained a new bathymetry database from the Sea Floor Mapping Lab, one that includes LIDAR data that describes the shallow mudflat and salt marsh regions. The new bathymetry has terrestrial (mudflat) LIDAR data acquired via aircraft merged with recent shipboard bathymetric surveys taken at high tide. As part of LOBO, we are currently working to implement an improved grid based on this bathymetry. (Figure 3.10) This transition is not smooth, however. To date, we have converted the one-meter raw data into the ten-meter format required for the model, initialized the boundary conditions for that grid, and are able to produce flow in the domain. (Figure 3.11) We are encountering difficulties with numerical instabilities in the domain, however. Once we have attained a stable flow or, more likely, in order to get a stable flow, we will have to modify areas of the grid on a point-by-point basis to ensure that the modeled domain represents the actual

morphology found there. As an example, the entrance to Parson's Slough will need to be modified to ensure that the number of cells representing the bridge underpass is appropriate. Finally, the LIDAR data measures the top of any vegetative structure. As a result, a good portion of the mudflat bathymetry is too high and this will need to be rectified in the long run.

Some of the defining features of Elkhorn Slough, namely the mudflats, have channels that are on the order of meters wide. The erosion of the smaller, tidal side channels is one of the more pressing issues with regard to habitat preservation within the slough. These features are impossible to accurately model in a grid with a ten-meter resolution. Aside from the computational costs that would come with resolving the slough at this detail on a Cartesian grid, data on erodability doesn't exist at this point to warrant including these details. Future work will focus on using a curvilinear unstructured grid. This will allow finer detail in areas of interest, such as the potential for erosion in mudflat tidal channels, while saving computational cost in areas such as the main channel where the scale of sediment and hydrodynamic variability is not as great. We also hope to include an existing model for Monterey Bay that could be coupled to the Elkhorn Slough model. This coupled modeling system will enable a more realistic long-range predictive capability as the fate of sediment exiting the slough on the ebb tide is of some uncertainty. Good bathymetry is crucial and it is expected that some of the difficulties we are having with improving the velocity amplitudes will be resolved with this new bathymetry set and that we will be able to calibrate the sediment transport with a reasonable degree of accuracy once better field data is available.

3.6 Summary

The current 10m grid/7 layer model does a good job of reproducing observed water levels, although, in light of the flat surface behavior, this is not a stringent test. Currents were reproduced with reasonable accuracy, although currents near Kirby Park were better predicted than were currents near the Highway 1 Bridge. This may reflect shortcomings in the bathymetry data, in particular, a general lack of data from the Parson's Slough drainage. Attempts at further improving the resolution has been stymied by instabilities of the wetting front (the water's edge during filling and emptying of the Slough), suggesting that the treatment of wetting and drying in TRIM3D may need improvement for application to systems like Elkhorn Slough. Besides problems with the bathymetry (e.g. missing data), the accuracy of current predictions may be

limited by the fixed resolution of the grid relative to the size of smaller channels and features in the slough, which may not be well represented by the 10m grid.

The sediment model shows clearly that the Slough is erosional. When run with the same parameters used previously for South San Francisco Bay, most of the Slough showed net erosion although there were also significant regions of deposition. In contrast, observations of changes in Slough bathymetry show only erosion. This highlights the need to obtain specific measurements of the needed sediment parameters, including some limited assessment of their spatial variability.

Computation of residence time by computing the transport of tracers that initially mark selected regions of the Slough show that downstream of Parson Slough, the residence time is quite short, possibly less than 1 day, depending on when in the spring-neap cycle and even at what phase of the tide the tracer is introduced. In contrast, upstream of Kirby Park, the residence time was appeared to be greater than the length of time the calculation was run (ca. 14 days).

Table 3.1 – Model specifications. Range in speed-up is based on number of output files generated.

Computer/Processor/RAM	Dell Precision 530 i686/Dual Intel Xeon/2 GB
Operating System	Linux FedoraCore 2.6
Compiler	Intel Fortran Compiler for Linux v8.0
Real time speed-up (30 sec time step, 2 layers)	6.5-7.4
Real time speed-up (30 sec time step, 7 layers)	5.0-5.4

Table 3.2– Computed tidal harmonics for field and model results at stations 1,2 & 5.

	M2 Tide - Field		M2 Tide - Model		M4 Tide - Field		M4 Tide - Model	
	Amplitude (m/s)	Phase (deg)	Amplitude (m/s)	Phase (deg)	Amplitude (m/s)	Phase (deg)	Amplitude (m/s)	Phase (deg)
Station 1	0.631,	252.8	0.399,	267.8	0.147	266.1	0.092	288.4
Station 2	0.609	254.0	0.322	267.7	0.136	290.0	0.070	309.5
Station 5	0.236	254.1.	0.190	273.7.	0.048	290.7	0.013	351.7

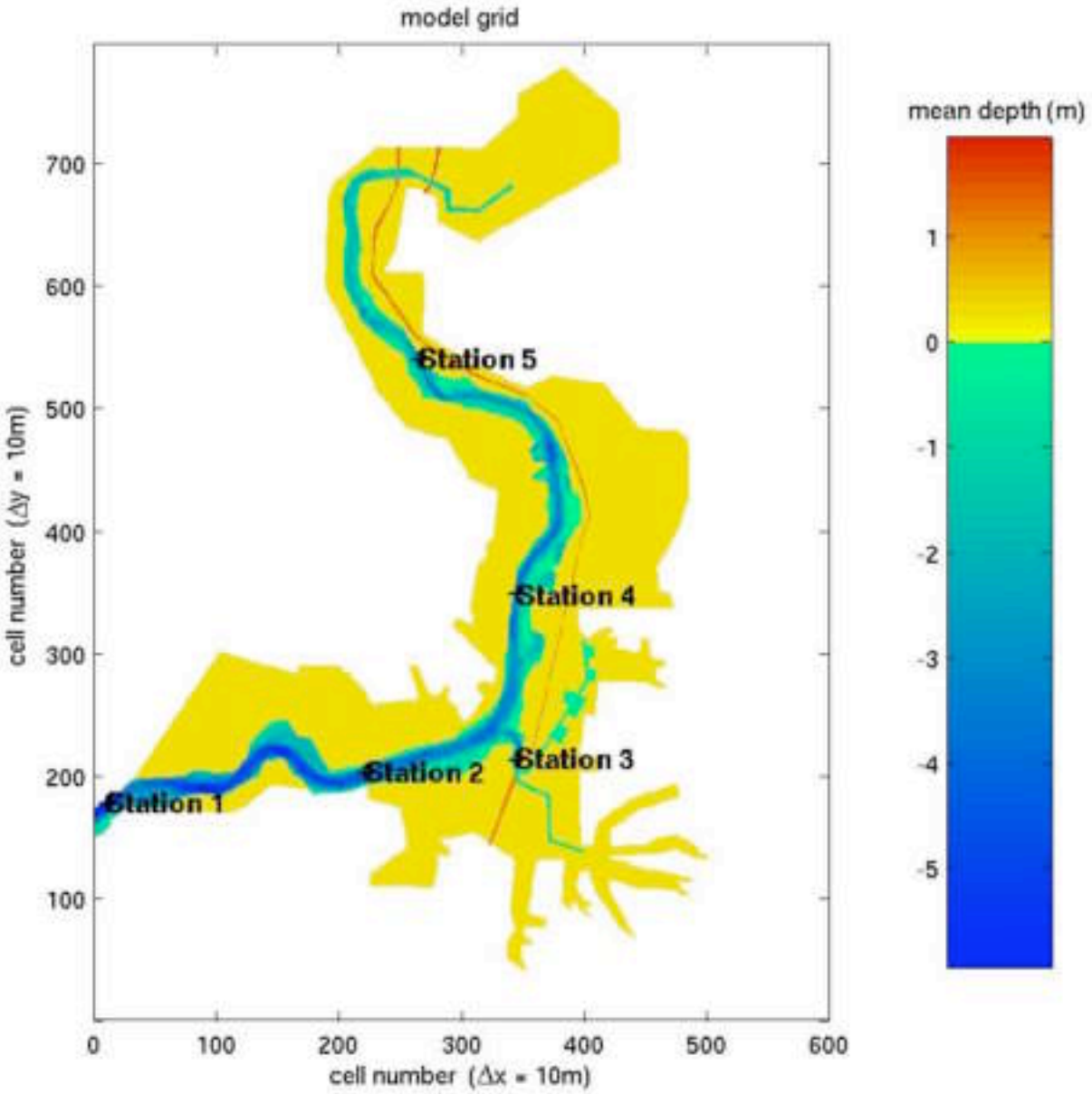

Figure 3.1 Model bathymetry and station locations for model output. Station locations match those of instruments deployed in 2002 and 2003.

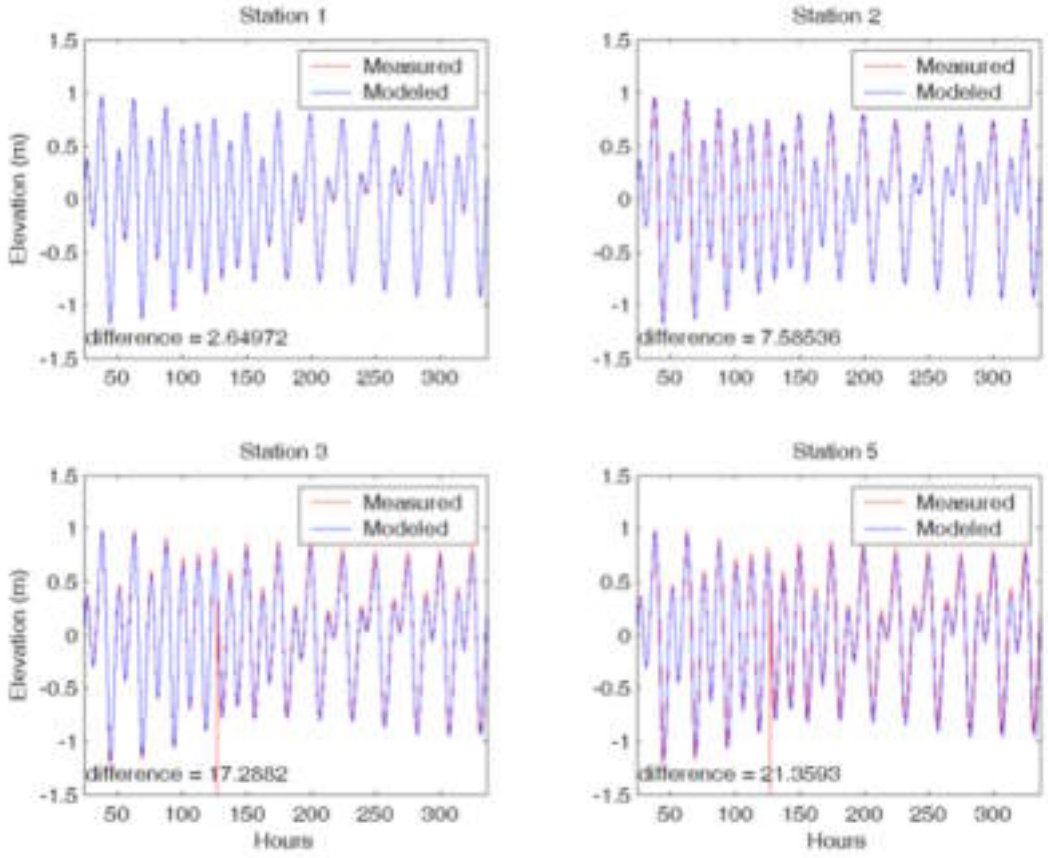

Figure 3.2 Measured and modeled water surface elevations Sept 2002.

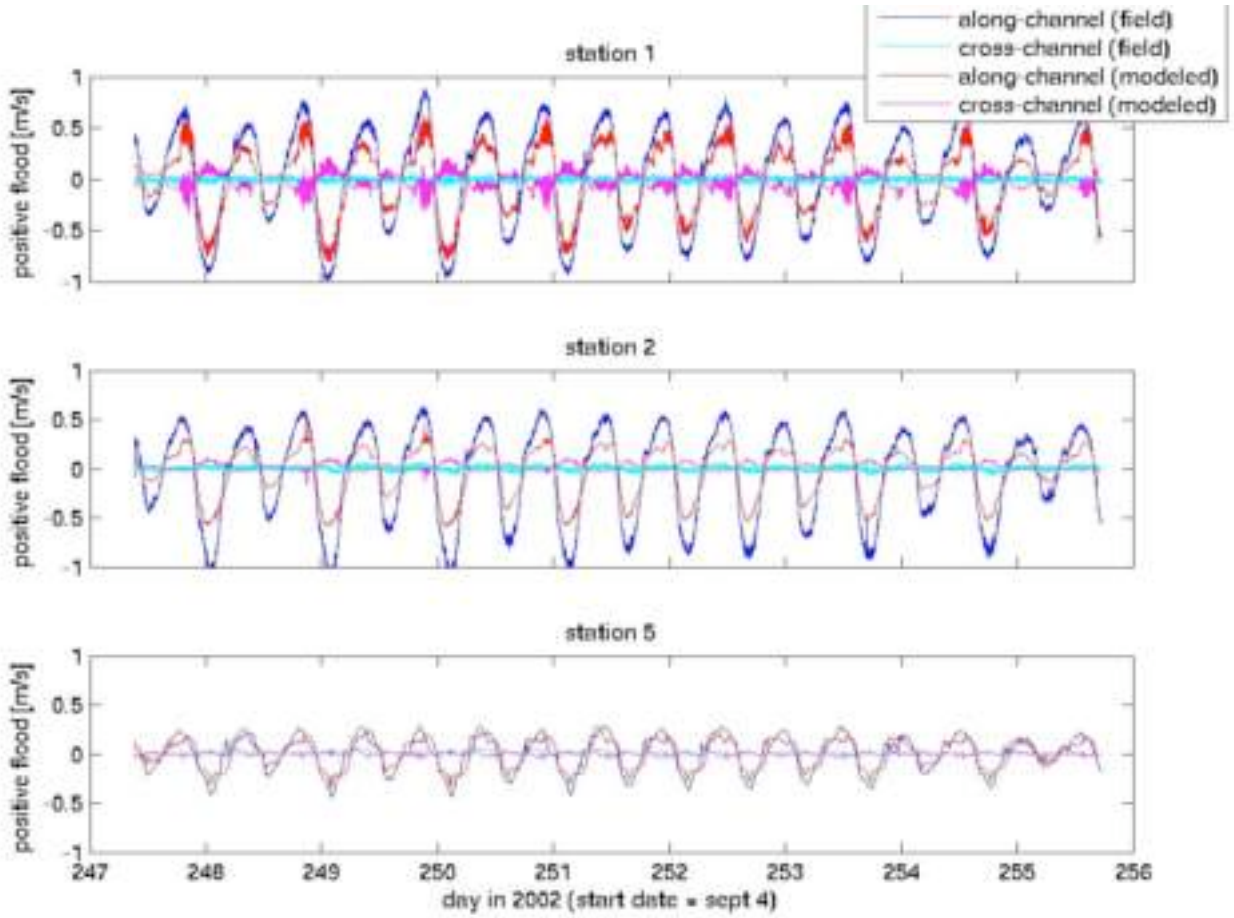

Figure 3.3 Comparison of measured and modeled along-channel and cross-channel velocities for the period September 3-12, 2002. Along-channel directions are indicated in Table 1.

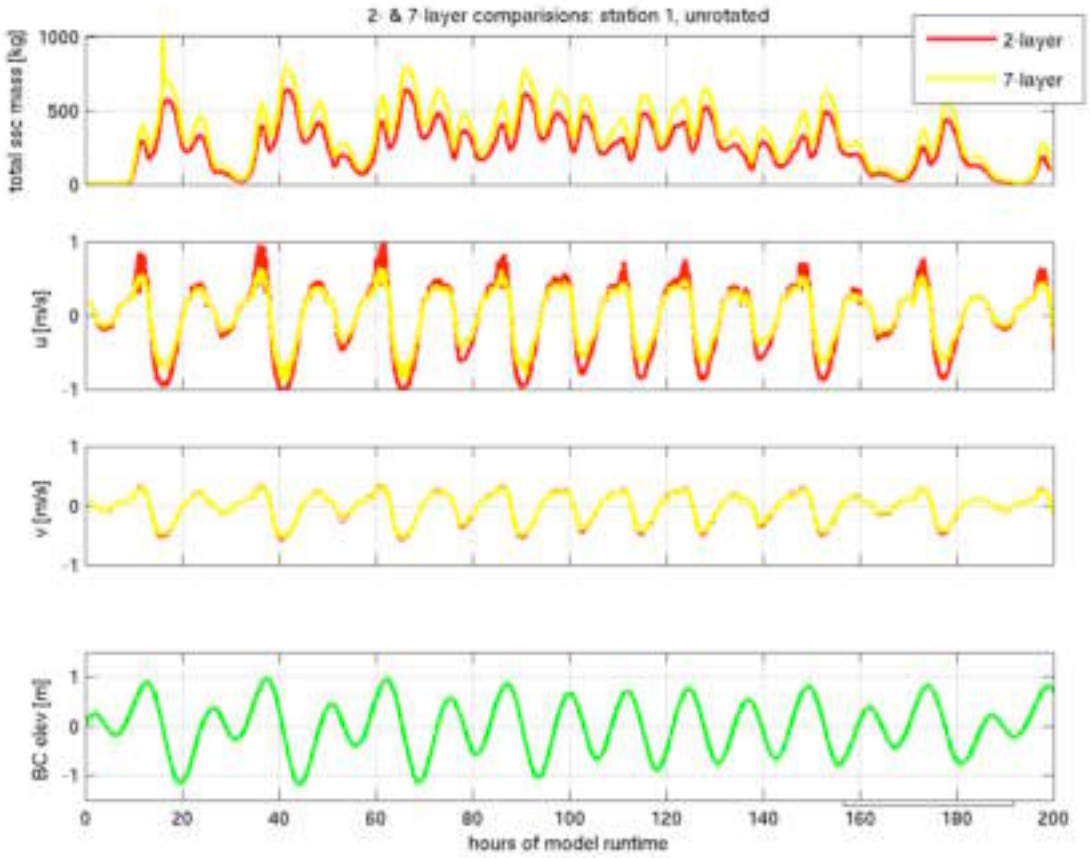

Figure 3.4 Comparison of output with two (red) and seven (yellow) vertical layers. The lower plot (green) is the surface elevation used to drive the model at the Highway 1 bridge.

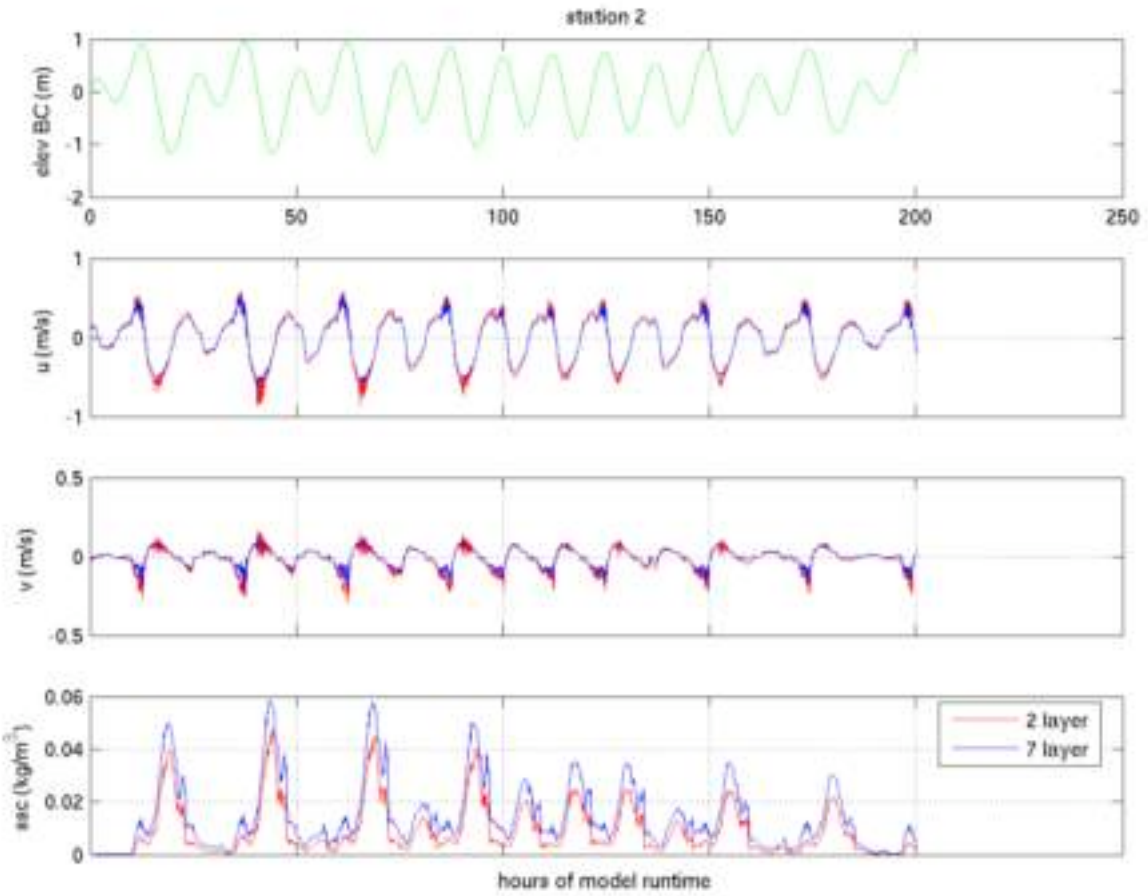

Figure 3.5 Comparison of along-channel velocities and suspended sediment at stations 2 and 5 for the 2-layer runs. The red represents $z_0 = 0.001$ in the shallows and $z_0 = 0.00002$ in the depths of the channels. Blue was run with $z_0 = 0.0025$.

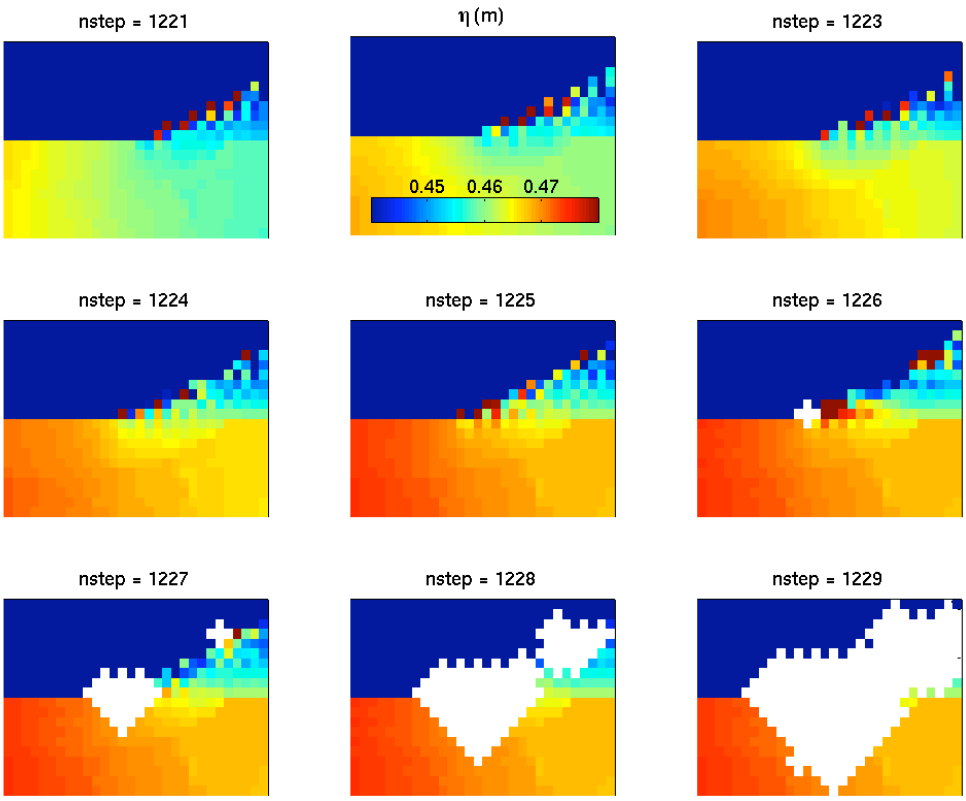

Figure 3.6 Development and growth of instabilities in the computed free surface elevation. Each panel is a plan view of the area (400 m x 300 m) immediately south of the Vierra property, at the north edge of the channel. Colors represent surface elevation, in meters, as indicated in the upper middle plot.

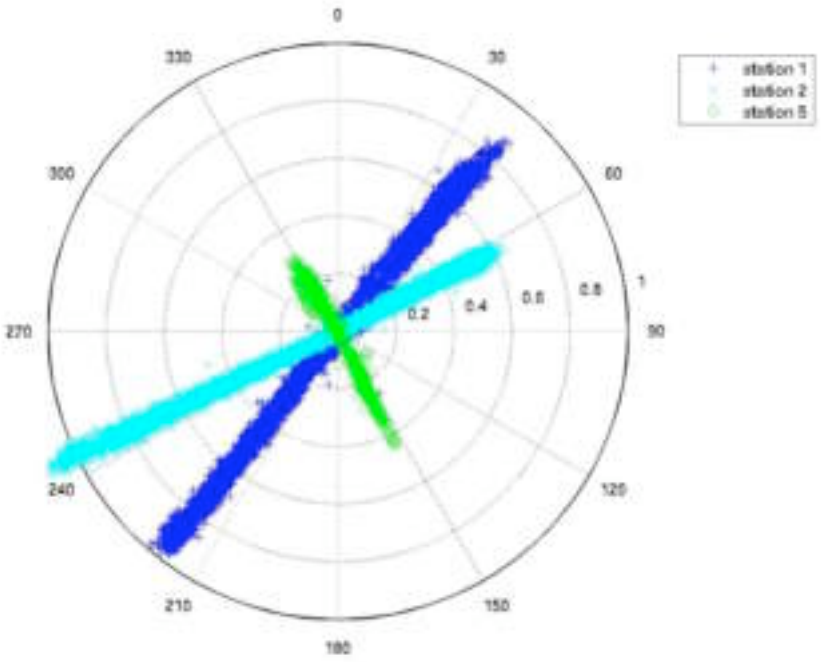

Figure 3.7 a) Direction and magnitude of measured current speeds, September 3-12, 2002.

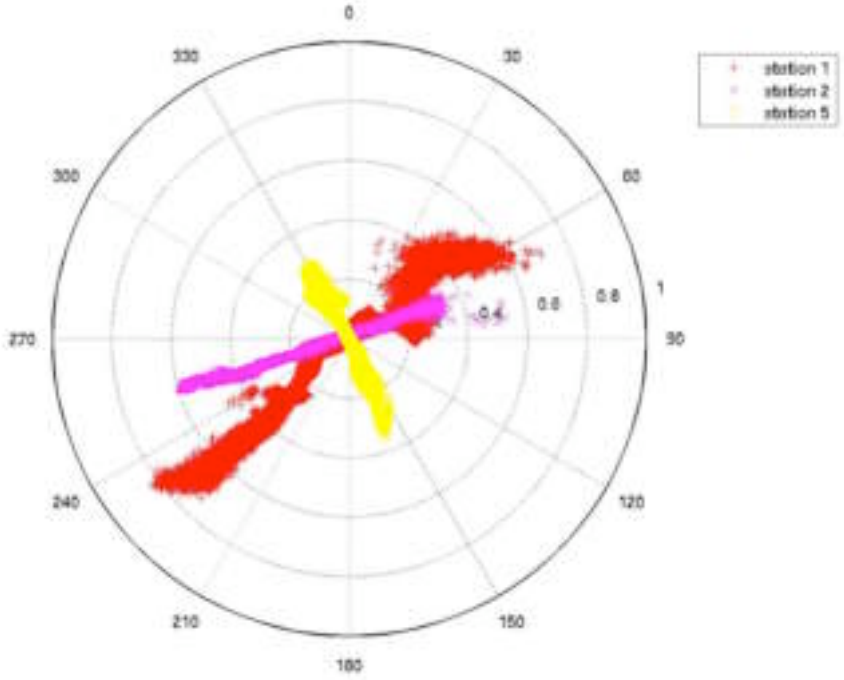

Figure 3.7 b) Direction and magnitude of modeled current speeds, September 3-12, 2002.

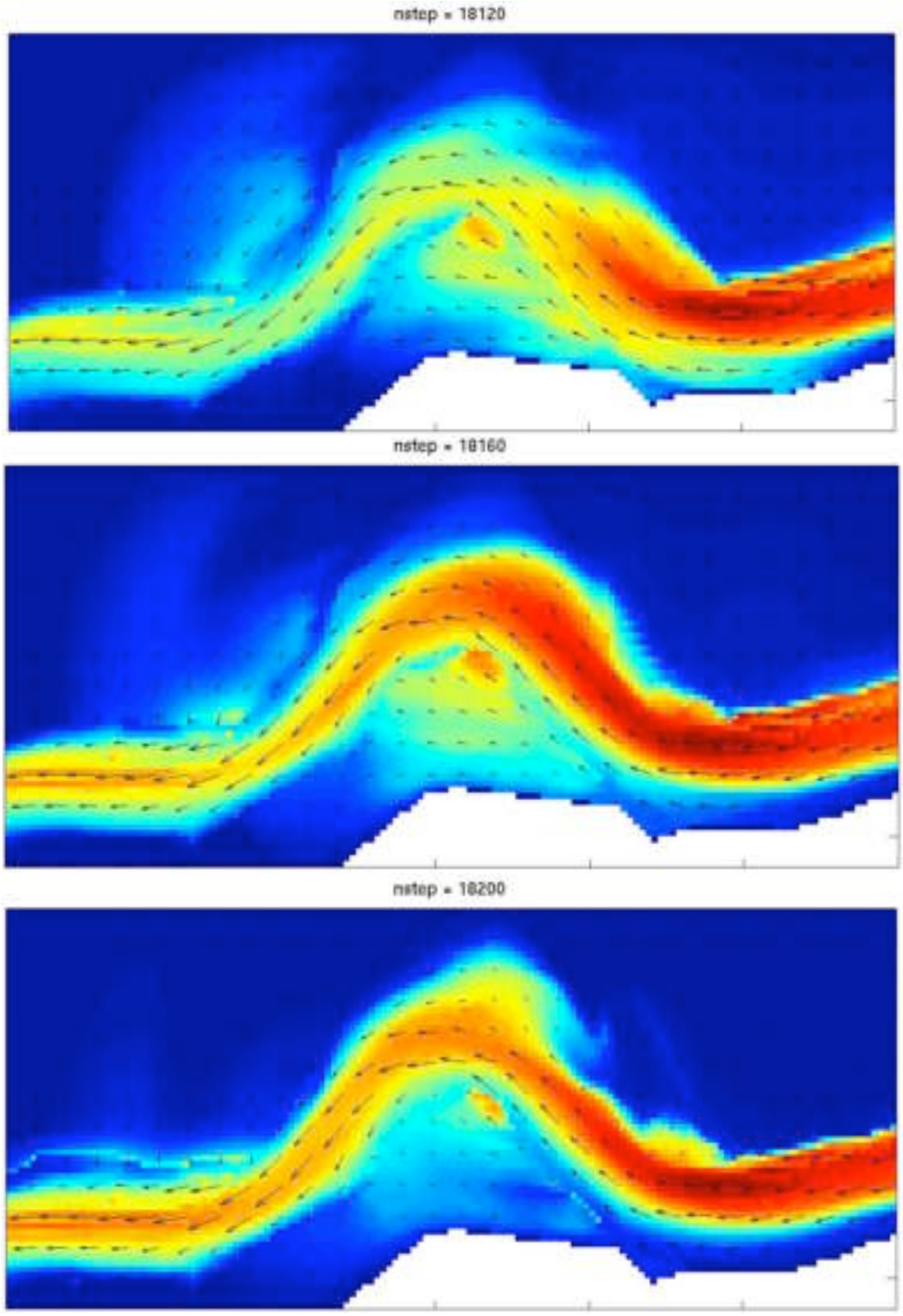

Figure 3.8 Velocity vectors and suspended sediment concentrations (0-0.05 kg/m3 – blue to red).

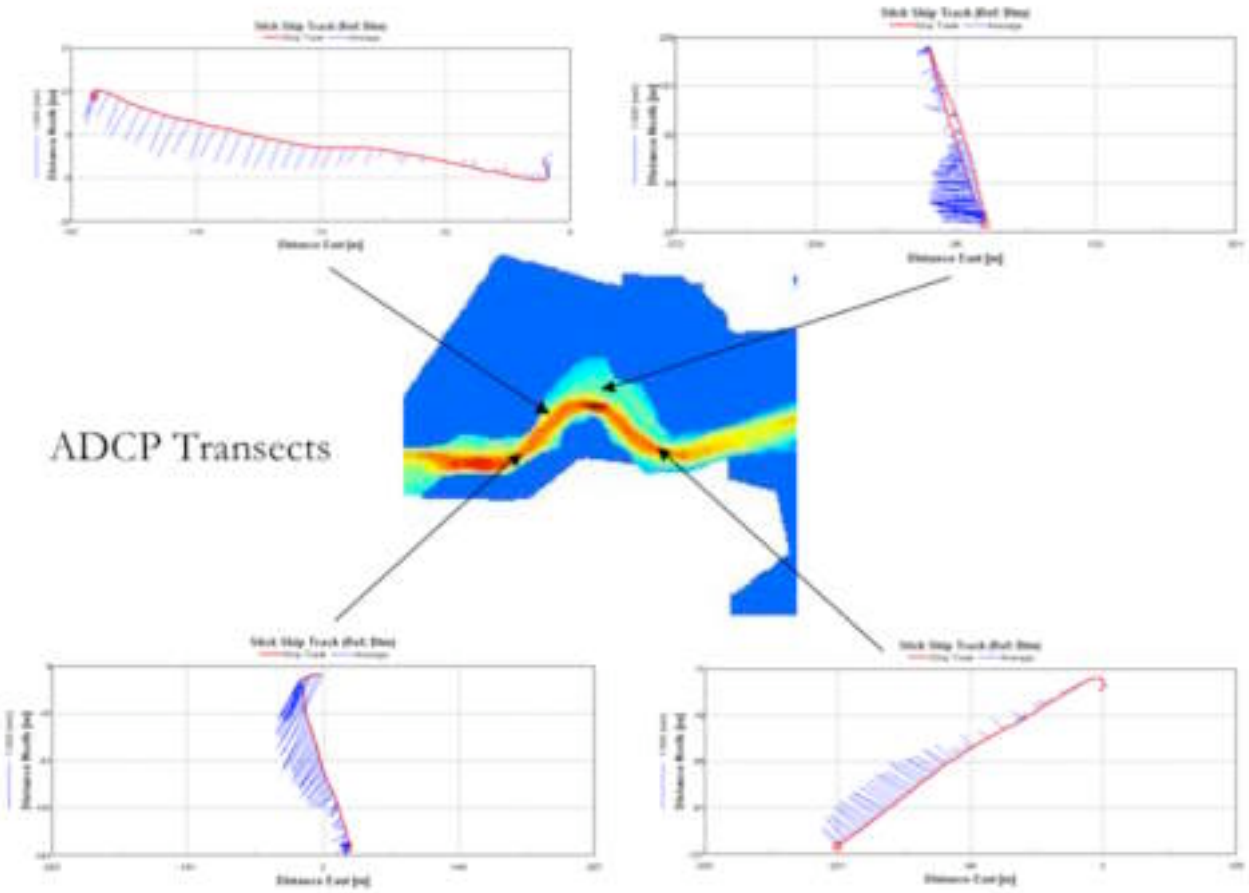

Figure 3.9 Velocity vectors at points along Seal Bend, as measured by ADCP transects, September 2002. Colors represent bathymetry.

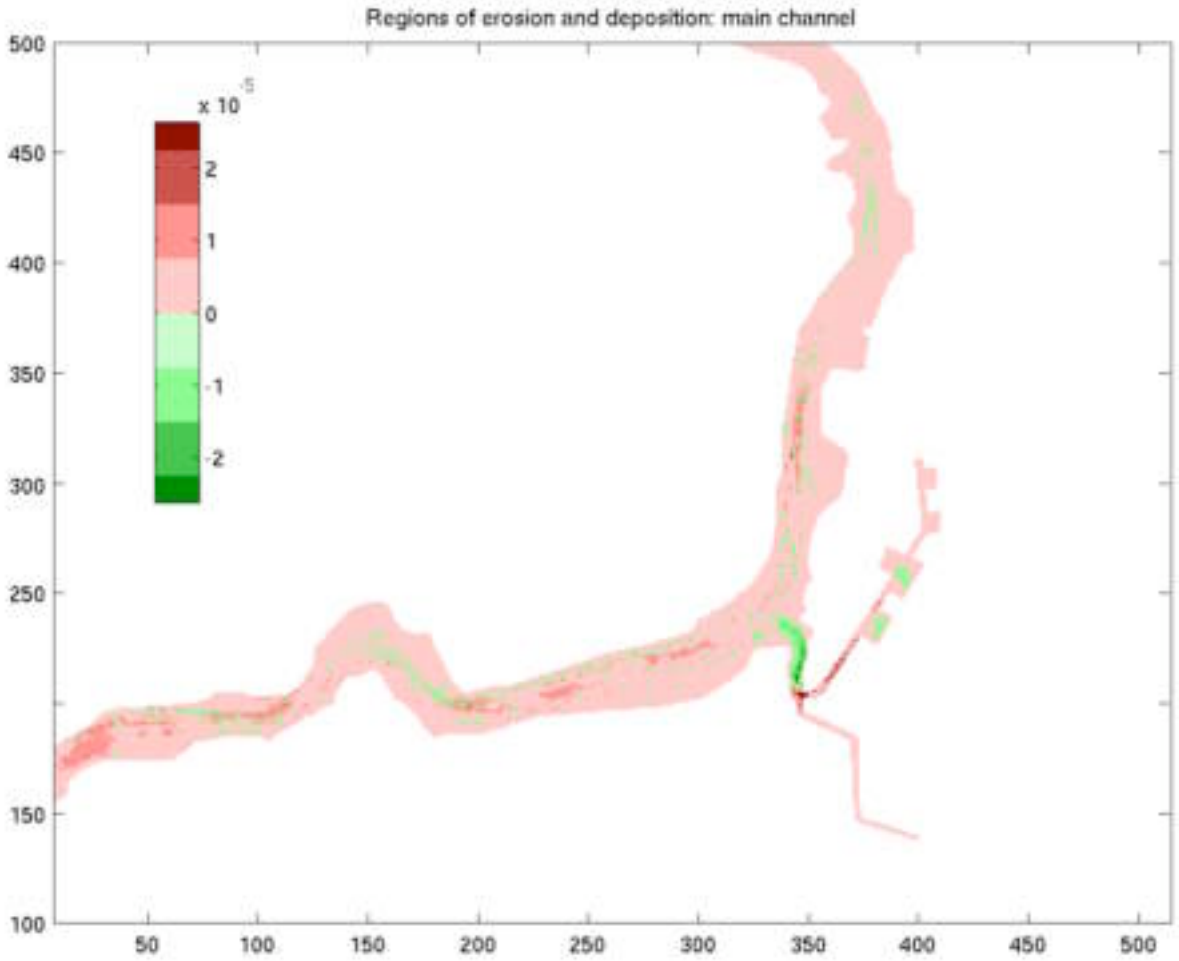

Figure 3.10 a) Areas of net erosion (red) and deposition (green) averaged over the course of the model run.

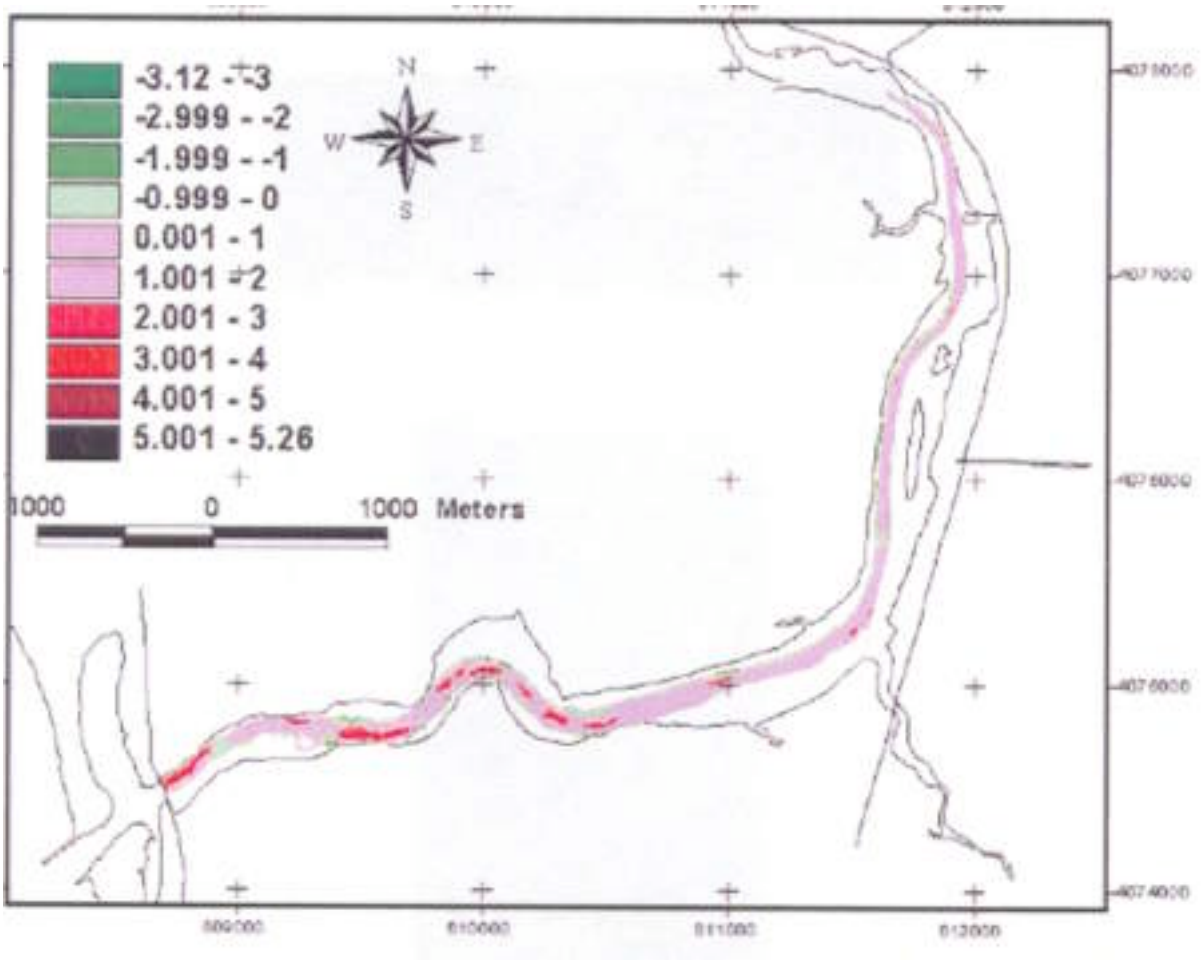

Figure 3.10 b) The main Slough channel showing rates of sediment loss between 1993 and 2001. Shades of red indicate areas of loss; gains in sediment are shown in greens. [Wasson et al 2002].

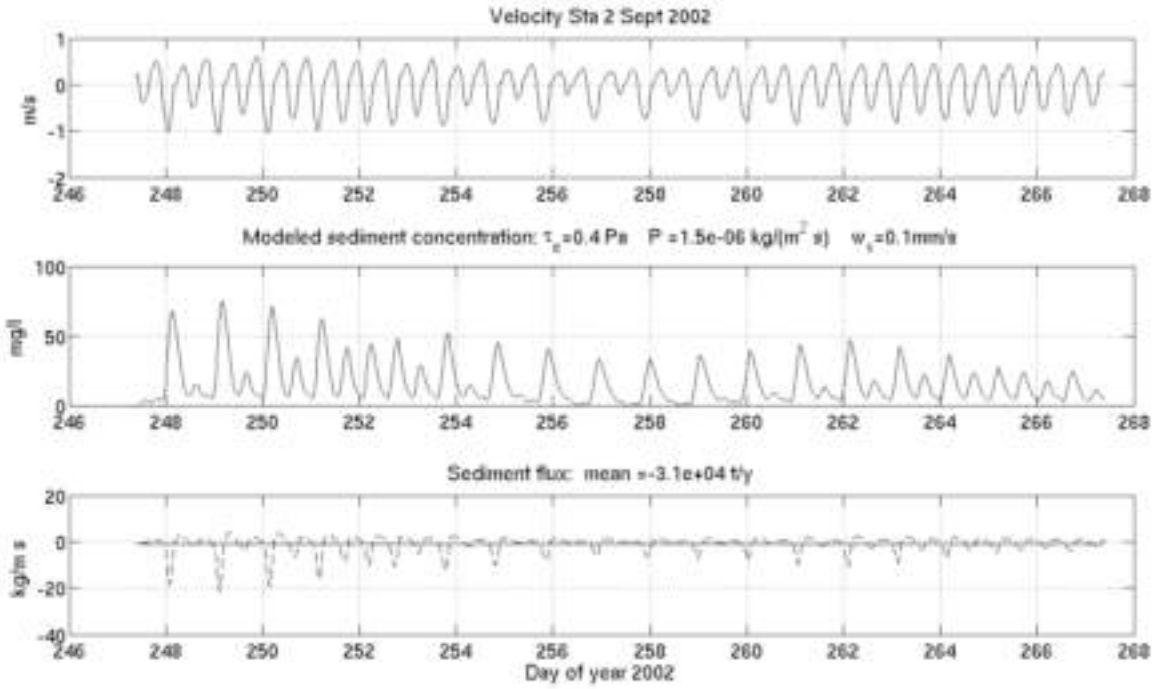

Figure 3.11 One dimensional model of sediment dynamics with "asymmetrical advection"

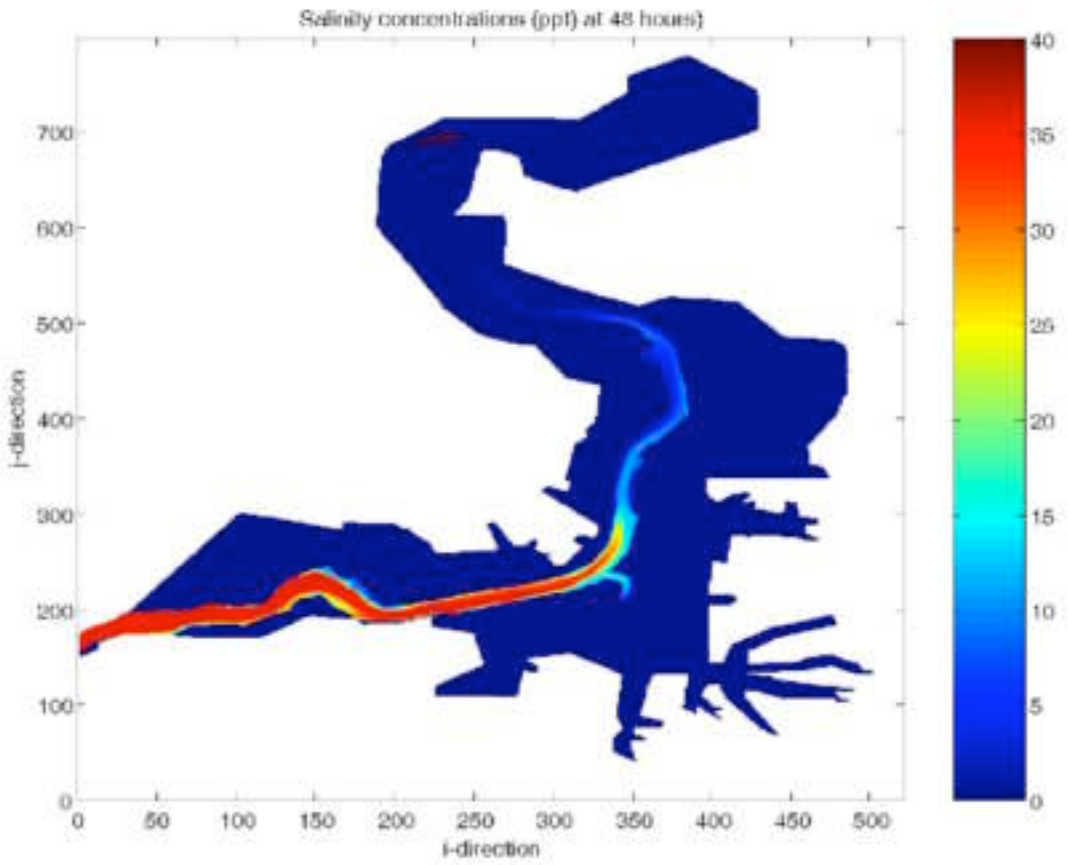

Figure 3.12a Computed salinity field 48 hours (during flood) after start up with a fresh Elkhorn Slough.

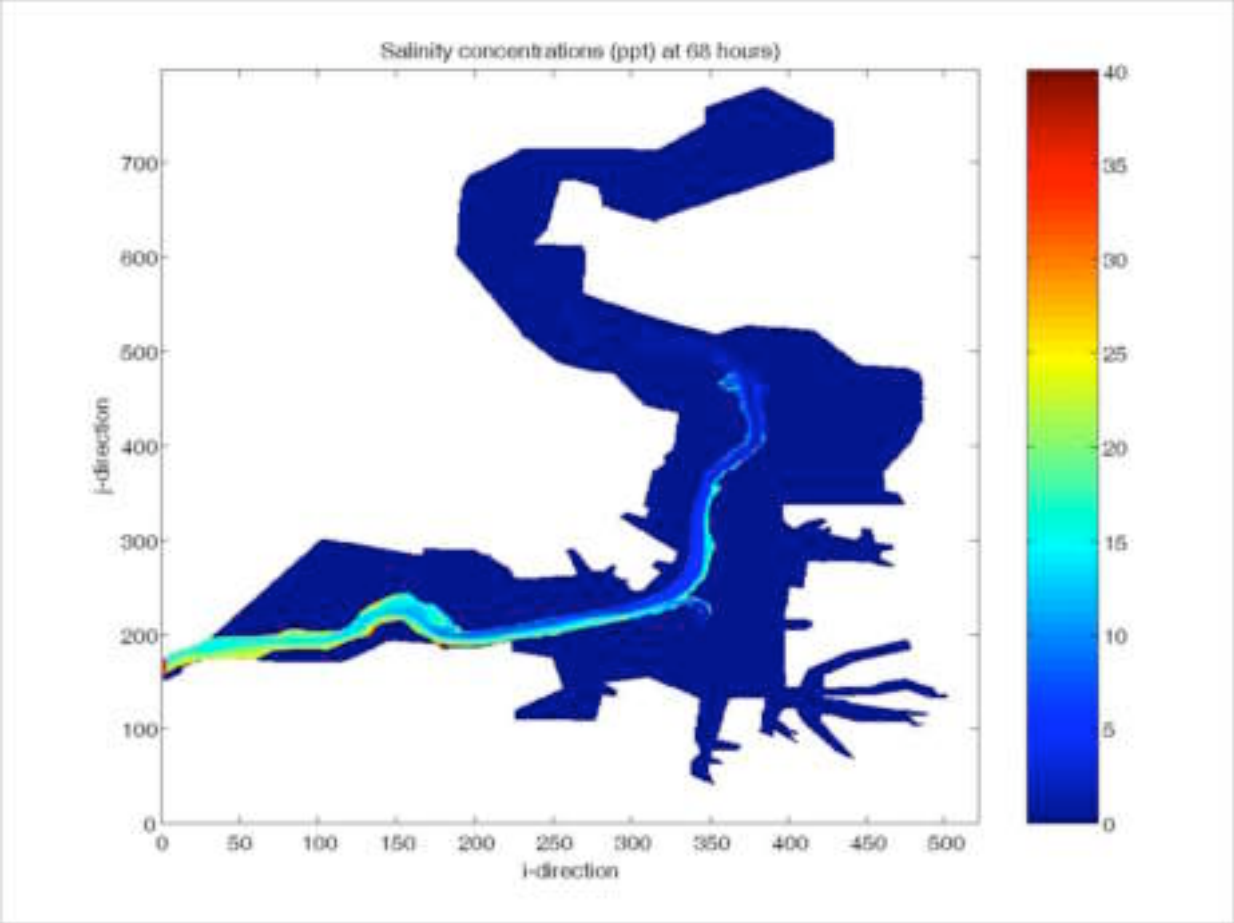

Figure 3.12b Computed salinity field 68 h (end of ebb) after start up

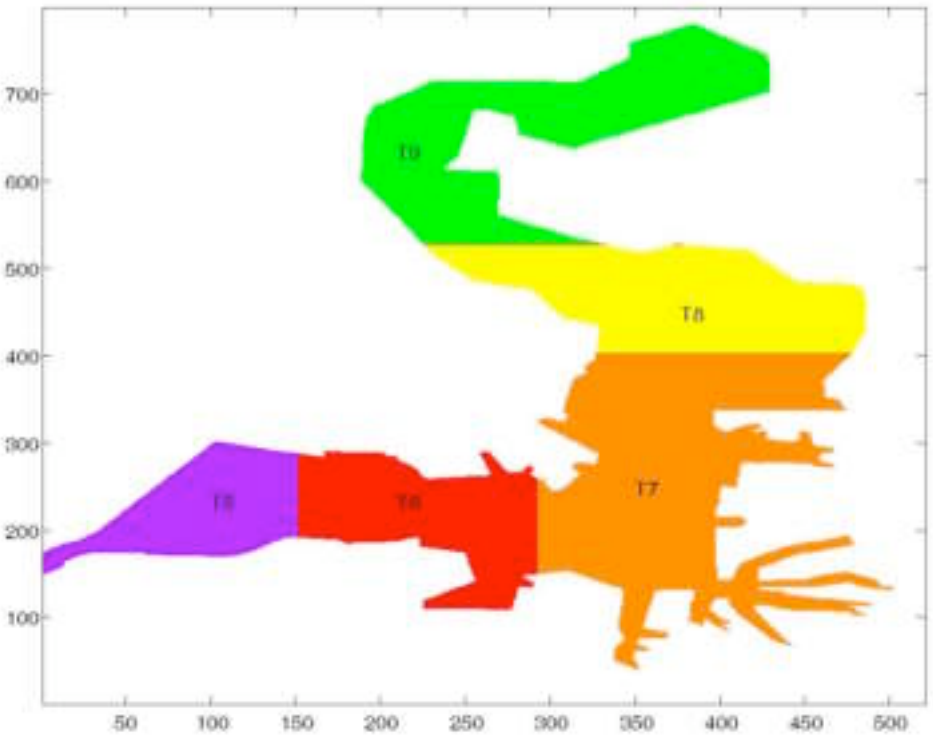

Figure 3.13 Definition of regions for tracer computations

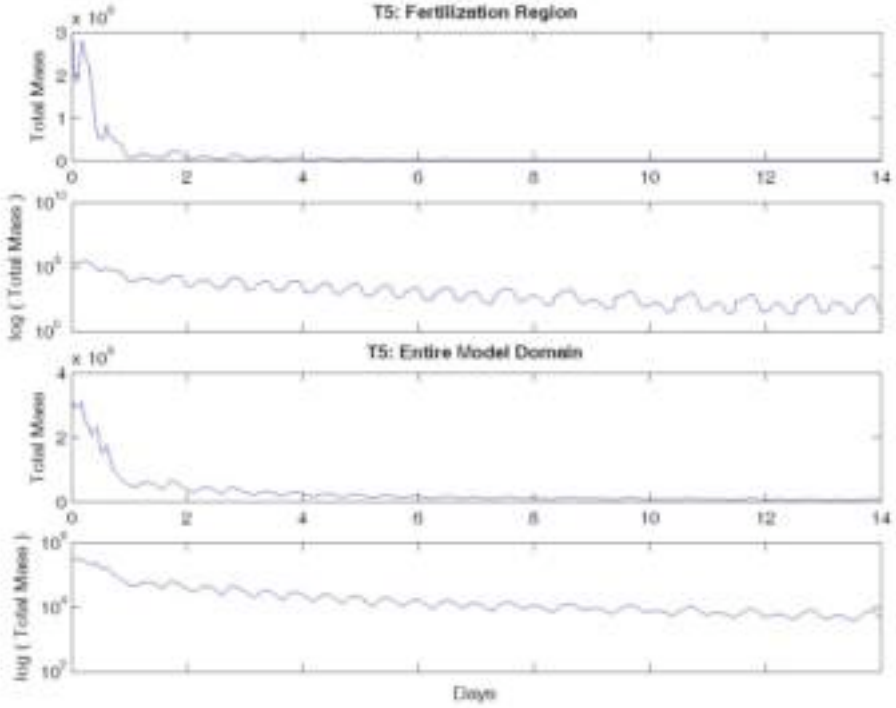

Figure 3.14a Tracer concentrations computed for Region 5

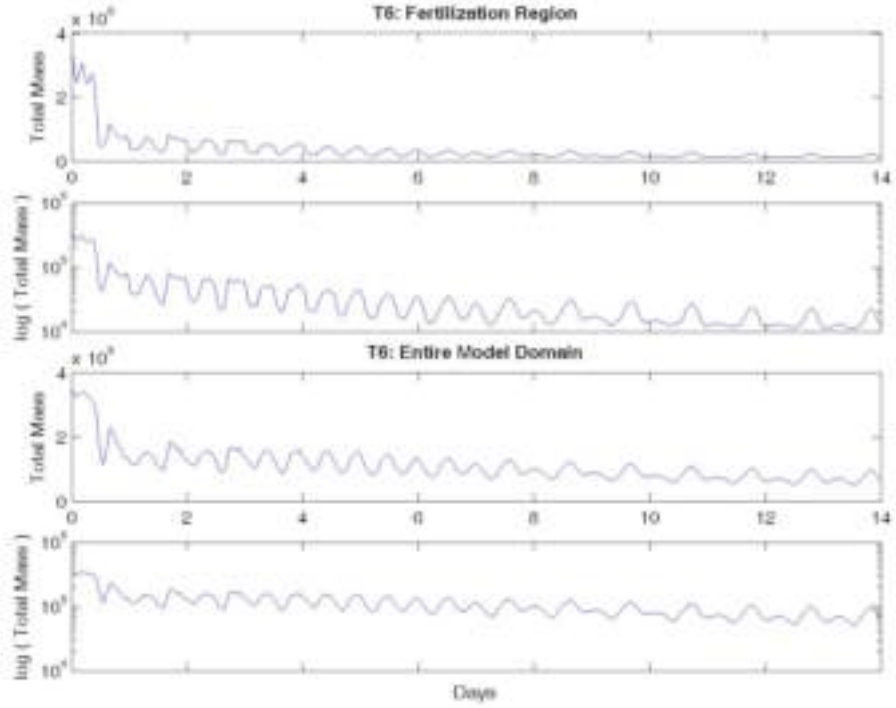

Figure 3.14b Tracer concentrations computed for Region 6

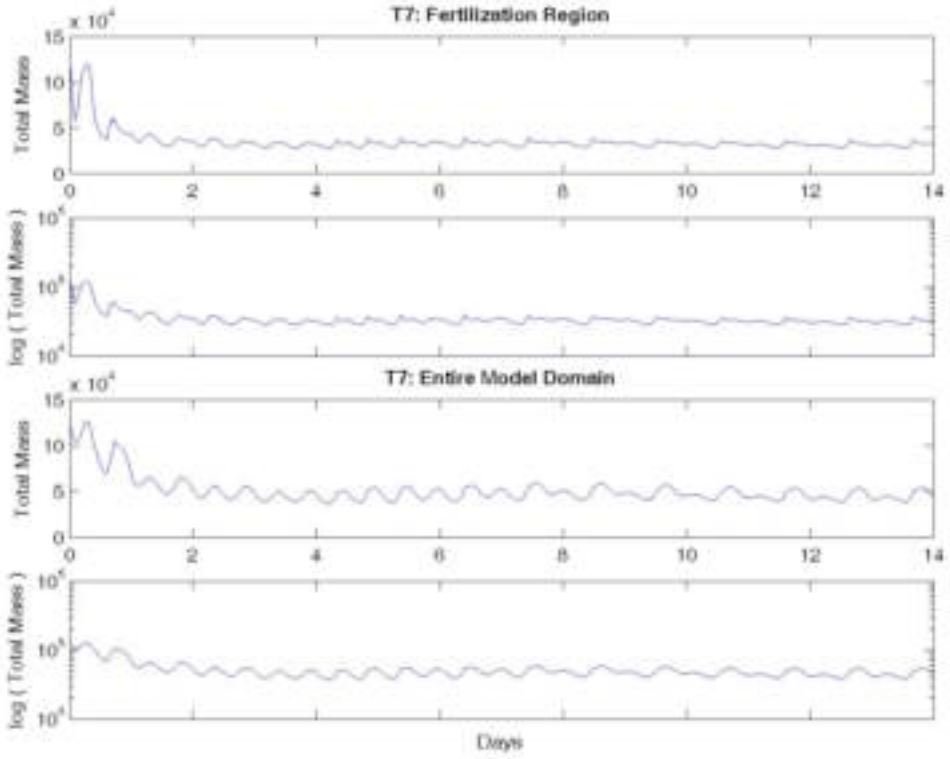

Figure 3.14c Tracer concentrations computed for Region 7

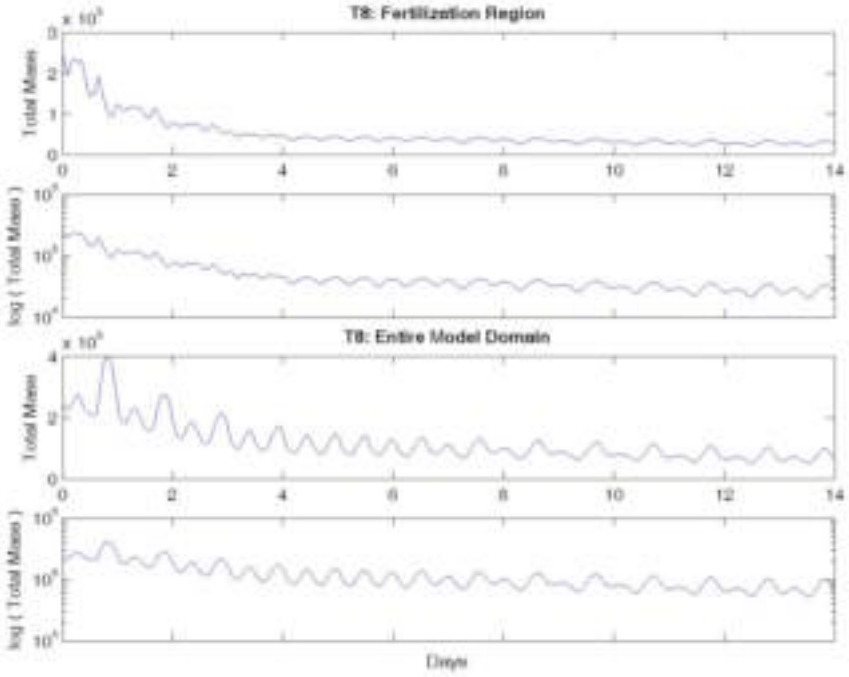

Figure 3.14d Tracer concentrations computed for Region 8

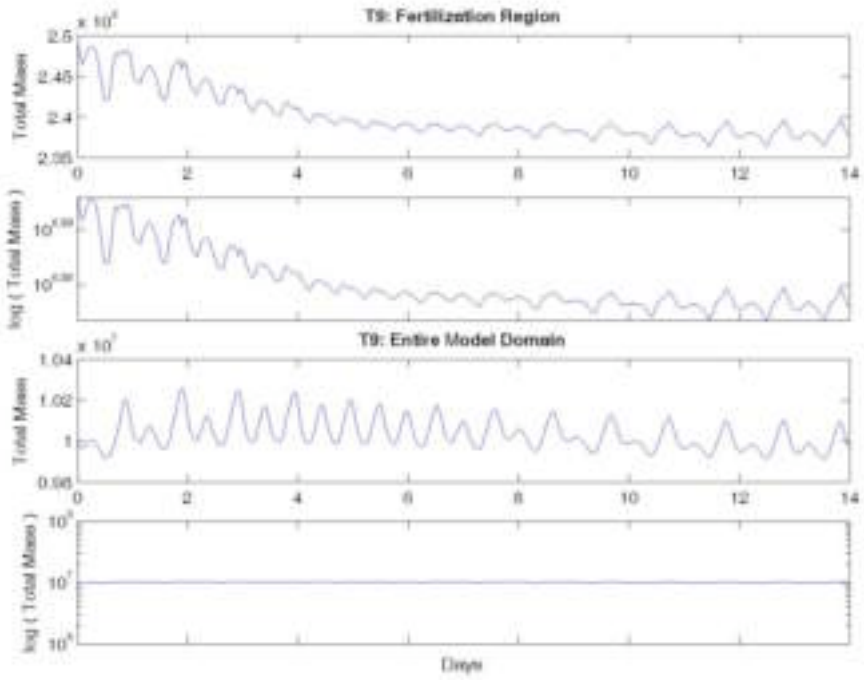

Figure 3.14e Tracer concentrations computed for Region 9

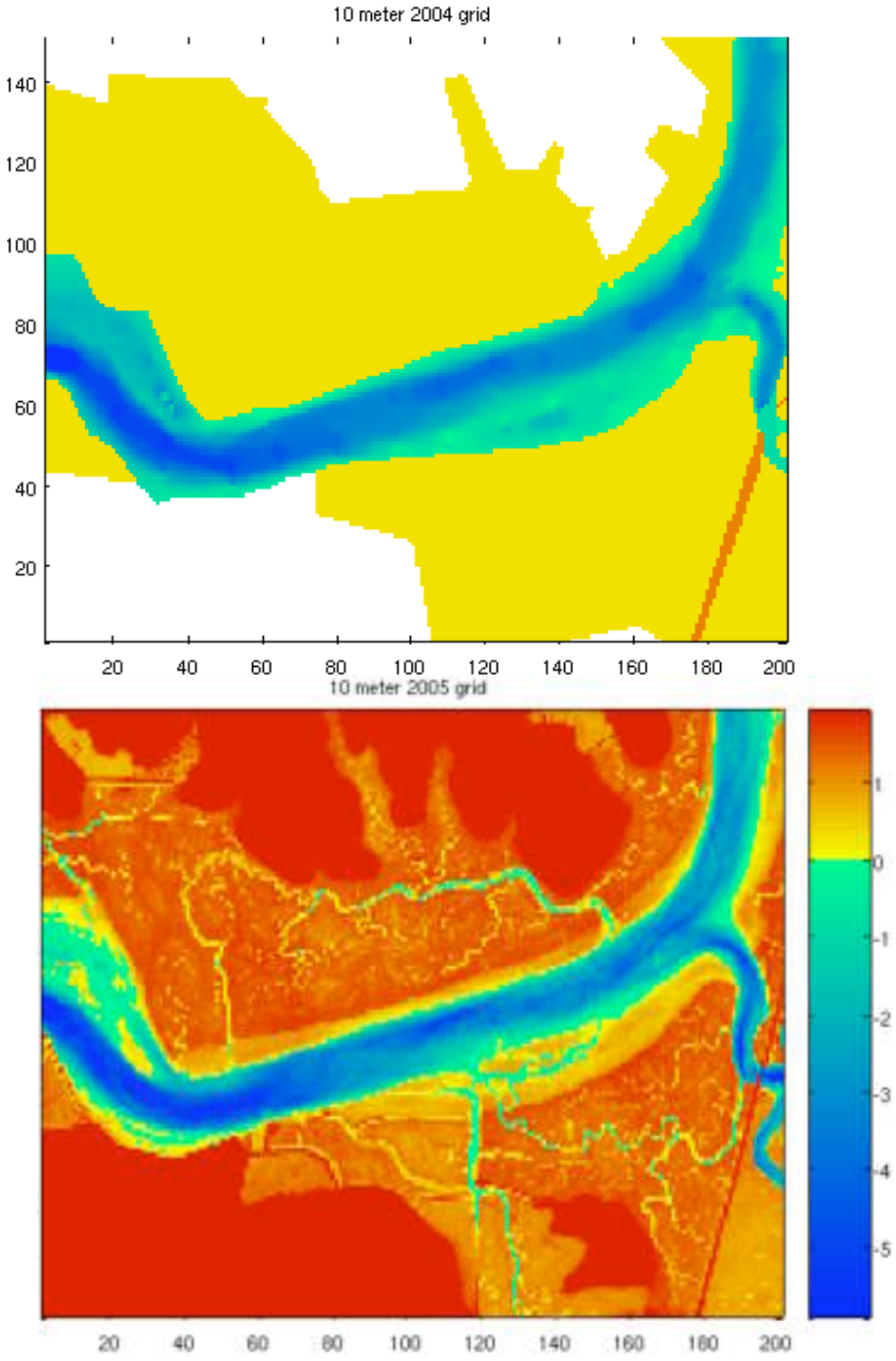

Figure 3.14 a) 10-meter resolution bathymetry used for data in this report. Mudflats are approximated at an elevation of 0.3 meters mean water; **b)** 10-meter resolution bathymetry currently in preparation, obtained via combination of LIDAR and bathymetric surveys. The color scale is in meters, from mean water.

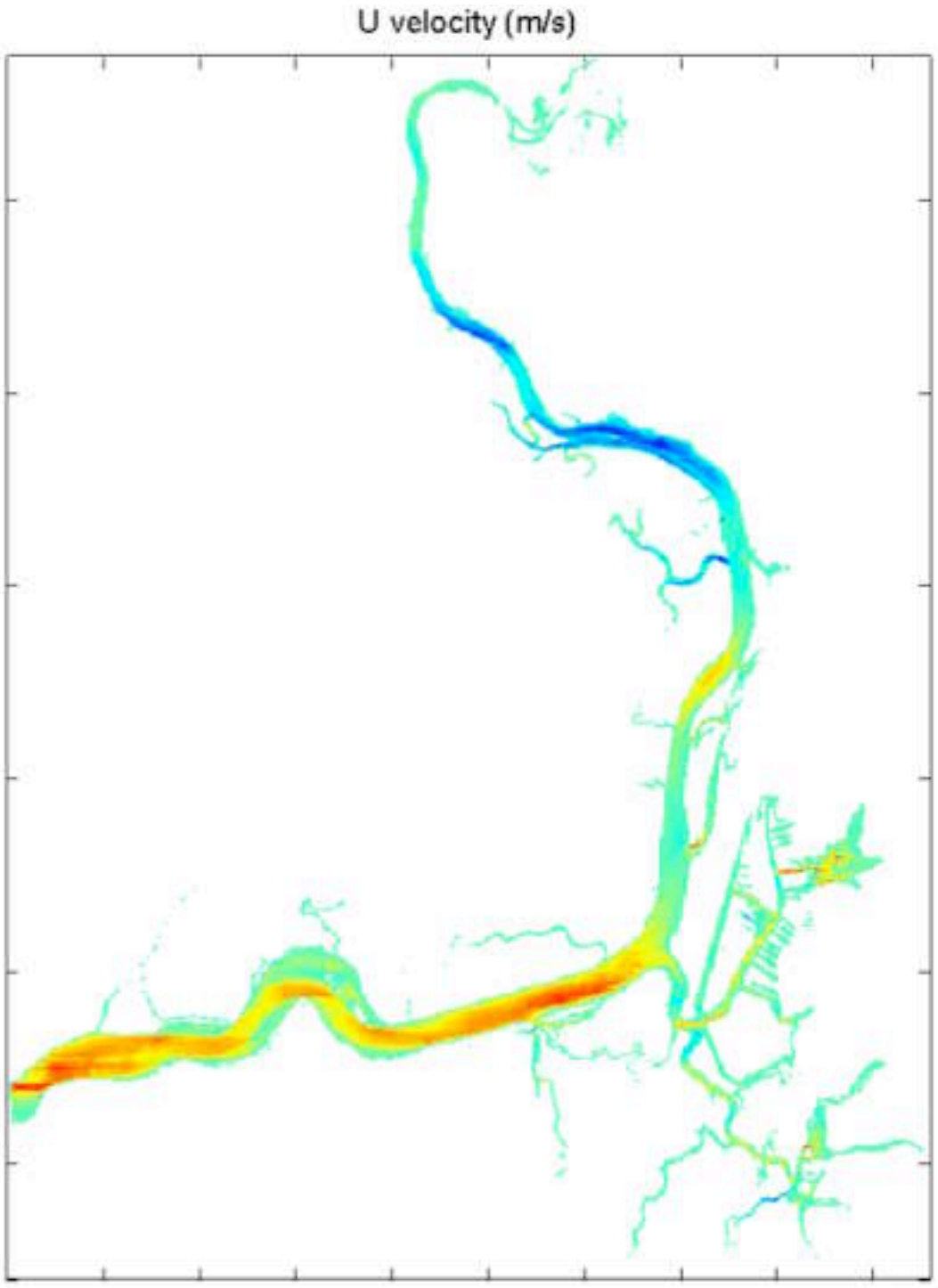

Figure 3.15 East (red)/west (blue) velocities at beginning of model run using new bathymetry.

4. Groundwater fluxes to Elkhorn Slough derived from measurements of Radium isotopes.

Activities of radium isotopes were measured several times at six sites in the Slough channel (Figure 4.1) in order to trace the spatial, tidal, and seasonal variability of groundwater and associated nutrient input to Elkhorn Slough. In all seasons, and under all tidal conditions, high activities of the short-lived isotopes ^{223}Ra ($t_{1/2}$ = 11.3 d) and ^{224}Ra ($t_{1/2}$ = 3.7 d) were measured near the head of the Slough at Kirby Park, declining toward oceanic activities at sites closer to the mouth of the Slough (Figure 4.2). Since the flushing time of the slough is short (~80% of the Slough volume is thought to exchange with the ocean each tidal cycle), this general pattern in Ra activity primarily reflects the discharge of groundwater to the northeastern end of the slough rather than radioactive decay. To test this conclusion we have examined ^{224}Ra: ^{223}Ra activity ratios at each of the sampling sites. If radioactive decay were a significant factor, the 224:223 ratio would be expected to decline as the ^{224}Ra activity dwindled relative to the longer-lived ^{223}Ra. No such decline is apparent in our data; instead, 224:223 generally increases toward the mouth of the Slough, possibly as a result of groundwater input from isotopically-distinct sources, such as the Salinas River and Parsons Slough (Figure 4.3).

Within the dominant pattern of decreased Ra activity (and, by proxy, the groundwater component) moving toward the mouth of the Slough lie several notable spatial and temporal trends. The highest Ra activities at all sites are seen shortly after the high tide maximum and appear to follow the tide by a few hours (Figure 4.4). This pattern may result from greater discharge as the tide starts to fall, or from tidal control of the salinity of discharging groundwater, which will in turn affect the degree of Ra desorption from aquifer sediments. This pattern appears to be augmented by a seasonal effect, as supported by the observation that ^{223}Ra and ^{224}Ra activities are often higher in the autumn than in the spring, particularly at high tide (Table 4.1). As the dry season progresses, groundwater probably becomes a larger component of the freshwater input to the slough than during the wet winter and spring months, when surface runoff is greater. Furthermore, the elevated Ra activities measured in the autumn suggest that the character of groundwater discharge may vary seasonally, with brackish or saline (and hence Ra rich) groundwater, including recirculated seawater, comprising a larger fraction of the total discharge during the dry season.

The long-lived radium isotopes, ^{228}Ra ($t_{1/2}$ = 5.6 yr) and ^{226}Ra ($t_{1/2}$ = 1600 yr), which over the timescales applicable to this study can be considered purely conservative tracers have also

been analyzed. For the most part, the long-lived isotope data corroborate the conclusions drawn from the short-lived isotopes, i.e., that groundwater discharge to the slough is dominated by input to the upper reaches (with the signal of a lesser source apparent in Moss Landing Harbor near the Salinas River tide gates) and that Ra activities, and perhaps groundwater discharge, peak just after the high tide. Seasonal differences in activity are still apparent for the long-lived tracers suggesting that the pattern is not merely a function of residence time and decay in the slough but rather an indication of seasonal variability in the groundwater contribution.

As a preliminary step toward quantifying the groundwater flux to Elkhorn Slough we have constructed a simple mass balance model to describe the mass of Ra (any isotope) that leaves the estuary:

$$\left(Q_{GW} + Q_{EX}\right)\overline{Ra}_{ES} + \lambda V_{ES}\overline{Ra}_{ES} = Q_{GW} Ra_{GW} \tag{27}$$

where

Q_{GW} = groundwater flow

Q_{EX} = exchange flow due to tides (effect of mixing)

λ= decay rate of given Radium isotope

$\overline{Ra}_{ES}$ = average Radium isotope concentration in estuary

Ra_{GW}= constant (by assumption) concentration of Radium isotope in groundwater

This equation can be re-arranged to solve for Q_{GW} (two isotopes) if we assume that Q_{EX} is known:

$$Q_{GW} = V_{ES}\lambda\left(1 + \frac{1}{\lambda T_R}\right)\frac{\overline{Ra}_{ES}}{Ra_{GW} - \overline{Ra}_{ES}} \tag{28}$$

where $T_R = V/Q_{EX}$ is the residence time for the box. Note that for the suite of 4 isotopes that we measured, (28) gives 4 estimates of the groundwater flow. Moreover if $\lambda T_R >> 1$, then the estimate of groundwater flow is mostly determined by the decay rate, whereas if $\lambda T_R << 1$, the estimate of groundwater flow is determined mostly by the assumed residence time.

Previous bathymetric work yielded an estimate of the slough volume of 10^7 m^3 (Malzone 1999), while a plausible of the water residence time is 3 days (see below). Because no groundwater sample representative of the dominant source to the upper slough has yet been located and collected, values used here for Ra_{GW} are from the slough channel at Kirby Park; as a

result, these calculated flows are preliminary and may overestimate the actual groundwater input. These estimates will be refined as soon as a groundwater end member is located and analyzed. Ranges of daily groundwater flow to Elkhorn Slough, given in Table 4.1, represent the solutions to equation (2) using the various Ra isotopes. It must be emphasized that this is not a pure freshwater input but a mixture of freshwater and recirculated seawater

We can check these estimates in another way. The governing equation for quasi-steady subtidal variations in Ra isotope concentrations, C, can be written as:

$$-Q_{GW}\frac{\partial C}{\partial x} = -\lambda A_c C + \frac{\partial}{\partial x}\left(K_x A_c \frac{\partial C}{\partial x} \right) \tag{29}$$

where K_x (m^2/s)is the shear flow dispersion coefficient (see Fischer et al 1979) and we have assumed that the groundwater flow enters the estuary near the head and is otherwise constant (other models are possible). If we integrate (29) from $x = 0$ (the mouth) to $x = L$, and assume that (a) dispersion near the head is much weaker than at the mouth (reasonable given that K_x is proportional to the square of the width and the rms tidal current both of which decrease substantially towards the head of the Slough)(b) the concentration gradient is roughly constant (see figure 2.27), we find that

$$-Q_{GW}C\Big|_0^L = -\lambda\int_0^L A_c(x)C(x)\,dx + K_x A_c \frac{\partial C}{\partial x}\Big|_0^L \tag{30}$$

or

$$-Q_{GW}\left(C(L) - C(0)\right) \simeq -\lambda V\overline{C} - K_x A_c \frac{\partial C}{\partial x}\Big|^L$$

$$Q_{GW}\Delta C \simeq \lambda V\overline{C} + K_x(0)A_c(0)\frac{\Delta C}{L}$$

which can be written as

$$Q_{GW} \simeq \lambda V\frac{\overline{C}}{\Delta C} + \frac{K_x(0)A_c(0)}{L} \tag{31}$$

From figure 2.27, we can assume that $\overline{C}/\Delta C \approx 2$, while for Ra^{223} $\lambda = 0.06$ day^{-1}, so that if dispersion were nil at the mouth, a lower bound on Q_{GW} would be 1.2 x 10^6 m^3/day. However, as discussed above, we can estimate that near the mouth K_x ! 200 m^2/s, and so with $A_c = 350$ m^2, and $L = 7000$ m, an upper bound on Q_{GW} would be

$$Q_{GW} \simeq 1.2\times10^{6}\,\tfrac{\mathrm{m}^3}{\mathrm{d}} + \frac{200\,\tfrac{\mathrm{m}^2}{\mathrm{s}}\times 86400\,\tfrac{\mathrm{s}}{\mathrm{d}}\times 350\,\mathrm{m}^2}{7000\,\mathrm{m}} \approx 2\times10^{6}\,\tfrac{\mathrm{m}^3}{\mathrm{d}}$$

These values are in reasonable agreement with the values estimated via the box model and suggest that there are considerable groundwater inputs, ca. 10 - 25 m^3/s, to Elkhorn Slough. We note that these fluxes are comparable to groundwater fluxes observed at Port Royal Sound (8.6 x 10^6 m^3/day), and other east coast estuaries (Crotwell and Moore 2003). However, given the variability we see both tidally and with time of year and the fact that we also observed hypersaline conditions in Sept 2002, this input waxes and wanes and may cease entirely at times.

Finally, using the nitrate concentration of the groundwater (2μM) and the above fluxes an input of 60-100 kg N/day into the slough form groundwater is calculated. Using a typical (Redfield) C:N ratio for marine productivity this nitrate flux if utilized efficiently may support the fixation of 400-660 kg C/day in the slough. These values should be considered minimum values since we are yet to sample a pure groundwater end member which based on data from many other locations is likely to have higher inorganic nitrogen concentrations.

Table 4.1 Estimates of groundwater Flux to Elkhorn Slough

Season	**Tide**	Q_{GW} (10^6 m^3/day) Based on Ra balance				Q_{GW} (10^6 m^3/day) Average Flux
		226	228	223	224	
Autumn	High	4	0.4	0.9	2	1.8
Autumn	Low	5	1	0.7	2	2.0
Spring	High	9	3	0.8	4	4.2
Spring	Low	8	2	2	1	5.9
Average		6.4	1.6	0.9	2.9	3.7

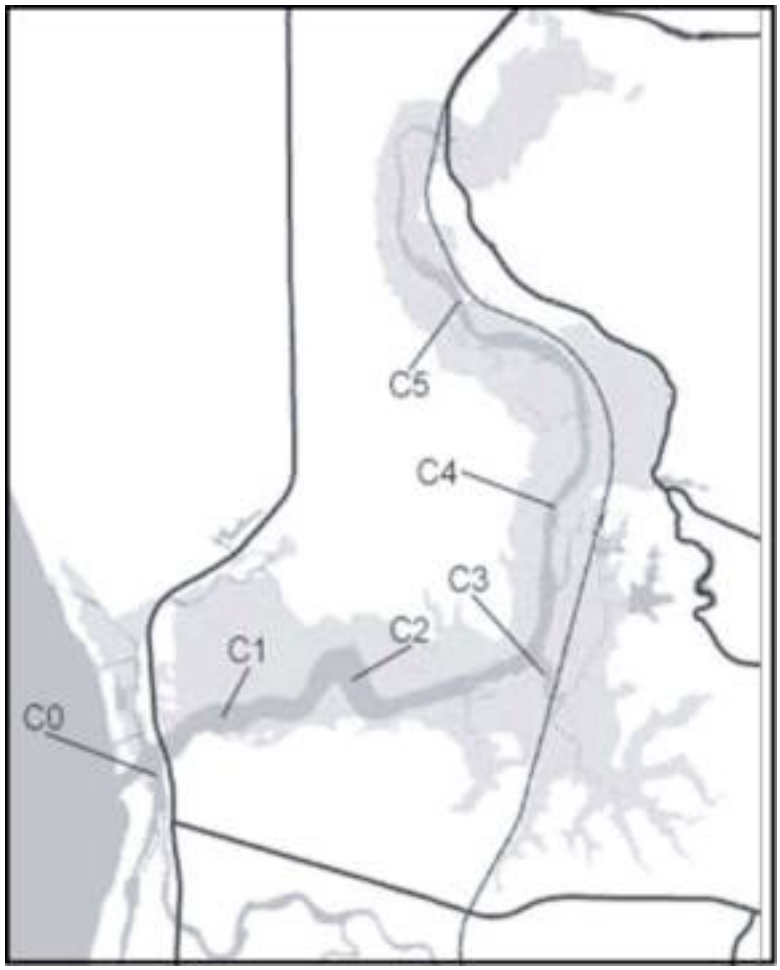

Figure 4.1 Location of Ra sampling sites in the main channel of Elkhorn Slough

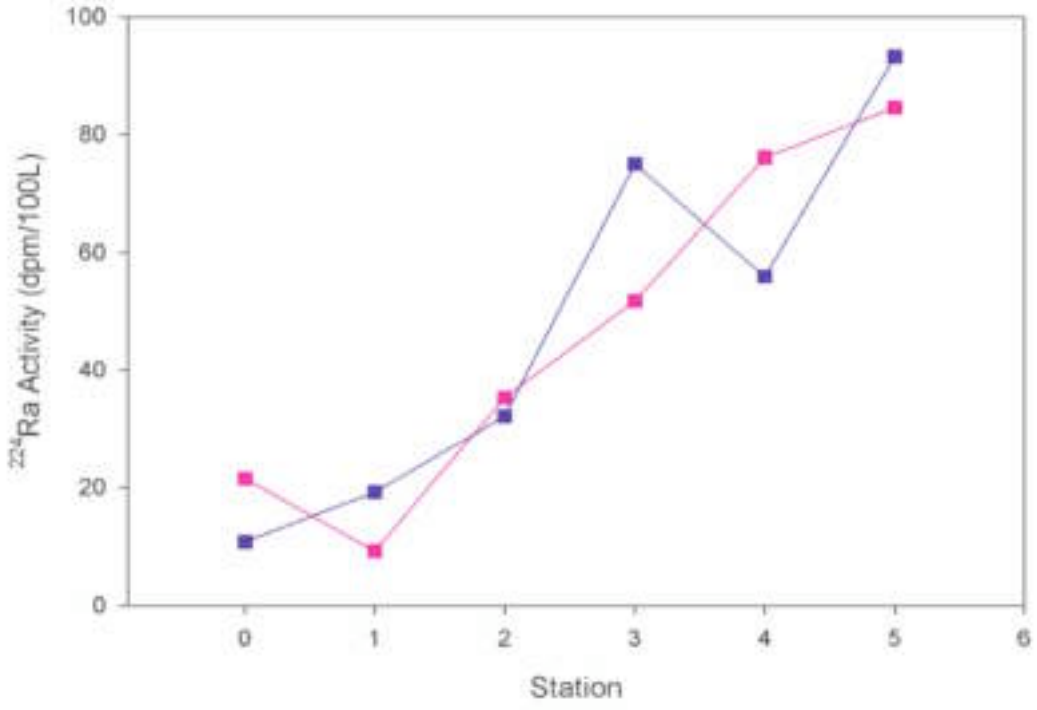

Figure 4.2 ^{224}Ra activity along the Elkhorn Slough main channel – Station numbers refer to sites on figure 3.1. Samples were collected in the Spring of 2003.

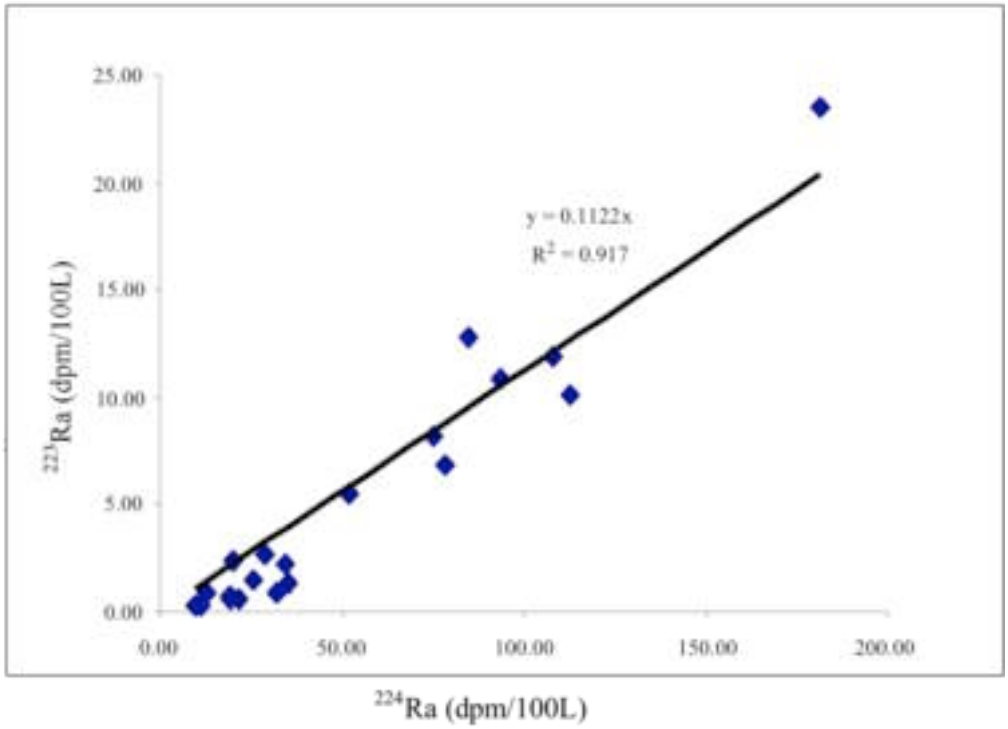

Figure 4.3 Correlation between ^{223}Ra and ^{224}Ra activities in Elkhorn Slough

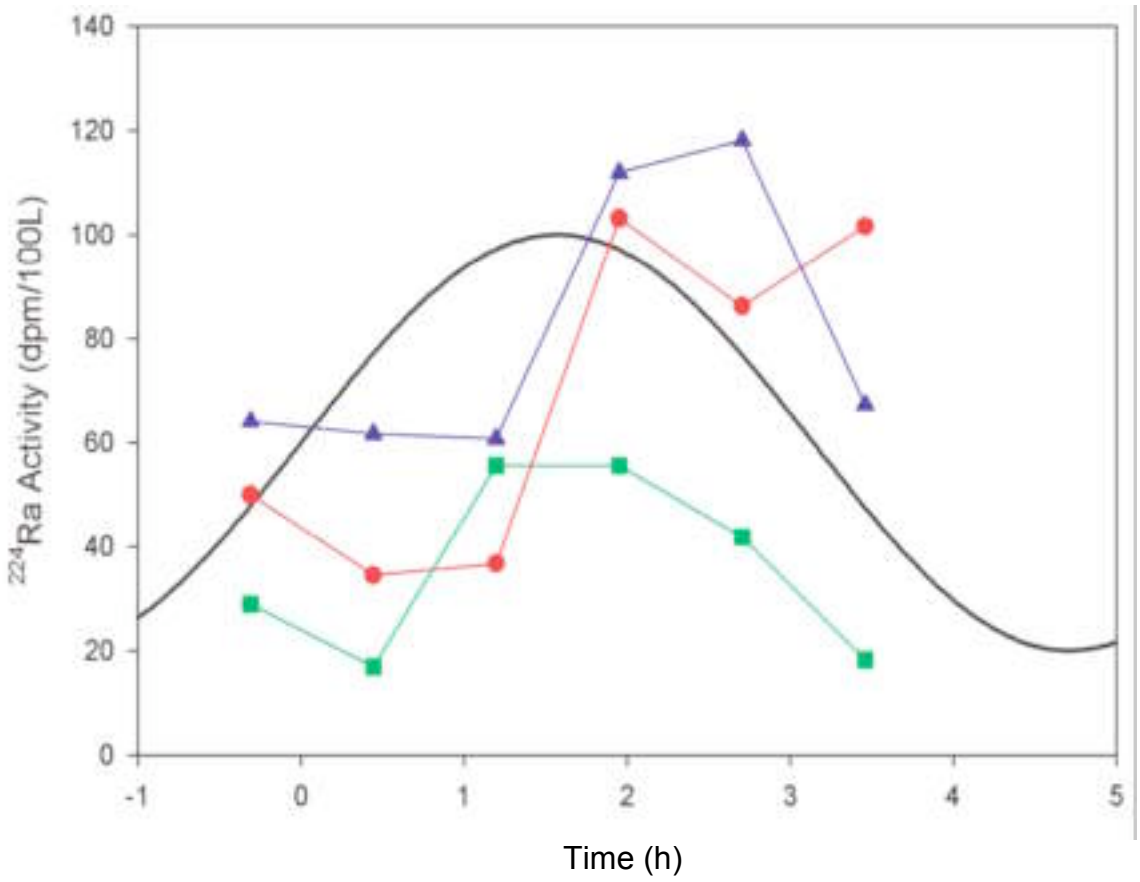

Figure 4.4 Tidal variability in Ra activity. Samples collected at 3 different locations (Kirby Park - blue, Mouth - green and MBARI Dock -red) on February 2003. The black line marks the tidal elevation scaled to fit on the plot.

5. Summary and conclusions

The goal of this project has been to develop a detailed understanding of the hydrodynamics and sediment dynamics of Elkhorn Slough through a combination of numerical modeling, hydrographic field measurements, and tracer chemistry.

The hydrographic field work we discuss in this report is primarily based on two 3 week long experiments, one carried out in September 2002, the other performed in April 2003. During each experiment we deployed a variety of instruments for measuring currents, water levels, and temperatures at a series of 5 stations arrayed along the length of the Slough. More limited measurements of salinity were made during the 2002 experiment.

The major results of the field work are:

(1) Water levels in the Slough are nearly in-phase – i.e., the water surface in the Slough moves up and down in response to tides in Monterey Bay as though it were a flat surface. As a result, tidal currents are proportional to the rate of change in sea-surface elevation, enabling first-order predictions of currents to be made using predicted water level variations.

(2) Currents below Parsons Slough are relatively constant in strength, partially reflecting the fact that much of the tidal prism of the system is upstream of the confluence of Parson's Slough and the main stem of Elkhorn Slough. The decrease in cross-sectional area with distance from the Highway 1 Bridge also contributes to maintaining the strength of tidal currents below Parson's Slough.

(3) Currents in Elkhorn Slough are ebb dominant – i.e., the shorter duration ebbs have stronger currents than are observed during floods. The likely effect of this on sediment transport is pronounced since bottom stresses, which drive erosion of sediments, are substantially larger on ebbs than on floods. The net effect is a mean ocean-ward flux of sediments. This flux would appear to be strongly modulated by the fortnightly spring-neap cycle.

(4) Tidal excursions are a considerable fraction of the length of the Slough. As observed in measured temperatures and inferred from integration of current measurements, at spring tides, a water parcel that is located at Kirby Park at the end of the flood can travel nearly the entire length of the Slough on the following ebb. During neap tides, water motions are somewhat reduced.

(5) Flows in many sections of Elkhorn Slough are spatially complex. In most cross-sections, flows are stronger in the deepest section, although in Seal Bend, the region of maximum ebb

current wanders from side to side through the bend. Immediately upstream of the Highway 1 Bridge, there are pronounced secondary flows on ebbs. These lead to predictable variations in acoustic backscatter intensity that suggest cross-sectional variations in the distribution of sediments.

(6) Bottom drag coefficients, "constants" that relate bottom stress to local velocity vary from the canonical value of 0.002 near Kirby Park to values as large as 0.0075 in the reach below Parson's Slough.

Numerical modeling of currents and sediments was carried out using the 3D circulation model TRIM3D, a hydrodynamic model that has been applied to a number of estuarine systems like San Francisco Bay, the Venice Lagoon Tomales Bay, and the low salinity zone of the Saint Lawrence River. The 10 m resolution bathymetric grid was based on data provided by the CSUMB Seafloor mapping laboratory and extended from the Highway 1 Bridge to the head of the estuary. Lacking data for major portions of the intertidal zone of the Slough, bathymetry for much of the shallowest parts of the system were based solely on edges defined by USGS topographic maps. Flows in the model were forced by imposing observed variations in sea level at the downstream boundary,

Driven by tides observed in September 2002, and using bottom friction coefficients (roughness lengths) that we have used in modeling other estuaries, the model did a good job of reproducing observed water levels, although, in light of the flat surface behavior, this is not a stringent test. Currents were reproduced with reasonable accuracy, although currents near Kirby Park were better predicted than were currents near the Highway 1 Bridge. This may reflect shortcomings in the bathymetry data, in particular, a general lack of data from the Parson's Slough drainage. Increasing the model resolution was from 2 vertical layers to 7 layers improved the predicted velocities, although instabilities of the wetting front (the water's edge during filling and emptying of the Slough) also emerged, suggesting that the treatment of wetting and drying in TRIM3D may need improvement for application to systems like Elkhorn Slough. A second limitation to the accuracy of current predictions is the effect of fixed resolution of the grid relative to the size of smaller channels and features in the slough, which are not well represented by 10m grid.

The hydrodynamic code was supplemented by a sediment "module" previously used to predict cohesive sediment behavior in South San Francisco Bay. Using velocities calculated by

the hydrodynamic code, this module computed the erosion, deposition and transport of sediments. Erosion and deposition were calculated using standard models of these processes, models that entail specifying 4 empirical parameters related both the sediments themselves and to the state of the bed from which they are eroded.

The sediment model shows clearly that the Slough is erosional. When run with the same parameters used previously for South San Francisco Bay, most of the Slough showed net erosion although there were also significant regions of deposition. In contrast, observations of changes in Slough bathymetry show only erosion. This highlights the need to obtain specific measurements of the needed sediment parameters, including some limited assessment of their spatial variability.

Computation of residence time by computing the transport of tracers that initially mark selected regions of the Slough show that downstream of Parson Slough, the residence time is quite short, possibly less than 1 day, depending on when in the spring-neap cycle and even at what phase of the tide the tracer is introduced. In contrast, upstream of Kirby Park, the residence time was appeared to be greater than the length of time the calculation was run (ca. 14 days).

Work with the hydrodynamic/sediment model is ongoing as part of LOBO (Land Ocean Biogeochemical Observatory, an NSF funded project lead by Ken Johnson of MBARI), and current efforts are focused on developing a new grid based on new bathymetric data (also from CSUMB) which includes LIDAR surveys of the intertidal zone. The new grid will also include Moss Landing Harbor and may extend into Monterey Bay so as to enable study of ocean-estuary exchange.

Measurement of four Radium isotopes (^{223}Ra, ^{224}Ra, ^{226}Ra, and ^{228}Ra) made at 5 stations along the length of the Slough show that there may be significant groundwater inputs to Elkhorn Slough, with computed flows varying from 5 to 50 m^3/s depending on the time of year and the isotope used to compute the flow. Averaging over all the Radium data, the groundwater flow we computed was 34 ± 29 m^3/s.

The picture these observations make is that while details of flows in Elkhorn Slough may be complex, overall, it is clear that because of its ebb dominance, Elkhorn Slough is currently exporting sediment to Monterey Bay. The fact that the water levels in the Slough are more or less the same as in Monterey Bay and change little along the length of the Slough also suggests that any measure, e.g. sills (P. Williams 1992), aimed at muting tides in the Slough would either need

to be of a length along the channel that is comparable to the wavelength of the tides, or would need to impose hydraulically critically conditions at the sill or contraction to regulate water levels in the Slough. In any case, the current hydrodynamic/sediment model could be used to assess the qualitative, order of magnitude response to engineered features like sills, although details of the predictions could not be made with any confidence at the present time.

6. Acknowledgements

This work was supported by a grant from the Monterey Bay National Marine Sanctuary Foundation through the SIMON program. Additional support came from the UPS Foundation, Stanford University, and the NSF through grant ECS-0308070 to MBARI. The authors wish to thank Juan Bustamente, Jeremy Bricker, Sandy Chang, Derek Fong, Jim Hench, Johanna Rosman, Greg Shellenbarger, and Scott Wankel, all of whom helped with the field work and Jan Wang who provided crucial help with the modellng.. We are indebted to Scott Hansen for his skilled boat operation during both experiments and to Billy Moore for his assistance with application of his Radium technique to Elkhorn Slough. Finally, we thank Rikk Kvitek and his group at CSUMB, particularly Pat Iampietro, for sharing their high quality bathymetric data with us.

7. References

Blumberg, A.F., L.A. Khan, and J.P. St. John 1999. Three dimensional hydrodynamic model of New York Harbor region. *J. Hydraulic Eng*. 125(8): 799-816.

Brennan, M.L., Schoellhamer, D.H., Burau, J.R. and Monismith, S.G. 2002. Tidal asymmetry and variability of cohesive sediment transport at a site in San Francisco Bay, California. In: INTERCOH-2000: *Fine Sediment Dynamics in the Marine Environment* / Ed. by J.C. Winterwerp, C. Kranenburg. Amsterdam u.a.: Elsevier (Proceedings in Marine Science; 5), pp. 93-108.

Bricker, J.D., Inagaki, S.and Monismith, S.G. ,2004. Bed Drag Coefficient Variability in a Tidal Estuary:Field measurements and Numerical Modeling, *Ann. J. Hyd. Eng., JSCE*, 48: 1237-1242.

Buddemeier, R.W. (ed.)1996. *Groundwater Discharge in the Coastal Zone: Proceedings of an International Symposium.* LOICZ/R&S/96-8, iv+179 pp. LOICZ, Texel, The Netherlands,.

Burnett, W. W., J. P. Chanton, J. Christoff, E. Kontar, S. Krup, M. Lambert, W.S. Moore, D. O Rourke, R. Paulsen, C. Smith, L. Smith, and M. Taniguchi. Assessing methodologies for measuring groundwater discharge to the ocean. EOS, Trans. AGU, 83:117–123, 2002.

Cable, J. E., Bugna, G.C., Burnett, W.C., and Chanton, J.P., 1996. Application of ^{222}Rn and CH_4 for assessment of groundwater discharge to the coastal ocean. *Limnol Oceanog*, 41: 1347-1353.

Casulli, V. and E. Cattani 1994. Stability, accuracy and efficiency of a semi-implicit method for three dimensional shallow water flow. *Computers and Mathematics with Applications* 27(4): 99-112.

Casulli, V. and R.T. Cheng 1992. Semi-implicit finite difference methods for three dimensional shallow water flow. *Intl. J. Num. Methods in Fluids* 15: 629-648.

Cheng, R. T., V. Casulli, and J. W. Gartner, 1993. Tidal, residual, intertidal mudflat (TRIM) model and its applications to San Francisco Bay, California, . *Est. Coastal Shelf Sci.* 36: 235-280.

Church, T.M. 1996. An underground route for the water cycle. *Nature* 380: 579-580.

Cooper, H.H. Jr. 1959. A hypothesis concerning the dynamic balance of fresh water and salt water in a coastal aquifer. *J. Geophys. Res.* 64: 461-467.

Crotwell, A.M. and W.S. Moore, 2003. Nutrient and Radium Fluxes from Submarine Groundwater Discharge to Port Royal Sound, South Carolina. *Aquatic Geochem.,* 9(3): 191-208.

Dronkers, J. and J.T.F. Zimmerman, 1982. Some principles of mixing in tidal lagoons. *Oceanologia Acta* SPO: 101-117.

Dyer, K. R. 1997. *Estuaries: A Physical Introduction (2^{ed})*, Wiley Chichester, England, 195 p.

Fischer, H.B., E.J. List, J. Imberger, R.C.Y. Koh, and N. H. Brooks 1979. *Mixing in Inland and Coastal Waters* Academic Press, New York, N.Y., 483 pp.

Friedrichs, C.T. and D.G. Aubrey 1988. Non-linear tidal distortion in shallow well-mixed estuaries: a synthesis. *Est. Coastal Shelf Sci*, 27, 521-545.

Friedrichs, C.T., D.G. Aubrey, and P.B. Speer 1990. Impacts of relative sea level rise on evolution of shallow estuaries. in: Residual currents and long-term transport (*Coastal and Estuarine Studies* v. 38) ed. R.T. Cheng, pp. 105-122.

Friedrichs, C.T. and O.S. Madsen 1992. Nonlinear diffusion of the tidal signal in frictionally dominated embayments. *J. Geophys. Res.,* 94(C4): 5637-5650.

Galperin, B. and L.H. Kantha, S. Hassid, and A. Rosati, 1988. A quasi-equilibrium turbulent energy model for geophysical flows. *J. Atmos. Sci.* , 45: 55-62.

Glover, RE. 1959. The pattern of fresh-water flow in a coastal aquifer. *Jour. Geophy. Res.* 64: 457-459.

Gross, E.S. 1999. *Numerical modeling of hydrodynamics and scalar transport in an estuary.* PhD thesis, Dept of Civil and Env. Eng. Stanford University, Stanford, Ca. 313 pp.

Gross, E.S., Koseff, J.R. Koseff, and S.G. Monismith, 1999a. Evaluation of advective schemes for estuarine salinity simulations. *J. Hydraulic Eng.* 125: 32-46.

Gross, E.S., Koseff, J.R. Koseff, and S.G. Monismith 1999b. Three-dimensional salinity simulations in South San Francisco Bay. *J. Hydraulic Eng.* 125(11): 1199-1209.

Henderson, F.M. 1966. *Open Channel Flow.* MacMillan 522 p.

Holdaway, G.P, P.D. Thorne, D. Flatt, S.E. Jones, and D. Prandle 1999. Comparison between ADCP and transmissometer measurements of suspended sediment concentration. *Cont. Shelf Res.* 19, 421-441.

Inagaki. S. 2000. Effects of a proposed San Francisco airport runway extension on hydrodynamics and sediment transport in South San Francisco Bay. Engineers thesis, Dept of Civil and Env. Eng. Stanford University, Stanford, Ca. 110 pp

Kalkwijk, J. P. T., and Booij R., 1986: Adaptation of secondary flow in nearly-horizontal flow. *J. Hydraul. Eng.,* **24**, 19–37.

Krest J., W. Moore, and Rama. 1999. Radium-226 and radium-228 in the mixing zones of the Mississippi and Atchafalaya Rivers: Indicators of groundwater input. *Marine Chemistry* 64(3): 129-152.

Krest, J.M. and J.W. Harvey. Using natural distributions of short-lived radium isotopes to quantify groundwater discharge and recharge. Limnol. and Oceanogr., 48(1): 290-298, 2003.

Krone, R.B., 1962. *Flume study of the transport of sediment in estuarial processes*. Final Report, Hydraulic Eng. Lab. and Sanitary Eng. Res. Lab., Univ. Calif., Berkeley, Calif., USA.

Largier, J. L., S. V. Smith and J. T. Hollibaugh. 1997 Seasonally hypersaline estuaries in Mediterranean-climate regions. Est Coastal Shelf Sci. 45:789-797.

Li Y.-H., G. Mathieu, P. Biscaye, and H. Simpson 1977. The flux of 226 Ra from estuarine and continental shelf sediments. *Earth and Planetary Science Letters* 37: 237-241.

Li, C. and J. O'Donnell, 1997. Tidally driven residual circulation in estuaries with lateral depth variations. *J. Geophys. Res.*, 102: 27913-27929.

McDonald, E. T., and R. T. Cheng, 1997, A Numerical Model of Sediment Transport Applied to San Francisco Bay, California, *J. Mar. Env. Eng*. 4: 1-41.

Malzone, C. M. 1999. *Tidal scour and its relation to erosion and sediment transport in Elkhorn Slough*, M.S. thesis, Dept of Geology, San José State University.

Malzone, V. and R. Kvitek 1994. Tidal scour, erosion and habitat loss in Elkhorn Slough, California, Report to the Elkhorn Slough Foundation, 22p.

McNeil, J., C. Taylor, and W. Lick 1996. Measurements of erosion of undisturbed bottom sediments with depth. *J. Hydraulic. Eng*. 122(6),: pp. 316-324.

Mehta, A. 1989. On estuarine cohesive sediment suspension behavior. *J. Geophys. Res*. 94(C10), pp. 14303-14314.

Monismith, S.G., W. Kimmerer, M.T. Stacey, and J.R. Burau, 2002. Structure and Flow-Induced Variability of the Subtidal Salinity Field in Northern San Francisco Bay. *J. Phys. Ocean*, 32(11): 3003-3019.

Monsen, N.E. 2000. *A study of sub-tidal transport in Suisun Bay and the Sacramento-San Joaquin Delta, California.* PhD thesis, Dept of Civil and Env. Eng. Stanford University, Stanford, Ca. 344 pp.

Monsen, N.E., J.E. Cloern, L. V. Lucas, and S. G. Monismith 2002. A comment on the use of flushing time, residence time, and age as transport time scales. *Limnol. Oceanog.*

Moore W. 1996. Large groundwater inputs to coastal waters revealed by ^{226}Ra enrichments. *Nature* 380: 612-614.

Moore. W. S. The subterranean estuary: a reaction zone of ground water and sea water. Marine Chemistry, 65:111–125, 1999.

Moore W. 2000a. Ages of continental shelf waters determined from ^{223}Ra and ^{224}Ra. *J. Geophys. Res.* 105(C9):22,117-22,122.

Moore W. 2000b. Determining coastal mixing rates using radium isotopes. *Continental Shelf Res.* 20: 1993-2007.

Moore. W. S., 2003. Sources and fluxes of submarine groundwater discharge delineated by radium isotopes. *Biogeochemistry*, 66 (1):75-93.

Moore, W.S and R. Arnold 1996. Measurement of ^{223}Ra and ^{224}Ra in coastal waters using a delay coincidence counter. *J. Geophys. Res.* 101:1321-1329

Moore W. and Todd J. 1993. Radium isotopes in the Orinoco Estuary and eastern Caribbean Sea. *J. Geophys. Res.* 98:2233-2244.

Nepf, H. 1999. Drag, turbulence and diffusivity in flow through emergent vegetation. *Water Resources Res.* 35(2): 479-489.

Phillip Williams & Assoc. 1992, *Elkhorn Slough tidal hydraulics erosion study*. Report submitted to US Army Corps of Engineers San Francisco District, August 1992, 33 pp.

Pope, S.B 2000. *Turbulent Flows.* Cambridge Press, 771 p.

Rama and W. Moore 1996. Using the radium quartet for evaluating groundwater input and water exchange in salt marshes. *Geochimica et Cosmochimica Acta* 60(23):4645-4652.

Reay, W.G. Gallagher, D.L. & Simmons, G.M. 1992. Groundwater Discharge and Its Impact on Surface Water Quality in a Chesapeake Bay Inlet. *Water Resources Bull.* **28**, 1121-1134.

Shaw T., Moore, W., Kloepfer J., and Sochaski M., The flux of barium to the coastal waters of the southeastern USA: Importance of submarine groundwater discharge. Geo. Chem. Aacta. 62: 3047-3054, 1998.

Speer, P.E. and D.G. Aubrey. 1985. A Study of Non-Linear Tidal Propagation in Shallow Inlet/Estuarine Systems. Part II: Theory. *Est. Coastal Shelf Sci.,* 21: 207-224.

Shureman, P. 1940. *Manual of harmonic analysis and prediction of tides*, US Dept of Commerce Speical Publication 98, 317 p.

Stacey, M.T., S.G. Monismith, and J.R. Burau, 1999. Observations of turbulence in a partially stratified estuary. *J. Phys. Oceanogr.*, 29: 1950-1970.

Torgersen, T., K.K. Turkenian, V.C. Turkenian, N. Tanaka, E. DeAngelo, J. O'Donnell 1996. ^{224}Ra distribution in surface and deep water of Long Island Sound: sources and horizontal transport rates. *Continental Shelf Res.* 16(12): 1545-1559.

Turkenian, K.K., V.C. Turkenian, T.Torgersen, and E. DeAngelo 1996. Transfer rates of dissolved tracers through estuaries based on ^{228}Ra: a study of Long Island Sound. *Continental Shelf Res.* 16(7): 863-873.

Veeh H., W. Moore, and S. Smith 1995. The behavior of uranium and radium in an inverse estuary. *Continental Shelf Research* 15(13):1569-1583.

Wasson K, Van Dyke E, Kvitek R, Brantner J, Bane S., 2002. "Tidal Erosion at Elkhorn Slough".In: Carless J. editor. Ecosystem observations for the Monterey Bay National MarineSanctuary, 2001. Monterey, CA: Monterey Bay National Marine Sanctuary.

Webster, I.T., G.J. Hancock and A.S. Murray. Use of radium isotopes to examine pore-water exchange in an estuary. Limnol. and Oceanogr., 39(8): 1917-1927, 1994.

Yang, H. S., D. W. Hwang, and G. B. Kim. Factors controlling excess radium in the Nakdong River estuary, Korea: submarine groundwater discharge versus desorption from riverine particles. Marine Chemistry, 78:1–8, 2002.

Zimmerman, J.T.F. 1976. Mixing and flushing of tidal embayments in the western Dutch Wadden Sea. Part I: Distribution of salinity and calculation of mixing time scales. *Neth. J. Sea Res.* 10(2):149-191.